Solitons in conducting polymers

A. J. Heeger

Department of Physics and Institute for Polymers and Organic Solids, University of California at Santa Barbara, Santa Barbara, California 93106

S. Kivelson

Department of Physics, SUNY at Stony Brook, Stony Brook, New York 11794-3800

J. R. Schrieffer

Department of Physics and Institute forTheoretical Physics, University of California at Santa Barbara, Santa Barbara, California 93106

W.-P. Su

Department of Physics, University of Houston, Houston, Texas 77004

Self-localized nonlinear excitations (solitons, polarons, and bipolarons) are fundamental and inherent features of quasi-one-dimensional conducting polymers. Their signatures are evident in many aspects of the physical and chemical properties of this growing class of novel materials. As a result, these polymers represent an opportunity for exploring the novel phenomena associated with topological solitons and their linear confinement which results from weakly lifting the ground-state degeneracy. The authors review the theoretical models that have been developed to describe the physics of polyacetylene and related conducting polymers and summarize the relevant experimental results obtained for these materials. An attempt is made to assess the validity of the soliton model of polyacetylene and its generalization to related systems in which the ground-state degeneracy has been lifted.

CONTENTS

I. INTRODUCTION

Since polymers are typically insulators, they are often considered uninteresting from the point of view of electronic materials. Although this is true for saturated polymers (in which all of the four carbon valence electrons are tied up in covalent bonds), the situation in conjugated polymers is much more interesting. In conjugated polymers, the sp^2p_z hybridization leads formally to one unpaired electron per carbon atom (see Sec. II). As a result, the electronic structure is determined by the chain symmetry (e.g., the number and kind of atoms in the repeat unit, etc.), with the result that such polymers can be expected to exhibit semiconducting or even metallic properties. Polyacetylene (see Sec. II) is a particularly important example, for, in this case, the π band is half-filled, implying the possibility of metallic conductivity. Because of the strong intrachain bonding (and weak interchain interactions) characteristic of such polymers, the π electrons are delocalized principally along the polymer chain. These systems are therefore electronically essentially one dimensional.

Quasi-one-dimensional metals tend to distort spontaneously (Peierls, 1955) (structurally) such that the spacing between successive atoms along the chain is modulated with period $2\pi/Q = 2\pi/2k_F$, where k_F is the Fermi wave number. When the band is half-filled, the tendency toward spontaneous symmetry breaking is particularly strong, and the distortion leads to a pairing of successive sites along the chain, or dimerization. This dimerization opens an energy gap at the Fermi surface, thereby lowering the energy of the occupied states and stabilizing the distortion. The competition between the lowering of the electronic energy and the increase of the elastic energy of the polymer (caused by the distortion) leads to an equilibrium bond-length modulation which is of order 0.03–0.04 Å in polyacetylene. Thus the lattice instability removes the high density of states at the Fermi surface and renders the system a semiconductor, in contrast to the metallic behavior expected of a corresponding three-dimensional system with a half-filled band.

Fortunately, there is more to the story. A chain of atoms (or, more generally, monomers made up of groups of atoms) can be dimerized in two distinct patterns, both of which have the same energy. Labeling the atoms (or monomers) 1,2,3, . . . , one could have the bonding structures 1═2—3═4—5═6— or 1—2═3—4═5—6═ which we denote the A and B phases, respectively. In this notation, — represents a single (or long) bond and ═ represents a double (or short) bond. Clearly if all monomers are equivalent and the chain is infinite in extent, the energies of these bonding structures are equal. In the language of quantum field theory, the vacuum state is twofold degenerate.

In the early 1960s, it was recognized that in addition to electron and hole excitations in such a dimerized semiconductor a new type of excitation could exist: namely, a domain wall separating regions of different bonding structure or different vacua. These excitations were called "misfits" (Longuet-Higgins and Salem, 1959; Pople and Walmsley, 1962; Salem, 1966). While no detailed analysis was carried out to estimate the width of the misfit, it was argued (Longuet-Higgins and Salem, 1959) that the region of the misfit would be confined to a finite number of atoms. As we shall see, the actual width of this nonlinear excitation is large (Rice, 1979; Su, Schrieffer, and Heeger, 1979, 1980) approximately $14a$, so that the excitation can be reasonably well described by a continuum model.

The large width of the domain wall leads to several important qualitative effects. First, the variation of the system energy as the center of the wall moves relative to the lattice is very small, so that the object is free to move in defect-free material except possibly at very low temperature. This would not be the case for a misfit with width of order a, since the excitation would have to pass over a high barrier in moving from site to site, leading to pinned or immobile excitations. Second, the large width leads to an extremely small effective mass for the excitation, of order the electron mass rather than the ionic mass. As a result of the smallness of the domain-wall effective mass, this object is truly a quantum particle.

In view of the fact that the domain wall is a nonlinear shape preserving excitation which propagates freely, it has been called a "soliton" (Zabusky and Kruskal, 1965). This term is not totally appropriate, since solitons are supposed to pass through one another, preserving their shape. This is certainly not the case with these domain-wall excitations. Nevertheless, the particlelike nature of these objects is dominant, and the term soliton has become standard. Since a moving soliton converts A-phase material into B-phase material (or vice versa), these objects act as topological solitons and can only be created or destroyed in pairs.

While the soliton has a remarkable effect on the lattice distortion pattern, it has an equally peculiar effect on the electronic spectrum. As noted in the early quantum chemical work (Longuet-Higgins and Salem, 1959; Pople and Walmsley, 1962; Salem, 1966), a single electronic state appears near the center of the energy gap when a soliton is created. This state is singly occupied for a neutral soliton. Since the unpaired electron has a spin $\frac{1}{2}$ and all other states in the system are spin paired, it follows that the neutral soliton has spin $\frac{1}{2}$. In chemical terms, this object is a neutral free radical (spatially delocalized over $\simeq 14a$). From the point of view of physics, this excitation is indeed peculiar (Su, Schrieffer, and Heeger, 1979, 1980), since a spin-$\frac{1}{2}$ object would be expected to carry charge $\pm e$, as in the case of an electron or a hole. Furthermore, since the midgap state is a solution to the Schrödinger equation in the presence of the structural kink, it can be occupied with 0, 1, or 2 electrons. Equally peculiar, therefore, is the fact that a charged soliton (having either 0 or 2 electrons in the gap state) carries charge $\pm e$ and has spin zero, rather than the spin $\frac{1}{2}$ as for an electron or a hole. These reversed spin-charge relations are a fundamental feature of the soliton model of polyacetylene and are supported by experiment. They are also closely related to the occurrence of fractional fermion number, which was first discovered in quantum field theory (Jackiw and Rebbi, 1976; Jackiw and Schrieffer, 1981).

A truly multidisciplinary approach has been necessary to unravel the fundamental properties of these intriguing systems. The discovery that these polymers can accept large concentrations of dopants, which donate or accept an electron, has enabled experimentalists to create charged solitons at will and over a wide range of densities. Photogeneration of these nonlinear excitations has been of great importance in probing the dynamics. Equally important has been the dramatic improvement of the materials quality as well as the introduction (through chemical synthesis) of new conducting polymer systems. New effects are found in materials such as polythiophene, in which the degeneracy between A and B phases is weakly lifted. In such cases, the solitons are confined by a potential that is approximately linear in their separation, reminiscent of the confinement potential of QCD.

A number of reviews of progress in the area of conducting polymers have appeared in recent years. These, together with the proceedings of topical conferences devoted to this subject, provide the interested reader with a chronological record of progress and with a focus on specific aspects (e.g., chemical, electrochemical, etc.) of the field. During the past ten years, more than 2000 papers have been written on polyacetylene alone; if one includes the extensive literature on other conducting polymers, the task of a comprehensive review of the literature becomes formidable.

We have therefore restricted ourselves to an overview of the theory and experiments related to the soliton model of quasi-one-dimensional conductors, using specific polymer systems as prototypical examples. We hope to clarify the relevant concepts in a coherent manner and to present a theoretical framework and an experimental methodology for studies of solitons, polarons, and bipolarons in the growing class of conducting polymers. We apologize to those whose contributions to this existing field are not specifically cited.

II. MATERIALS

A. Conducting polymers: Polyacetylene and polythiophene as model systems

In this review, we shall discuss the application of the theoretical concepts outlined in the preceding section in relation to experiments on conducting polymers (for earlier reviews, see Etemad *et al.*, 1982; Fincher *et al.*, 1983; Brazovskii and Kirova, 1984; Brédas and Street, 1985; Schrieffer, 1985; Frommer and Chance, 1986; Kivelson, 1986; Skotheim, 1986; Conwell, 1987). Although this field has grown rapidly with the emergence of a relatively large (and rapidly growing) number of novel systems, we shall focus on two particularly well-studied examples, which illustrate the fundamental concepts and for which a somewhat more complete data base exists.

(1) Polyacetylene, $(CH)_x$, in which the degenerate ground state leads to solitons as the important excitations and the dominant charge storage species. The concepts developed for polyacetylene can be generalized to include systems in which the degeneracy is weakly lifted, leading to fundamental interesting phenomena such as the *linear confinement* of soliton pairs into doubly charged bipolarons (Brazovskii and Kirova, 1981; Heeger, 1981; Lauchlan *et al.*, 1981). The chemical structure of polyacetylene is shown in Fig. 1.

(2) Polythiophene, a specific example of a conjugated polymer in which the ground-state degeneracy is weakly lifted so that polarons and confined soliton pairs (bipolarons) are the important excitations and the dominant charge storage configurations. The chemical structure of polythiophene is shown in Fig. 2.

Many other conducting polymers exist (Etemad *et al.*, 1982; Fincher *et al.*, 1983; Brazovskii and Kirova, 1984; Brédas and Street, 1985; Schrieffer, 1985; Frommer and

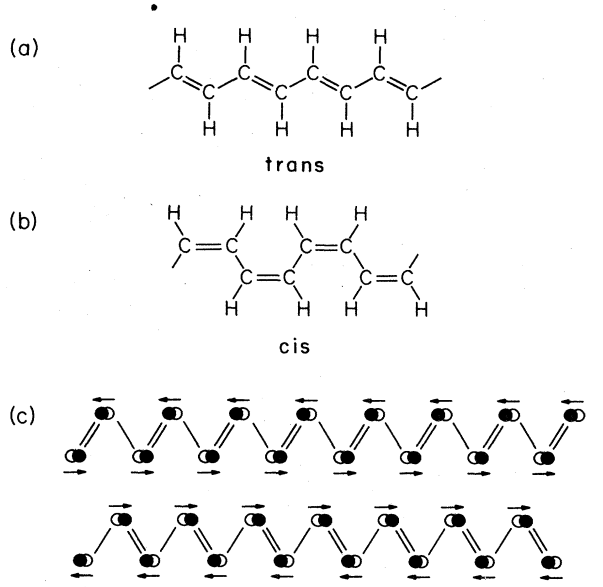

FIG. 1. Structural diagrams for polyacetylene: (a) *cis*-$(CH)_x$; (b) *trans*-$(CH)_x$; (c) the two degenerate ground states of *trans*-$(CH)_x$.

Chance, 1986; Kivelson, 1986; Skotheim, 1986; Conwell, 1987); since most of these have a nondegenerate ground state, such systems can be considered as fundamentally similar to the polythiophene example. Those polymers which have a degenerate ground state are directly analogous to polyacetylene.

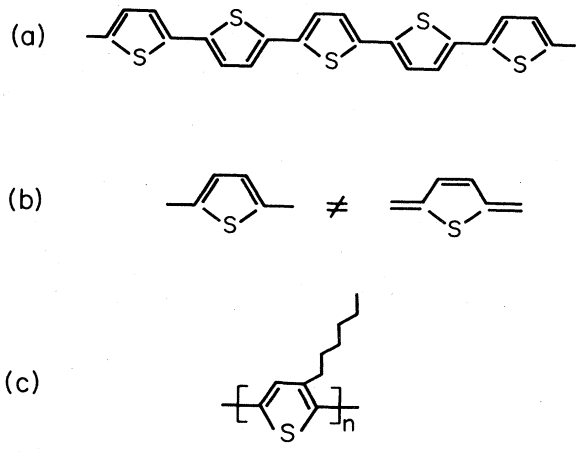

FIG. 2. Structural diagrams for polythiophene and the alkylthiophene derivatives: (a) chemical structure of polythiophene; (b) the two valence-bond configurations are not equivalent; (c) chemical structure of the soluble and processible poly(3-alkylthienylenes)—the P3AT's.

B. Polyacetylene, the simplest conjugated polymer

Polyacetylene is a linear polymer; it consists of weakly coupled chains of CH units forming a quasi-one-dimensional lattice. Three of the four carbon valence electrons are in sp^2 hybridized orbitals; two of the σ-type bonds connect neighboring carbons along the one-dimensional (1D) backbone, while the third forms a bond with the hydrogen side group. The optimal bond angle of 120° between these three bonds can be obtained by two possible arrangements of the carbons, *trans*-$(CH)_x$ and *cis*-$(CH)_x$, with two and four CH monomers per unit cell, respectively [see Figs. 1(a) and 1(b)]. In either isomer, the remaining valence electron has the symmetry of a $2p_z$ orbital with its charge-density lobes perpendicular to the plane defined by the other three. In terms of an energy-band description, the σ bonds form low-lying, completely filled bands, while the π bond leads to the partially filled energy band responsible for the important electronic properties.

If all the bond lengths were equal, pure *trans*-$(CH)_x$ would be a quasi-1D metal with a half-filled band. Such a system is unstable with respect to a dimerization distortion, the Peierls instability (Peierls, 1955), in which adjacent CH groups move toward each other forming alternately short (or "double") bonds and long (or "single") bonds (Fincher *et al.*, 1982; Yannoni and Clarke, 1983), thereby lowering the energy of the system [see Fig. 1(c)]. Clearly, by symmetry, one could interchange the double and single bonds without changing the energy. Thus there are two lowest-energy states, A and B, having two distinct bonding structures. This twofold degeneracy leads to the existence of nonlinear topological excitations (Rice, 1979; Su, Schrieffer, and Heeger, 1979, 1980), bond-alternation domain walls or solitons, which appear to be responsible for many of the remarkable properties of *trans*-$(CH)_x$. In *cis*-$(CH)_x$, no such symmetry relates the two possible senses of the dimerization; hence the ground state is nondegenerate.

Both *cis* and *trans* forms can be prepared using the techniques originally developed by Shirakawa and colleagues (Shirakawa and Ikeda, 1979/1980, and references therein to earlier work). The polymer can be prepared as silvery flexible films, which can be made either free-standing or on a variety of substrates, such as glass or metal, with thicknesses varying from $<10^{-5}$ cm to ≈ 0.5 cm. The *trans*-$(CH)_x$ isomer is the thermodynamically stable form. Any *cis-trans* ratio can be maintained at low temperatures, but complete isomerization from *cis*- to *trans*-$(CH)_x$ can be accomplished after synthesis by heating the film to temperatures above 150 °C for a few minutes.

Electron microscopy studies (Shirakawa and Ikeda, 1979/1980) of Shirakawa polyacetylene show that the as-grown $(CH)_x$ films consist of randomly oriented fibrils (typical fibril diameter ~ 200 Å; see Fig. 3). The fibril diameter can be varied somewhat with different polymeri-

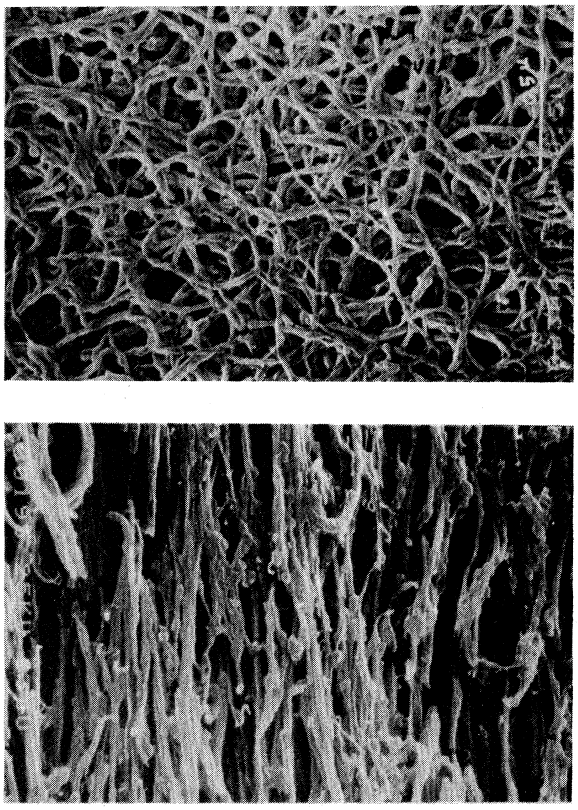

FIG. 3. Electron micrographs of polyacetylene; the upper panel shows the as-grown morphology, and the lower panel shows the effect of modest orientation by stretching. The typical fibril diameter is approximately 200 Å (from Shirakawa and Ikeda, 1979/1980).

zation conditions. The films can be stretch oriented in excess of three times their original length, with concomitant partial alignment of the fibrils. The bulk density of unoriented films is about 0.4 g/cm^3, compared with 1.2 g/cm^3 as obtained by flotation techniques. Therefore the polymer fibrils fill only about one-third of the total volume, and the effective surface area is quite high ($\sim$60 m^2/g).

Alternative methods for synthesis of polyacetylene have been explored. Of these, the synthesis developed at Durham University (so-called Durham polyacetylene) offers particular advantages (Edwards and Feast, 1980; Edwards *et al.*, 1984; Feast, 1986). The synthesis utilizes a soluble prepolymer that is converted to polyacetylene as a final step. The Durham polyacetylene can be studied in the as-grown amorphous form, or it can be stretch oriented simultaneous with isomerization into crystalline, highly anisotropic free-standing films (Bradley *et al.*, 1987; Kahlert *et al.*, 1987). The fibrillar morphology of Shirakawa $(CH)_x$ is *not* present in Durham polyacetylene; the latter is high-density material with no microstructure visible by electron microscopy.

X-ray studies (Shirakawa and Ikeda, 1979/1980; Fincher *et al.*, 1982; Bradley *et al.*, 1987; Kahlert *et al.*, 1987) have shown that $(CH)_x$ films made by either the Shirakawa method or the Durham method (Bott *et al.*, 1986) are highly crystalline (Akaishi *et al.*, 1980), and detailed analysis of the scattering data have provided important information on the chain structure and packing.

Although the existence of bond alternation in long-chain polyenes has been a question of importance to quantum chemistry for many years, only recently has direct experimental evidence of the dimerization been obtained. From analysis of the x-ray diffraction data obtained from oriented films, of *trans*-$(CH)_x$, the crystal structure (see Fig. 4) was determined (Fincher *et al.*, 1982). The space group is $P2_1/n$ with two chains per unit cell, as proposed earlier (Baughman *et al.*, 1979). The chain structure is dimerized (Fincher *et al.*, 1982) with the symmetry-breaking distortion parameter $u_0 \sim 0.03$ Å.

The dimerized chain structure was confirmed through a novel NMR experiment in which the dipolar splitting associated with the two different distances between neighboring (C-H) units was measured (Yannoni and Clarke, 1983). Unambiguous evidence of the dimerization was obtained; the symmetry-breaking parameter was determined to be $u_0 = 0.035$ Å.

There is continuing activity in the area of structural studies of polyacetylene. For example, the evolution of the structure on isomerization from *cis* to *trans* has been followed (Robin *et al.*, 1983a, 1983b). Although this is not a controversial area, some aspects of the structure

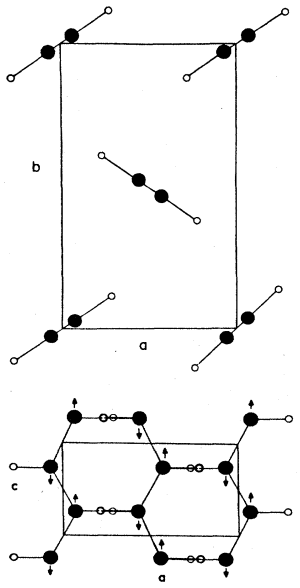

FIG. 4. Two schematic projections of the structure of *trans*-$(CH)_x$. $a = 4.24$ Å, $b = 7.32$ Å, $c = 2.46$ Å, and $\beta = 91.5$. The arrows are a schematic representation of the bond-alternation atomic displacements (from Fincher *et al.*, 1982).

remain unsettled. In particular, there has been disagreement on the precise phasing of the two chains in the unit cell, whether short bonds on one chain next to short bonds on the other (Kahlert *et al.*, 1987) or short bonds on one chain next to long bonds on the other (Fincher *et al.*, 1982; Robin *et al.*, 1983a, 1983b; Moon *et al.*, 1987).

Simple estimates lead to a picture of $(CH)_x$ as a broad-band, quasi-one-dimensional semiconductor. The overall bandwidth associated with electronic motion along the chain, W, can be estimated from tight-binding theory, $W=4t_0$, where t_0 is the intercarbon transfer integral for π electrons. From theoretical and spectroscopic studies of aromatic ring systems and short-chain polyenes, t_0 can be estimated as ≈ 3 eV, so that $W \simeq 12$ eV. The transverse bandwidth due to interchain coupling is much less. The large nearest-neighbor interchain spacing (>4.2 Å) implies a transverse bandwidth much smaller, i.e., of order 0.1 eV. Weak interchain coupling is therefore implied, and the system can be regarded as quasi-one-dimensional (1D). Because of the bond alternation, *trans*-$(CH)_x$ is a highly anisotropic semiconductor with an energy gap of $E_g^{1D} \approx 1.8$ eV. The interchain transfer leads to weak dispersion for k transverse to the chain axis, resulting in a three-dimensional energy gap of about 1.5 eV. These qualitative estimates have been confirmed through detailed band calculations (Grant and Batra, 1979; Ashkanazi *et al.*, 1985).

For undoped *trans*-$(CH)_x$, the reflection coefficient (see Fig. 5) resembles that of a 1D semiconductor with band gap $E_g^{1D} \simeq 1.8$ eV (Moses *et al.*, 1982). This value for the 1D gap is also inferred from resonance Raman scattering experiments (Vardeny, Ehrenfreund, *et al.*, 1983; Vardeny, Orenstein, and Baker, 1983a, 1983b; Horovitz *et al.*, 1984). The 1D divergence in the joint density of states at the band edge is smeared by a combination of effects due to interchain coupling, disorder, and dynamical one-dimensional fluctuations of the lattice (Brazovskii, 1980; Su and Schrieffer, 1980; Sethna and Kivelson, 1982; Su and Yu, 1983; Mele and Hicks, 1986). The effect on interchain (transfer) interactions has been investigated through measurements of the pressure dependence of the absorption edge (Moses *et al.*, 1982), with the conclusion that $E_g^{3D} \approx 1.5$ eV.

Electron energy-loss spectroscopy has been utilized to probe the excitation spectrum of neutral polyacetylene (Fink and Leising, 1986). The results, obtained from measurements carried out on highly oriented Durham material, are shown in Fig. 6. The single-particle spectrum was analyzed in terms of the simple 1D tight-binding model with energy bands

$$\varepsilon(k)=\pm(t_1^2+t_2^2+2t_1t_2\cos ka)^{1/2}\ , \tag{2.1}$$

where k is the wave vector (along the chain axis), a is the unit cell length, and t_1 and t_2 are the transfer integrals between successive sites. Because of the dimerized structure, t_1 and t_2 are not the same. Figure 6 is plotted (Fink and Leising, 1986) with $t_1=3.65$ eV and $t_2=2.75$ eV.

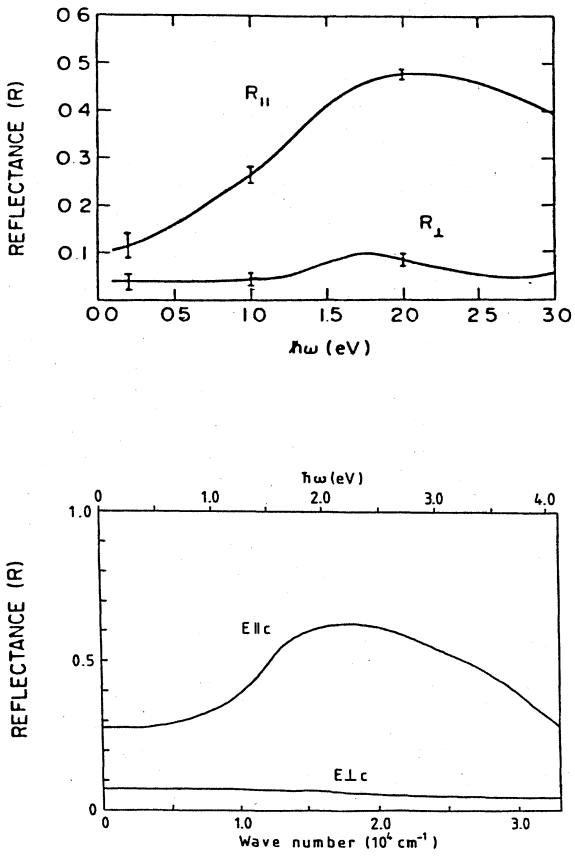

FIG. 5. Reflectance spectra of neutral *trans*-polyacetylene: (a) neutral *trans*-$(CH)_x$, stretch-oriented Shirakawa material with $l/l_0 \approx 2.5$, with light polarized parallel and perpendicular to the chain axis (Fincher, Ozaki, Tanaka, *et al.*, 1979); (b) neutral *trans*-$(CH)_x$, stretch-oriented Durham material with $l/l_0 \approx 20$, with light polarized parallel and perpendicular to the chain axis (from Leising, 1987). The improved orientation in (b) is evident in the optical properties.

These values of the transfer integrals correspond to an energy gap of $E_g=2(t_1-t_2)=1.8$ eV and to a total bandwidth between the bottom of the valence band and the top of the conduction band of $W=4t_0=2(t_1+t_2)=12.8\pm0.1$ eV. The k dependence of the peak in the π-π^* transition is shown as the solid circles in Fig. 6. The measured dispersion is in excellent agreement with that calculated from the 1D tight-binding band structure. These beautiful results demonstrate without ambiguity that a well-defined band structure exists for this polymer system and that the band structure can be accurately modeled by 1D tight-binding theory (Fink and Leising, 1986). Moreover, they provide a solid foundation on which one can begin to build a more complete theoretical understanding.

The experimentally determined π-plasmon dispersion relation (i.e., the zero crossing of ε_1) is also plotted in Fig. 6. Detailed calculations of the longitudinal dielec-

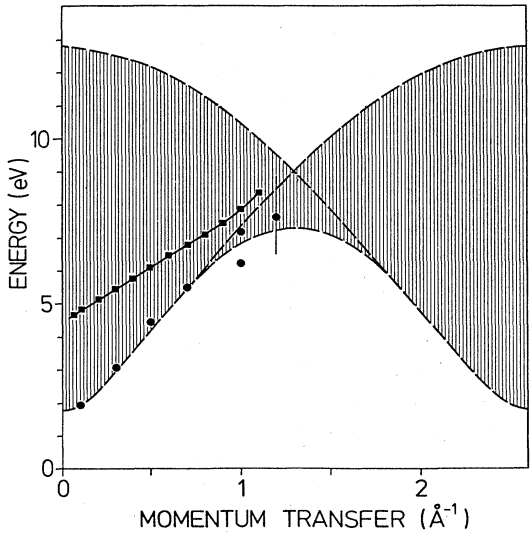

FIG. 6. Excitation of π electrons in polyacetylene with momentum transfer parallel to the chain axis. The solid circles represent maxima of the π-π^* transitions as derived from the experimentally determined joint density of states. The vertical bar indicates the broader distribution of interband transitions. The hatched area indicaes the region of possible interband transitions calculated in the tight-binding scheme [Eq. (2.1)]; dashed lines show the maxima in the calculated joint density of states. The transitions near the upper dashed line (starting at 12.8 eV and $q=0$ and ending at 1.8 eV and $q=2.6$ Å) are suppressed by the matrix element. The solid squares represent the observed π-plasmon spectrum; i.e., the zero crossing of ε_1 (from Fink and Leising, 1986).

tric function have been carried out (Lee and Kivelson, 1984; Drechsler and Bobeth, 1985; Neuman and van Boltz, 1988) and compared with the electron energy-loss data (Fink and Leising, 1986). The results are in excellent agreement with experiment and lead to an estimate of the π-band width $W \approx 11$ eV.

C. Doping of conducting polymers

The discovery that polyacetylene can be doped after synthesis, at room temperature, and with a variety of dopants, opened the field of conducting polymers (Chiang *et al.*, 1977; Shirakawa *et al.*, 1977; Chiang, Druy, *et al.*, 1978). Subsequently, the doping methodology was generalized and applied to a large number of conjugated systems (Frommer and Chance, 1986). The ability of these π-electron polymers to be reversibly doped at room temperature, and after synthesis, makes them fundamentally different from conventional covalent semiconductors.

The term "doping" is properly used here in contrast to "oxidation" or "reduction." The doping of conductive polymers implies (i) charge transfer (by oxidation, *p* type, or reduction, *n* type), (ii) the associated insertion of a counter ion (for overall charge neutrality), and (iii) the simultaneous control of the Fermi level or chemical potential. Through doping the electronic and optical properties of conducting polymers can be controlled over the full range from insulator to metal.

The ability to dope $(CH)_x$ *after synthesis* using chemical or electrochemical techniques is due to a combination of its open morphology with associated high surface area and the weak interchain forces that allow diffusion of the dopant ions between the polymer chains. The 200-Å-diameter fibrillar morphology of Shirakawa polyacetylene ensures that a dopant molecule has to diffuse less than ~ 100 Å to reach any chain (thus yielding relatively rapid doping kinetics). On the other hand, the strong intrachain bonding maintains the integrity of the polymer during the diffusion process and thereby ensures the reversibility of the doping.

The reversibility of the doping and undoping process has been monitored through absorption coefficient (α) measurements (Feldblum *et al.*, 1982). The results from *n*- and *p*-type doped polyacetylene are similar and resemble free-carrier absorption from a metal at high doping levels ($y \simeq 0.07$). Furthermore, chemical compensation (Chiang, Gau, *et al.*, 1978; Clarke and Street, 1980; Chung *et al.*, 1981; François *et al.*, 1981) or electrochemical "undoping" (Feldblum *et al.*, 1982) of either *n*- or *p*-type doped samples gives back the spectrum of the undoped *trans*-$(CH)_x$. These results demonstrate that doping *reversibly* transforms the electronic structure of the polymer from a semiconductor to a metal. The reversibility has also been demonstrated through *in situ* structural studies (Moon *et al.*, 1987; Winokur *et al.*, 1987).

The carriers generated by the doping of $(CH)_x$ result from charge transfer (Chiang, Park, *et al.*, 1978; Seeger *et al.*, 1978; Kwak *et al.*, 1979). Charge transfer occurs from polymer to acceptor (A), with the polymer chain acting as a poly(cation) in the presence of an A species. For a donor (D), the polymer chain acts as a poly(anion) in the presence of D^+ species. The A^- or D^+ counter ions reside between polymer chains. Doping can be carried out by exposure of the polymer to the vapor phase of an electron acceptor (such as iodine or AsF_5, etc.) or donor (such as the vapor of an alkali metal), by means of chemical charge transfer in solution, or by electrochemical oxidation or reduction (Nigrey *et al.*, 1979; MacInnes *et al.*, 1981; Etemad *et al.*, 1982; Fincher *et al.*, 1983; Brazovskii and Kirova, 1984; Brédas and Street; 1985; Schrieffer, 1985; Frommer and Chance, 1986; Kivelson, 1986; Skotheim, 1986; Conwell, 1987).

The solution doping method is convenient. For *p*-type doping, the following reaction may be used:

$$2(NO^+PF_6^-)_{y/2}+(CH)_x \rightarrow (N_2O_2)\,|_{\text{gas}} + [(CH)^{+y}(PF_6^-)_y]_x \ .$$

In this (or analogous) reaction the NO^+ is the oxidizing

agent, and the (PF_6^-) counter ion enters the structure to assure charge neutrality; the reaction is carried out in a suitable solvent. Similarly, for *n*-type doping, the following reaction may be used:

$$y(Na^+)(Naphth^-)+(CH)_x \rightarrow (Naphth)_{neutral} + [(Na_y{}^+(CH)^{-y}]_x \ .$$

The ($Naphth^-$) act as the reducing agent and the Na^+ as the counter ion.

In the case of electrochemical doping, the reaction is carried out in an electrochemical cell with the polymer as one electrode (MacDiarmid and Kaner, 1986, and references therein). The polymer is reduced or oxidized (i.e., electrons are added or removed) electrochemically through the external circuits. Electrical neutrality is provided by an ion from the electrolyte. For example, polyacetylene can be used as one electrode and Li metal as the counter electrode, with $Li^+ClO_4^-$ as the electrolyte (dissolved in a suitable solvent).

The electrochemical method is the most elegant of the doping methods, for it is reversible, it allows control at the resolution of parts per million, and it makes possible a novel experimental methodology based on *in situ* experiments (Heeger, 1985). Moreover, the doping is accomplished by directly controlling the electrochemical potential μ of the polymer (the cell voltage is precisely μ measured with respect to the reference electrode). Since the doping involves first-order phase transitions (Chen *et al.*, 1985; Moraes *et al.*, 1985; Shacklette and Toth, 1985), both electronic and structural, it is useful to control μ rather than the dopant concentration whenever possible.

The technique of electrochemical voltage spectroscopy (EVS) has been used to measure μ vs y (the doping level) (Kaufman *et al.*, 1983; Kaufman, Chung, and Heeger, 1984). A series of phase transformations (with dopant ordering) were discovered by EVS measurements on alkali-doped polyacetylene (Shacklette and Toth, 1985); these show up as steps in μ vs y, and were identified as structural transitions by examining samples at fixed concentration with x-ray diffraction.

The process of doping is structurally very demanding, since it involves diffusion of the dopant species into the structure with associated rearrangements of the polymer chains (Baughman *et al.*, 1985; Shacklette, Murthy, and Baughman, 1985; Shacklette, Toth, *et al.*, 1985). It is, nevertheless, true that reversible structural changes have been observed [at least at moderate doping levels (Moon *et al.*, 1987)]. The reversible doping-induced structural transitions have been studied by x-ray scattering carried out *in situ* on Na-doped polyacetylene (Winokur *et al.*, 1987). The results indicate an unusual sequence of reversible transitions within a channel structure, in which the local unit is a column of Na ions surrounded by three $(CH)_x$ chains. The ability to monitor continuously the evolution of the scattering data made it possible to characterize the full series of transformations as a function of dopant level. (i) At the lowest doping levels ($<0.5\%$), the Na^+ ions appear to go into the $(CH)_x$ structure at random. (ii) At moderate doping levels, Na^+ channels form (with three polyacetylene chains per channel) and develop into a strongly modulated incommensurate lattice in the plane normal to the polymer chains [see Fig. 7(a)]. Below 6 mol %, this incommensurate lattice of Na^+ channels coexists with the lightly (random) doped PA. (iii) At higher doping levels (≈ 11 mol %), the sodium lattice becomes commensurate, forming a $\sqrt{3}\times\sqrt{3}$ superlattice relative to the average triangular spacing of the *rearranged* $(CH)_x$ chains [see Fig. 7(b)]. (iv) Finally, at the highest doping levels (>11 mol %), the sodium superlattice transforms into a dense disordered state, which is best characterized as a highly modulated fluid. These features represent an unusual example of two interpenetrating mass-density waves with continuously varying periodicities; the strong interaction between the two results in the formation of a novel discommensuration-domain channel structure (Winokur *et al.*, 1987).

D. Charge carriers and electrical conductivity

The electrical conductivity of conducting polymers results from mobile charge carriers introduced into the π-electronic system through doping. At low doping levels,

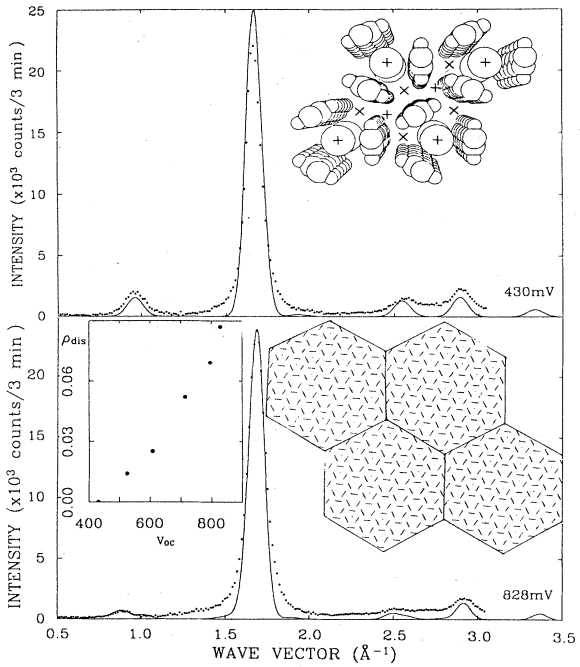

FIG. 7. Structure of Na-doped polyacetylene, $[(Na^+)_y(CH)^{+y}]_x$ (from Winokur *et al.*, 1987): (a) comparison between data (dots) and calculated diffraction profile (solid curve) for the commensurate $\sqrt{3}\times\sqrt{3}$ superlattice channel structure, $y\approx 0.11$; (b) comparison between data (dots) and calculated diffraction profile (solid curve) for discommensurate-domain structure shown in the inset, $0.06<y<0.10$.

these charges self-localize and form the nonlinear configurations (solitons, polarons, and bipolarons) that are the principal focus of this review. At higher doping levels, a transition to a degenerate Fermi sea is observed, with associated metallic behavior. Because of the large intrachain transfer integrals (Grant and Batra, 1979; Moses *et al.*, 1982; Ashkanazi *et al.*, 1985; Fink and Leising, 1986), the transport of charge is believed to be principally along the conjugated chains, with interchain hopping as a necessary secondary step.

In conducting polymers, as in all metals and semiconductors, charge transport is limited by a combination of intrinsic electron-photon scattering and sample imperfection. Although relatively high conductivities ($\sigma > 10^4$ S/cm) have been reported for partially oriented and heavily doped polyacetylene (Basescu *et al.*, 1987), the absence of a metal-like temperature dependence (see Fig. 8) suggests that the observed values are not intrinsic. In doped polyacetylene, electrical transport can be limited both by microscopic defects (leading to scattering and localization) and by the more macroscopic complex fibrillar morphology and associated interfibrillar contacts. Thus, with improvements in material quality, one might anticipate corresponding improvements in the electrical conductivity.

A modified technique has been developed by Naarmann and Theophilou (Naarmann, 1987a, 1987b; Naarmann and Theophilou, 1987) to synthesize polyacetylene with fewer sp^3 defects than in material prepared by other methods. Since the perfect $(CH)_x$ structure would have only sp^2p_z hybridization, the reduction of sp^3 defects implies longer conjugation length (localization lengths), fewer crosslinks, and fewer (unspecified) chain interruptions. The higher-quality material exhibits substantially higher electrical conductivity; maximum values (Basescu *et al.*, 1987, 1988; Naarmann, 1987a, 1987b; Naarmann and Theophilou, 1987) in excess of 20 000 S/cm are obtained after doping with iodine, and even higher values with other dopants (such as PF_6^-). The conductivity has been measured as a function of temperature (room temperature to 0.48 K) and pressure (1 atm to 15 kbar); at 0.48 K and 10 kbar, iodine-doped samples remain highly conducting ($\sigma \approx 9000$ S/cm; Basescu *et al.*, 1987, 1988; Naarmann, 1987a, 1987b; Naarmann and Theophilou, 1987). The polymer synthesized by the Naarmann/Theophilou technique has been thoroughly characterized. In most respects it is essentially identical to polyacetylene prepared by the Shirkawa technique. The material has the characteristic fibrillar morphology (approximately the same fibril diameter as Shirakawa material) with a density of 0.5 g/cm^3. X-ray scattering studies show features that are indistinguishable from Shirakawa material. The principal difference appears to be a major reduction in the number of sp^3 defects to a level that is not detectable by high-resolution ^{13}C NMR. No bands corresponding to —CH_3— or —CH_2— could be detected at wavelengths of 2960, 2910, and 2830 μm in the infrared spectrum. The low density of sp^3 defects implies a higher degree of chain perfection in this material.

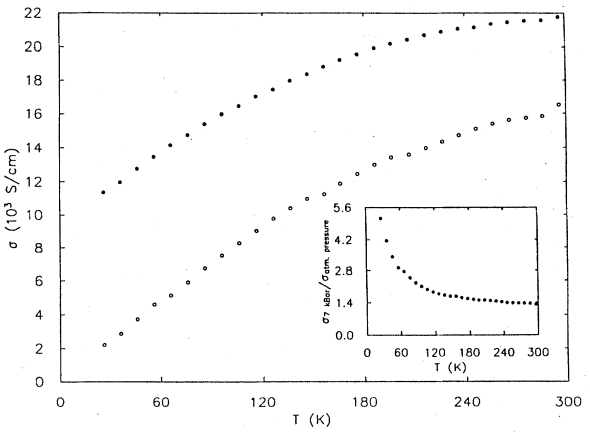

FIG. 8. Temperature dependence of the conductivity (parallel to the stretch direction $\sigma_\parallel$) of heavily doped polyacetylene, $[(CH)^{+y}(I_3)_y]_x$ with $y \approx 0.08$, prepared via the Naarmann method; solid dots, 7 kbar; open circles, 1 atm. The stretch ratio was 6:1 (Basescu *et al.*, 1987).

The most striking feature of the Naarmann polyacetylene is the high electrical conductivity of the heavily doped material (Basescu *et al.*, 1987). Figure 8 shows $\sigma_\parallel$ as a function of temperature for a fourfold stretched sample at 10 kbar. At room temperature, the conductivity is greater than 20 000 S/cm; at 0.5 K the conductivity is still above 9000 S/cm. The inset shows the temperature dependence below 4 K in more detail. Even more recent improvements in synthesis and orientation have resulted in $\sigma = 1.5 \times 10^5$ S/cm (Naarmann and Theophilou, 1987). It now appears quite clear that the intrinsic conductivity for doped polyacetylene is greater than that of copper and that these remarkable transport properties should be attainable through improvements in synthesis and processing.

The fact that the conductivity of heavily doped polyacetylene is sensitive to the presence of a few ($\ll 1$ mol %) sp^3 defects is remarkable. Evidently, the conduction process involves long-distance coherent motion of electrons along the polymer backbone, with relatively long mean free paths [of order several hundred angstroms (Basescu *et al.*, 1987, 1988)]. This implies that even in the heavily doped state (in which the polymer contains of order 10% charged impurities), the wave functions are delocalized over many lattice constants along the polymer chain.

The anisotropy of the conductivity (Basescu *et al.*, 1987; Naarmann, 1987a, 1987b; Naarmann and Theophilou, 1987) is relatively large compared to that obtained from previous measurements on material prepared by the Shirakawa method; $(\sigma_\parallel/\sigma_\perp) \approx 80$ at 7 kbar. The anisotropy is somewhat higher at high pressure, since $\sigma_\parallel$ increases with pressure while $\sigma_\perp$ remains essentially constant.

The observation of a temperature- and pressure-dependent anisotropy suggests that the transport data are beginning to provide information on intrinsic processes. The magnitude and temperature independence of $\sigma_{\parallel}(T)$ below 1 K implies genuine metallic behavior for heavily doped polyacetylene (consistent with specific heat, thermopower, and susceptibility data) and rules out transport by hopping among strongly localized states. Note, however, that $\sigma_{\parallel}(T)$ increases with increasing temperature, implying that phonon-assisted transport (either through microscopic localized states or across interfibrillar barriers) is involved. Thus, although this modified synthesis yields significantly higher-quality polyacetylene (Naarmann, 1987a, 1987b; Naarmann and Theophilou, 1987), with $\sigma_{\parallel}$ comparable to the conductivity of copper, the transport is still limited by material imperfection (Basescu *et al.*, 1987, 1988).

E. Polythiophene (and polythiophene derivatives)

The chemical structures of polythiophene and the poly(3-alkylthiophene) derivatives are shown in Fig. 2. High-quality polythiophene has been prepared as powders by chemically induced polymerization (Kobayashi *et al.*, 1985; Mo *et al.*, 1985) (chemical coupling) or as free-standing films through oxidative electrochemical polymerization (Diaz, 1981; Tourillon and Garnier, 1982; Bargon *et al.*, 1983; Kaneto *et al.*, 1983; Hotta *et al.*, 1984, 1985; Sato *et al.*, 1985). The soluble poly(3-alkylthienylene) (P3AT) derivatives (see Fig. 2) have also been prepared using electrochemical polymerization (Jen *et al.*, 1986; Sato *et al.*, 1986; Hotta *et al.*, 1987). As synthesized, the electrochemically polymerized films are relatively heavily doped from *in situ* doping with anions of the supporting electrolyte during electrochemical polymerization. Consequently the as-synthesized films have relatively high electrical conductivities, with values as high as 500 S/cm reported in the literature (Jen *et al.*, 1986; Sato *et al.*, 1986; Hotta *et al.*, 1987). These films can be reversibly undoped (and subsequently redoped) by electrochemical reduction (oxidation); standard chemical doping techniques can also be used.

Quantum chemical calculations of the band structure of polythiophene have been carried out (Brédas, 1985, 1987; Brédas *et al.*, 1986). Relatively broad bands are obtained (comparable to those of polyacetylene), with an energy gap of about 2.1 eV. This gap value is in good agreement with experimental values inferred from optical absorption measurements (see Fig. 9) and from resonance Raman scattering experiments.

Both as-synthesized and solution-cast films of the P3AT's can be doped with resulting electrical conductivities that are quite high, for example, $\sigma \sim 40$ S/cm for films of poly(butylthienylene) (Jen *et al.*, 1986; Sato *et al.*, 1986; Hotta *et al.*, 1987; Nowak *et al.*, 1987). Ultraviolet visible absorption spectra of these soluble polythiophenes (see Fig. 9) have been obtained for solid films (as-synthesized and solution-cast) and for the polymers in solution. The spectral characteristics of the solution-cast films are essentially identical to those of the as-synthesized films, both in the neutral state and after doping. From a comparison of the spectra of the as-grown and solution-cast films, the following were concluded.

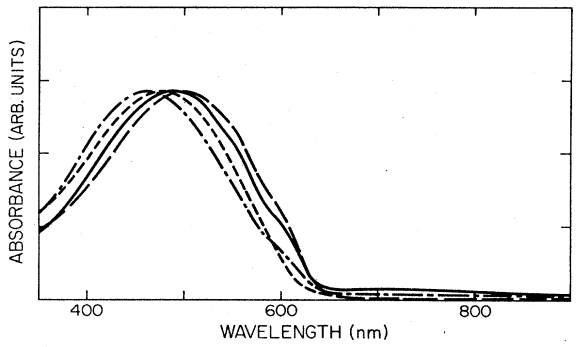

FIG. 9. Absorption spectra of polythiophene (PT) and a few derivatives of 3-substituted PT's; PT (short-dashed line), P3MT (long-dashed line), P3BT (dashed-dotted line), P3HT (solid line). The onset of absorption is at ≈ 620 nm (implying a 3D gap of about 1.9 eV); E_g^{1D} is estimated to be about 2.1 eV (580 nm). From Hotta *et al.*, 1987.

(a) The electronic structure of the P3AT's is unchanged after dissolution and subsequent processing into thin solid films.

(b) The solution-cast films have a well-defined electronic structure, which is equivalent in overall features to that of the most highly crystalline polythiophene (in fact, the absorption edge is even sharper and the residual absorption below the edge is even weaker than observed for chemically coupled, annealed polythiophene).

These conclusions imply relatively weak interchain electronic transfer interactions, i.e., the electronic structure is highly anisotropic or quasi-one-dimensional. This quasi-one-dimensionality is consistent with the good solubility of the alkyl-substituted polymer. In this context, the excellent electrical conductivities found after doping are particularly interesting. The combination of high conductivity and weak interchain coupling implies that electronic motion along the conjugated chains is the dominant transport mechanism. The results on the poly(3-alkylthienylenes) therefore suggest that for conducting polymers, in general, solubility (and processibility, etc.) and excellent electrical and optical properties are not necessarily mutually exclusive (Hotta *et al.*, 1987; Nowak *et al.*, 1987).

Chemically coupled polythiophene (Kobayashi *et al.*, 1985) has been particularly useful for structural studies. X-ray scattering (Mo *et al.*, 1985; Brückner, Porzio, and Wudl, 1988) has been used to investigate the crystallinity and crystal structure. Heat treatment of polythiophene (Mo *et al.*, 1985) leads to a significant increase in the

crystallinity and to the improvement of coherence within the crystalline regions. The chain growth and extension is implied by the structural data and confirmed by chemical analysis. After 30 min of annealing at 300 °C, the residual iodine content is consistent with growth of the polythiophene chains to approximately 1200 thiophene units or a molecular weight of nearly 10^5.

The crystallographic data lead to the structure of polythiophene (Mo *et al.*, 1985; Brückner, Porzio, and Wudl, 1988). The results are consistent with an orthorhombic unit cell with lattice constants $a=7.80$ Å, $b=5.55$ Å, and $c=8.03$ Å, or a monoclinic unit cell with $a=7.83$ Å, $b=5.55$ Å, $c=8.20$ Å, and $\beta=96°$. In either case, the polymer axis is along c, and there are two polymer chains per unit cell. More detailed information on the chain packing and the precise determination of the monoclinic angle β will require a more detailed analysis based upon an enlarged data set from polythiophene of even higher crystallinity.

Results on the structure of doped polythiophene indicate that substitution at the β carbon (poly-3-methylthiophene) leads to higher regularity in the corresponding polymer (Garnier *et al.*, 1985). The electron diffraction and x-ray data are consistent with a hexagonal lattice. A helicoidal structure was proposed for highly doped, crystalline poly(3-methylthiophene).

F. Conducting polymers: Intrinsically anisotropic (quasi-one-dimensional) electronic materials

A unique aspect of conducting polymers is their intrinsic anisotropy in electrical and optical properties. This uniaxial anisotropy arises directly from π-electron delocalization along the polymer backbone and from the weak interchain coupling inherent in the polymer structure; conducting polymers are intrinsically quasi-one-dimensional materials. This anisotropy offers the promise of special materials properties that are not currently available to technology with other classes of electronic materials. However, in order to realize this intrinsic anisotropy, oriented (chain-aligned) materials are required. There is ample evidence that chain alignment can yield the expected anisotropy and major improvements in material properties. Particularly illustrative and impressive in this respect has been the development of ultra-high-strength/modulus polymer fibers and films. Because of the extraordinary level of molecular orientation that is achieved in processing, these materials exhibit mechanical properties close to the theoretical limits for the carbon-carbon bond. Analogous enhancement of electrical properties can be expected from highly oriented samples (Basescu *et al.*, 1987, 1988; Naarmann, 1987a, 1987b; Naarmann and Theophilou, 1987). The modest orientation of polyacetylene that can be achieved by stretching resulted in a clear demonstration of the expected anisotropy. Alternatively, alignment has been achieved directly in the course of synthesis by suspending the catalyst in oriented liquid-crystal solvent during polymerization (Akagi *et al.*, 1987).

As noted above, crude stretch orientation, together with improved synthetic methods, has resulted in the achievement of a room-temperature electrical conductivity in excess of 1.5×10^5 S/cm along the drawing axis (Naarmann, 1987a, 1987b; Naarmann and Theophilou, 1987). Use of the Durham route (Fincher *et al.*, 1978; Fincher, Ozaki, Tamaka, *et al.*, 1979; Edwards and Feast, 1980; Edwards *et al.*, 1984; Townsend *et al.*, 1985; Feast, 1986; Bradley *et al.*, 1987; Fink *et al.*, 1987; Kahlert *et al.*, 1987; Townsend and Friend, 1987) to obtain stretch-aligned polyacetylene has resulted in excellent orientation with associated anisotropy in optical properties. For example, doped Durham polyacetylene has the optical properties of a one-dimensional metal; for light polarized along the chain, the reflectance is that of a metal with a beautiful plasma edge (Leising, 1987), whereas for light polarized perpendicular to the chain the reflectance is that of an insulator (small and nearly constant); see Fig. 10. The conclusion is clear: orientation of conducting polymers has been demonstrated to lead to highly anisotropic electrical and optical properties and to significant improvement in those properties. Further progress in the field is materials limited; only through the generation of higher-quality oriented materials can scientific (and technological) progress be made.

Although improvement of solid-state properties through higher-quality materials is a general feature of materials science, there has been little optimism that this rule would be applicable to conducting polymers. Perhaps the reason for this was the argument that the high level of impurities in doped conducting polymers would negate any improvements toward molecular chain

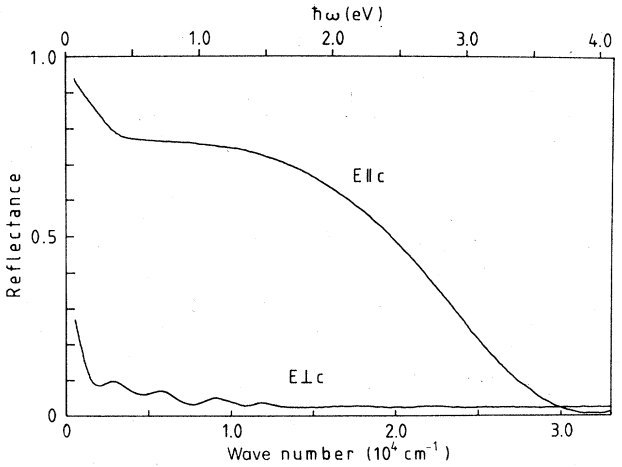

FIG. 10. Reflectance of heavily doped metallic polyacetylene (stretch-oriented Durham material, $l/l_0\approx20$) with the light polarized parallel and perpendicular to the chain axis. The long-wavelength oscillations for perpendicular polarization are interference fringes from multiple reflections. The dc conductivity of this samples is 1200 S/cm (from Leising, 1987).

perfection. The recent progress (Basescu *et al.*, 1987, 1988; Naarmann, 1987a, 1987b; Naarmann and Theophilou, 1987) has demonstrated, however, that this is not the case in polyacetylene or (by implication) in other conducting polymers: the achievement of still higher-quality material from improved synthesis and processing can be expected to lead to correspondingly better electronic properties.

III. MODEL HAMILTONIAN

A. Band structure and important interactions

The many degrees of freedom (e.g., σ bands, π bands, lattice vibrations, etc.) and the complicated interactions in real conducting polymers, coupled with the importance of fluctuations and nonlinear phenomena characteristic of one-dimensional systems, make a complete theoretical description impractical. However, if one is interested primarily in the low-energy, long-wavelength excitations of the system, it is in many cases possible to construct a simple effective model as in Landau theory (Pines, 1961) of a normal Fermi liquid. This is a consequence of the fact that in many conducting polymers the characteristic correlation length ξ is much larger than the lattice constant a, so the low-energy excitations of the systems are relatively insensitive to details of the underlying lattice structures. ($\xi/a = W/2\Delta$ is large since the π-band width W is large compared to the band gap 2Δ.) For this reason, various different simple models that share the same electronic structure in the vicinity of the Fermi surface can be used interchangeably. From the point of view of Landau theory, the continuum model obtained by expanding all interactions about the Fermi surface is the most natural approach.

It is, of course, obvious that the neglect of electron-electron interactions is never justified in a solid; however, in many cases, such as in a normal metal, the physics can most easily be described in terms of weakly interacting quasiparticles. While there are some fundamental problems associated with defining a Fermi-liquid theory in a one-dimensional metal, a quasiparticle description of a one-dimensional semiconductor, such as polyacetylene, is quite straightforward. Thus the electron-phonon coupling and the Hubbard model should always be viewed as Fermi-liquid parameters in which screening and other high-energy effects, have already been taken into account.

Therefore it is possible to derive the essential properties of the system from an effective Hamiltonian (Takayama *et al.*, 1980) that describes a field theory with a finite cutoff. There are only a few relevant interactions in the continuum limit, and the general forms of these interactions can be determined easily. However, the effective interaction strengths in the model are extremely difficult to derive from first principles and must generally be deduced from experiment. Despite appearances, the interactions are not truly bare microscopic interactions. An analogous situation occurs in the theory of superconductivity where the gap, 2Δ, is $\sim 10^{-4}$ eV. The BCS theory, which is based on the Landau theory, works extremely well in spite of the fact that the normal-state correlation energy is on the order of 1 eV per particle (Schrieffer, 1964).

It is sometimes more useful to use a lattice or tight-bonding model (see Figs. 11 and 12), since this correctly includes the effect of the underlying lattice periodicity. Moreover, a tight-binding model, such as the SSH (Su, Schrieffer, and Heeger, 1979, 1980) model, is closer in spirit to the underlying quantum chemistry of the polymers and, hence, allows us to develop some physical intuition for what the parameters in the model actually mean. In this review, we shall treat both the continuum and the tight-binding models.

Since any simple model is only an approximate representation of the real material, it is important from the outset to examine the conditions for the validity of these models. Although the band structure of polyacetylene is described by tight-binding theory with remarkable accuracy (see Figs. 6 and 13), the simple models only give a satisfactory description of the electronic structure of the real materials relatively near the Fermi energy (see Figs. 11–13). Those properties of the models which depend only on states near the Fermi surface are independent of the details of the model. Those which depend on the states near the band edges are model dependent. Since

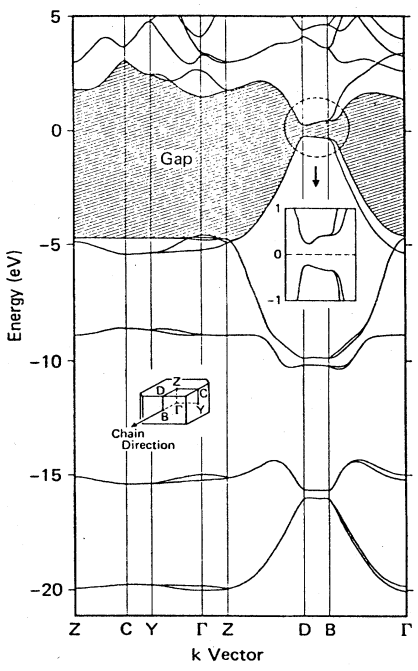

FIG. 11. Calculated band structure of *trans*-$(CH)_x$ from Grant and Batra (1979).

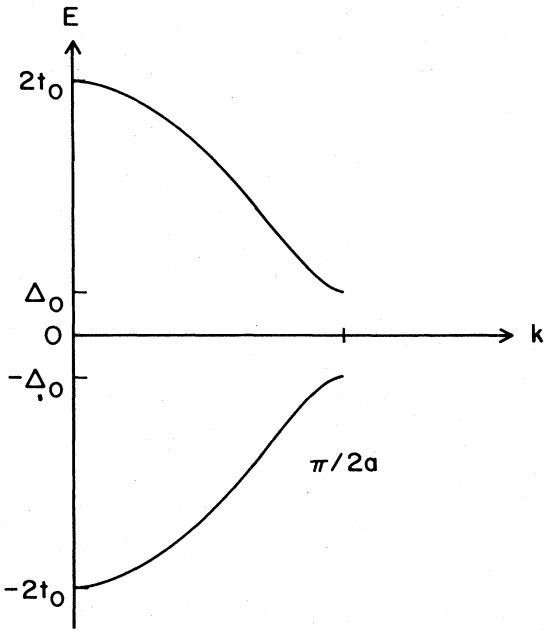

FIG. 12. One-dimensional tight-binding band structure.

the simple models may be incorrect near the band edges, only the low-energy features are meaningful. It is in this sense that, for example, the "band structure" of the continuum model can be expected to yield meaningful results.

We thus obtain two important criteria for the validity of the simple models. First, the band gap 2Δ, which sets the scale of interesting energies, must be small compared to the π-band width W; equivalently, the characteristic correlation length ξ must be large compared to the lattice constant a,

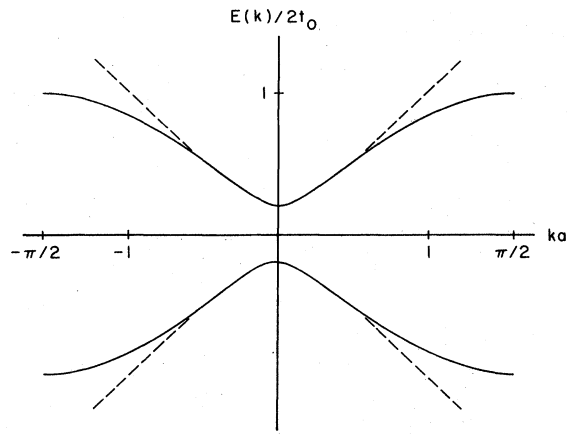

FIG. 13. Band structure of lattice (solid line) and continuum (dashed line) models of *trans*-$(CH)_x$.

$$2\Delta/W \simeq a/\xi \ll 1 . \tag{3.1}$$

Second, the characteristic magnitude U of the short-range electron-electron interactions must be small compared to the valence-band width

$$U/W \ll 1 . \tag{3.2}$$

This second condition emerges from detailed analysis of the structure of high-order perturbation theory (Kivelson and Wu, 1986a; Wu and Kivelson, 1986). It can be understood on the basis of a simple intuitive argument. An interaction with strength U will strongly mix the states with energy

$$|E - E_F| \leq U , \tag{3.3}$$

where E_F is the Fermi energy. Clearly, only if condition (3.3) is satisfied will the results be independent of the band structure near the band edges. Therefore conditions (3.2) and (3.3) are neccesary for the validity of the simple models. Note that, even if the condition (3.2) is satisfied, there may be a nonperturbative regime in which correlation effects are important (Krivnov and Ovchinnikov, 1986).

Since most conducting polymers have a small band gap compared to the π-band width, condition (3.1) is generally satisfied. However, condition (3.2) indicates that the simple models are valid only when electron-electron interactions are weak ($U/W \ll 1$). Detailed comparison with experiment of results obtained from the simple models, even from the exact solution of the models, is extremely difficult to justify when Coulomb interactions are not weak. We conclude that model calculations are valid only to lowest order in U/W. At best, the results are qualitatively correct outside this regime, but even that is not guaranteed. For instance, in the presence of strong electron-electron interactions, charge-conjugation symmetry (which is a feature of the simple models) is strongly broken (Kivelson and Wu, 1986a, 1986b).

The successes of the simple noninteracting models in explaining many experimental observations suggests that the effective electron-electron interactions in these materials are indeed weak. For instance, the dimerization in $(CH)_x$ was found to have the magnitude predicted on the basis of the noninteracting SSH model, and an analysis of the Raman spectrum has shown that the Peierls relation between the gap and the electron-phonon coupling constant is well obeyed (see Sec. V). Another piece of evidence that strongly supports both the claims that the properties of conducting polymers are insensitive to the band structure far from the Fermi surface, and that the interactions are weak, comes from a comparison of the optical-absorption spectra of different materials (Kivelson and Wu, 1986a; Wu and Kivelson, 1986). In Fig. 14 we have plotted the optical-absorption coefficient $\alpha(\omega)$ normalized to its peak value $\alpha(\omega_p)$ versus frequency ω in units of the peak frequency ω_p for several conducting polymers: *trans*- and *cis*-$(CH)_x$, polythiophene, polypyrrole, and polydiacetylene. The curves in Fig. 14(a)

display a remarkable similarity among the four different conducting polymers. They all lie within about 30% of an average curve. For comparison, note that fact that samples of thermally and electrochemically isomerized *trans*-$(CH)_x$ differ by about 20% [see Fig. 14(b)]. In view of the enormous differences in the structures of these materials, the observed similarity in $\alpha(\omega)$ is remarkable.

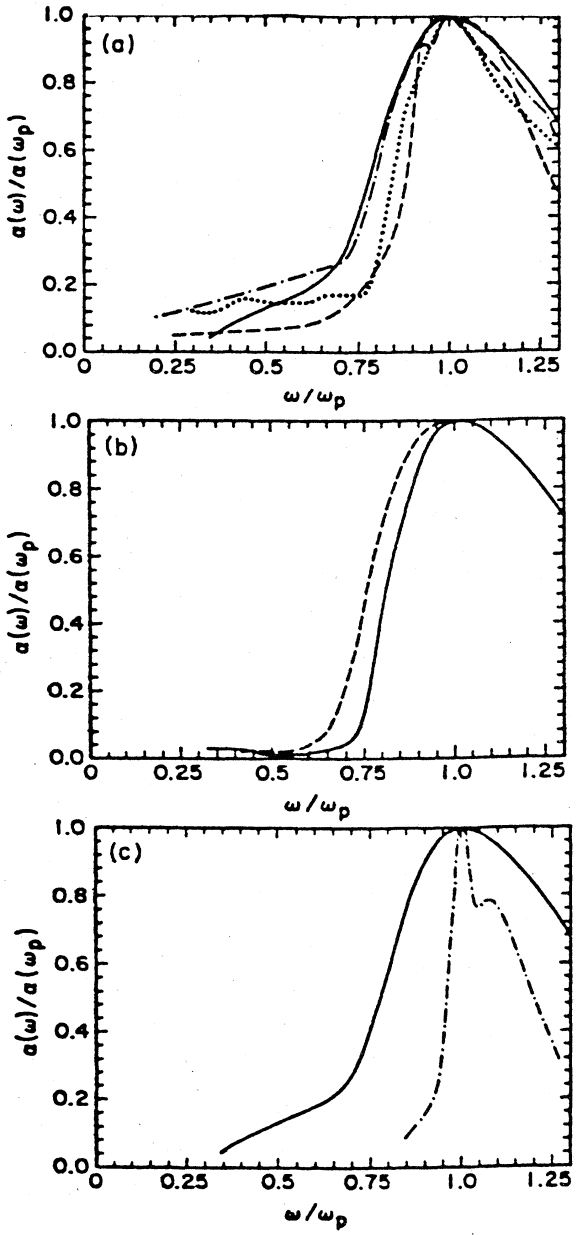

FIG. 14. Absorption spectra of selected conjugated polymers. (a) Rescaled absorption coefficients for various conducting polymers: solid line, *trans*-$(CH)_x$; dashed line, *cis*-(CH); dashed-dotted line, polythiophene; dotted line, polypyrrole. (b) Rescaled optical-absorption coefficients for thermally (solid line) and electrochemically (dashed line) isomerized *trans*-$(CH)_x$. (c) Rescaled optical-absorption coefficients for *trans*-$(CH)_x$ (solid line) and polydiacetylene (dashed line). From Kivelson and Wu (1986a, 1986b; Wu and Kivelson, 1986).

If the interactions were weak, this similarity could be readily understood, since the simple models would be accurate, and to zeroth order a single parameter, namely the gap Δ, would determine the entire spectrum. The rescaled optical absorption would thus lie on a universal curve. The striking universality demonstrated in the $\alpha(\omega)$'s thus strongly suggests that in most conducting polymers conditions (3.1) and (3.2) are fairly well satisfied. However, the fact that the optical data of polydiacetylene do not lie on this curve [see Fig. 14(c)] suggests that the interactions in this material may be quite different from those in the others; presumably they are much stronger than in $(CH)_x$. We shall show in Sec. VII that the long-ranged Coulomb interactions may contribute to this difference.

In view of the simplicity and successfulness of the noninteracting models, we shall start by ignoring explicit electron-electron interactions entirely. In Sec. VII we shall consider how the results of the noninteracting model are modified when electron-electron interactions are included. In particular, we shall show that over a large range of interaction strengths the results of the noninteracting model are not greatly modified and that the effects of interactions can be computed by straightforward perturbation theory. This justifies *a posteriori* our use of the noninteracting model.

B. The tight-binding model with electron-phonon interactions

To get a clearer idea of this model, we consider the system of *trans*-$(CH)_x$, shown in Fig. 1. As shown in Fig. 15, while each (CH) group has six degrees of freedom for nuclear translation, only the so-called dimerization coordinate u_n specifying the displacement of the nth group along the molecular-symmetry axis x is of importance at this point in our discussion. We therefore focus on a simple tight-binding Hamiltonian of the following form (the SSH model):

$$H_{\rm SSH}=H_{\pi}+H_{\pi\text{-ph}}+H_{\rm ph}\ , \tag{3.4}$$

where

$$H_{\pi}=-t_0\sum_{n,s}(c^{\dagger}_{n+1,s}c_{n,s}+c^{\dagger}_{n,s}c_{n+1,s}) \tag{3.5}$$

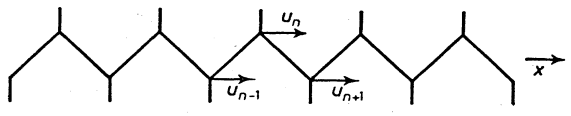

FIG. 15. Dimerization coordinate u_n defined for *trans*-$(CH)_x$.

describes the hopping of $\pi(p_z)$ electrons along the chain without spin flip. The π-electron-phonon interaction is given by

$$H_{\pi\text{-ph}}=\alpha\sum_{n,s}(u_{n+1}-u_n)(c^{\dagger}_{n+1,s}c_{n,s}+c^{\dagger}_{n,s}c_{n+1,s}) , \quad (3.6)$$

where the terms linear in u_n dominate higher-order terms for the weak-coupling systems of interest to us, i.e., the mean displacement $\langle u_n\rangle$ in the broken-symmetry phase is $\simeq 0.03$ Å compared to the lattice spacing of order 1.22 Å. Higher-order terms in $(u_{n+1}-u_n)$ lead to small renormalization effects of the α in Eq. (3.6). Finally, the phonon Hamiltonian is taken to be

$$H_{\text{ph}}=\sum p_n^2/2M+K/2\sum(u_{n+1}-u_n)^2 , \quad (3.7)$$

where M is the mass of the (CH) group and p_n is the momentum conjugate to u_n.

C. The continuum model

In the weak-coupling limit, only the electrons with energies within $\sim\Delta$ of the Fermi surface are strongly affected by the dimerization. Thus it is not at all unreasonable to make a further approximation and linearize the band structure as shown in Fig. 16. The advantage of this approximation is that the resulting theory is a continuum, or field theory (Campbell *et al.*, 1986), which is generally more amenable to analytic solution than the tight-binding model. The resulting electronic band structure (see Fig. 16) has two branches for each spin s and wave number k: a right-going branch ($j=1$) with energy $\varepsilon_k\approx\hbar v_F(k-k_F)$ and a left-going branch ($j=-1$) with $\varepsilon_k\approx-\hbar v_F(k-k_F)$. One can describe the electronic wave function by a two-component field $\psi_s(x)$, where $[\psi_s^{\dagger}(x)]_j$ creates an electron of spin s on branch j. The electron gas is coupled to the local value of the dimerization, as represented by a real scalar order-parameter field $\Delta(x)$. Since the dimerization has wave number $2k_F$, it causes scattering from one side of the Fermi surface to the other, or, in other words, it mixes the components of ψ. If we assume that these are the only important processes, we obtain (up to a possible isospin rotation) the continuum Hamiltonian [the TLM model (Takayama, Lin-Liu, and Maki, 1980)],

$$H_{\text{TLM}}=\sum\int dx\,\Psi_s^{\dagger}(x)[-i\hbar v_F\sigma_z\partial/\partial x+\Delta(x)\sigma_x]\Psi_s(x)$$
$$+\int dx\,[\dot{\Delta}(x)^2/\Omega_0^2+\Delta^2(x)]/2\pi\hbar v_F\lambda , \quad (3.8)$$

where σ_x and σ_z are the Pauli matrices in the branch index, v_F is the Fermi velocity, λ is the dimensionless electron-phonon coupling constant, Ω_0 is the bare optical-phonon frequency, and $[\dot{\Delta}/(\pi\hbar v_F\lambda\Omega_0^2)]$ is the momentum conjugate to Δ. This same Hamiltonian can be derived directly from the SSH model by expanding about the Fermi surface and keeping terms only to lowest order in (a/ξ). As we shall see, ξ is the electronic correlation length, $\xi=\hbar v_F/\Delta$. If we derive the TLM model in this way, we find that $\hbar v_F=2t_0a$, $\lambda=(4\alpha)^2/2\pi Kt_0$, $\Omega_0^2=4K/M$, and

$$\Delta(na)=(-1)^n4\alpha u_n . \quad (3.9)$$

The fermion fields have the interpretation that

$$c_{ns}=\psi_{+1,s}(na)\exp(ik_Fna)-i\psi_{-1,s}(na)\exp(-ik_Fna) .$$

There is an obvious disadvantage of the TLM model, namely that the electronic spectrum is unbounded below. The same trouble is encountered in the Dirac equation. This is not surprising, since Eq. (3.8) can be viewed as the one-dimensional Dirac Hamiltonian with a position-dependent mass $\Delta(x)$. Thus we could imagine that there exists an infinite full Dirac sea and treat the problem as a proper field theory. However, this approach in no way reflects the actual physics of $(CH)_x$, in which the spectrum is certainly bounded. Thus we shall adopt the strategy of artificially cutting off the spectrum at $E=-W/2\sim-2t_0$, where $W\gg\Delta$. We expect that no physically interesting quantity, other than an overall scale of energy, will depend on W. (To the extent that this expectation is not realized, a more realistic model is necessary.) In $(CH)_x$, many properties are well approximated by the continuum model. However, obvious exceptions exist. For instance, the order parameter $\Delta(x)$ represents the near-zone-center optical-phonon degrees of freedom. The acoustic modes, which are certainly present in the SSH model (and in the real material), are lost in the continuum limit. They appear only if terms are kept to next order in (a/ξ).

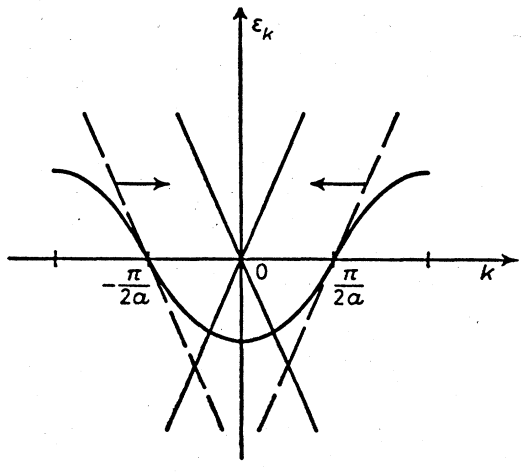

FIG. 16. The transformed energy bands entering the Takayama–Lin-Liu–Maki continuum limit of the Su, Schrieffer, and Heeger model.

IV. SOLITON EXCITATIONS: SUMMARY OF THEORETICAL RESULTS

A. Ground state

Peierl's theorem (Peierls, 1955) shows that within the mean-field approximation the ground state of the one-dimensional metal is spontaneously distorted to form a change-density wave with $\langle u_n \rangle \neq 0$. Since the strongest instability occurs for a charge-density wave of wave number $Q=2k_F=\pi/a$, we consider the adiabatic ground-state energy E_0 as a function of the mean amplitude of distortion u, where the u_n's are constrained to be

$$u_n \rightarrow \langle u_n \rangle = (-1)^n u \ . \tag{4.1}$$

By definition, E_0 is the total energy of the system, electronic plus elastic energy with $M \rightarrow \infty$. We shall see that, while quantum effects due to nuclear motion are not negligible, we can safely begin with a classical description, treating only the electrons quantum mechanically. For u_n given by Eq. (4.1), $H_{\pi\text{-ph}}$ is invariant under spatial translations $2ma$, $m=\pm 1, \pm 2, \ldots$, and H can be diagonalized in k space in the reduced zone, $-\pi/2a < k < \pi/2a$, for the two bands, valence $(-)$ and conduction $(+)$. One has

$$H(u) = -\sum_{n,s} [t_0 + (-1)^n 2\alpha u](c^{\dagger}_{n+1,s} c_{n,s} + c^{\dagger}_{n,s} c_{n+1,s}) + 2NKu^2 \tag{4.2}$$

for a chain of N monomers in a ring geometry. For $\alpha = 0$, $H(u)$ is brought to diagonal form by the usual Bloch operators,

$$c_{ks} = (N^{-1/2}) \sum_{n,s} \exp(-ikna) c_{ns} \tag{4.3}$$

in the extended zone, where $-\pi/a < k \leq \pi/a$. For $\alpha \neq 0$, it is convenient to fold the big zone into the little zone as shown in Fig. 17, with valence- and conduction-band operators defined as

$$c_{ks-} = (N^{-1/2}) \sum_{ns} \exp(-ikna) c_{ns} \ , \tag{4.4a}$$

$$c_{ks+} = -i(N^{-1/2}) \sum_{ns} \exp(-ikna)(-1)^n c_{ns} \ . \tag{4.4b}$$

In terms of these operators, one finds

$$H(u) = \sum [\varepsilon_k (c^{\dagger}_{ks+} c_{ks+} - c^{\dagger}_{ks-} c_{ks-}) + \Delta_k (c^{\dagger}_{ks+} c_{ks-} + c^{\dagger}_{ks-} c_{ks+})] + 2NKu^2 \ , \tag{4.5}$$

where the energy-gap parameter is defined by

$$\Delta_k = 4\alpha u \sin ka \ . \tag{4.6}$$

The unperturbed band energy in the reduced zone is defined as

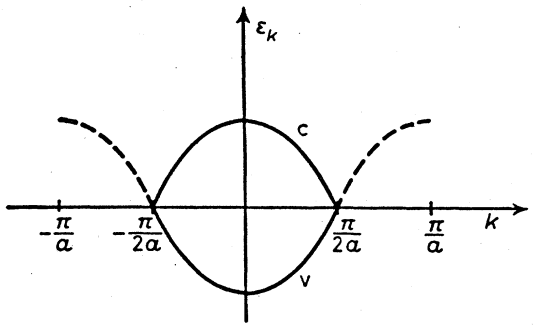

FIG. 17. The extended and reduced zone schemes.

$$\varepsilon_k = 2t_0 \cos ka, \quad (-\pi)/(2a) < k < (\pi)/(2a) \ ; \tag{4.7}$$

ε_k describes particles for $(+)$ and holes for $(-)$. Finally, H is brought to diagonal form by the transformation

$$a_{ks-} = \alpha_k c_{ks-} - \beta_k c_{ks+} \ , \tag{4.8a}$$

$$a_{ks+} = \beta_k c_{ks-} + \alpha_k c_{ks+} \ . \tag{4.8b}$$

For the a's to satisfy Fermi anticommutation relations, we must have

$$|\alpha_k|^2 + |\beta_k|^2 = 1 \ . \tag{4.9}$$

By requiring that H have no terms mixing the $(-)$ and $(+)$ operators, one finds

$$H = \sum E_k (n_{ks+} - n_{ks-}) + 2NKu^2 \ . \tag{4.10}$$

As in superconductivity theory, the quasiparticle energy is given by

$$E_k = (\varepsilon_k^2 + \Delta_k^2)^{1/2} \tag{4.11}$$

and

$$\alpha_k = [(1+\varepsilon_k/E_k)/2]^{1/2} \ ,$$
$$\beta_k = [(1-\varepsilon_k/E_k)/2]^{1/2} \operatorname{sgn}\Delta_k \ , \tag{4.12}$$
$$\alpha_k \beta_k = \Delta_k/(2E_k) \ .$$

For the half-filled band of $(CH)_x$, the ground-state energy $E_0(u)$ as a function of u is given by taking $n_{ks-}=1$ and $n_{ks+}=0$, so that, for a ring of circumference L, one has

$$E_0(u) - 2NKu^2 = -2L/\pi \int_0^{\pi/2a} E_k dk = -(4Nt_0)/\pi \times \int_0^{\pi/2} [1-(1-z^2)\sin^2 x]^{1/2} dx \ , \tag{4.13}$$

or the energy per site is

$$E_0(u)/N = -(4t_0/\pi) E(1-z^2) + 4t_0^2 z^2/2\alpha^2 \ , \tag{4.14}$$

where $E(1-z^2)$ is the complete elliptic integral of the second kind and

$$z=2\alpha u/t_0 \ . \tag{4.15}$$

Since for small z

$$E(1-z^2)\simeq 1+\tfrac{1}{2}[\ln(4/z)-\tfrac{1}{2}]z^2+\cdots \ , \tag{4.16}$$

the energy varies for small u as

$$E_0(u)/N\approx -4t_0/\pi-(2t_0/\pi)[\ln(4/z)-\tfrac{1}{2}]z^2 +Kt_0^2z^2/2\alpha^2+\cdots \ . \tag{4.17}$$

As $|z|\to 0$, the logarithmic term dominates, and E_0 has a maximum at $u=0$, consistent with the Peierls theorem. In field theory, $E_0(u)$ is analogous to the Coleman-Weinberg (Coleman and Weinberg, 1980) potential. E_0 is plotted versus u in Fig. 18 for parameters characteristic of polyacetylene (Su, Schrieffer, and Heeger, 1979, 1980). For an assumed energy gap of $2\Delta=1.4$ eV, $\alpha=4.1$ eV/Å, $K=21$ eV/Å^2, and $t_0=2.5$ eV. These parameters lead to the minimum-energy mean-field distortion $u_0\approx 0.04$ Å. The structural studies (Fincher *et al.*, 1982) and the NMR results (Yannoni and Clarke, 1983) give $u_0\approx 0.035$ Å, in good agreement with this estimate. More recent results indicate that the one-dimensional gap is somewhat larger, $2\Delta\approx 1.8$ eV, the absorption at lower energies being due to a combination of interchain interactions (3D band structure; Moses *et al.*, 1982) and dynamical fluctuations (Sethna and Kivelson, 1982; Su and Yu, 1983). Using this larger value for 2Δ and keeping $u=0.04$ Å yields somewhat different parameters: $\alpha=5.6$ eV/Å and $K=40$ eV/Å.

B. Soliton excitations

If one were to clamp u_n at the ground-state mean-field value, $(-1)^n u$, the chain would behave as a conventional semiconductor with electron and hole excitations. However, because of the twofold-degenerate ground state $E(u_0)=E(-u_0)$, the system supports nonlinear excitations, which act as moving domain walls separating regions having different ground states: A phase $(+u_0)$ and B phase $(-u_0)$. Since these walls are shape-preserving excitations, which alter the medium after they have passed a given point, they act as topological solitons. To determine the shape of the soliton, it is convenient to introduce the staggered displacement field

$$\varphi_n=(-1)^n u_n \ , \tag{4.18}$$

analogous to the staggered magnetization in antiferromagnets, so that

$$\varphi_n=u_0, \quad A \text{ phase}, \quad \varphi_n=-u_0, \quad B \text{ phase} \ . \tag{4.19}$$

For a long chain, a soliton (antisoliton) corresponds to a phonon field configuration that approaches the B phase for $N\to-\infty$, approaches the A phase as $N\to+\infty$, and minimizes the total energy; such a configuration is shown in Fig. 19. The soliton width is the result of the competition of two effects. If φ_n suddenly changes from $-u_0$ to u_0, say at $n=0$, the electronic energy will be quite large due to the uncertainty principle. Alternatively, if φ_n changes very slowly from $-u_0$ to u_0, there will be a large region surrounding $n=0$ where the condensation energy per site is greatly reduced, again raising the energy. Thus there is a preferred width ξ of the soliton that minimizes the total energy. Numerical calculations (Su, Schrieffer, and Heeger, 1979, 1980) show that the form of φ that minimizes the adiabatic energy with these boundary conditions is

$$\varphi_n\simeq u_0\tanh[(n-n_0)a/\xi] \ , \tag{4.20}$$

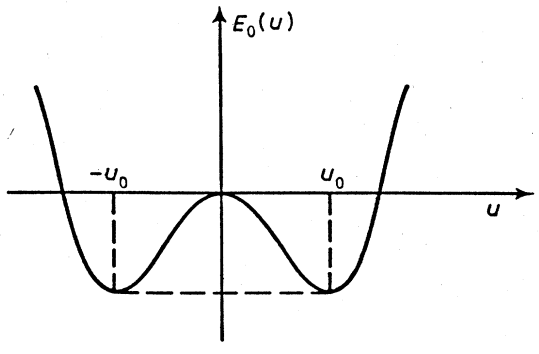

FIG. 18. The total energy (electronic plus lattice distortion) as a function of u. Note the double minimum associated with spontaneous symmetry breaking and the twofold-degenerate ground state.

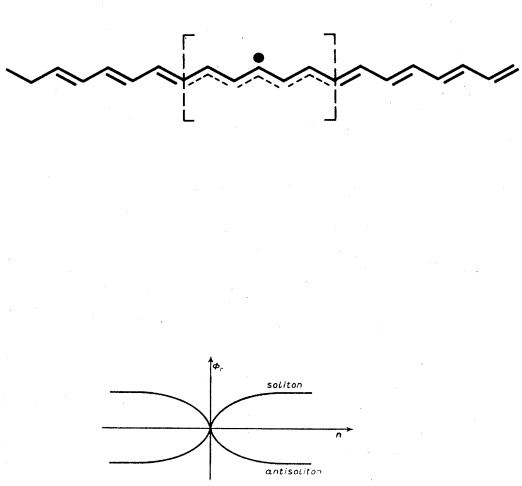

FIG. 19. Solitons (or bond-alternation domain walls in polyacetylene): schematic form of a neutral soliton on a *trans*-$(CH)_x$ chain; (b) the order parameter for a soliton and an antisoliton.

where $\xi \simeq 7a$ for the SSH set of parameters, and n_0 is the location of the center of the soliton. With the above parameters, the energy to create a soliton at rest is $E_s \simeq 0.42$ eV, which is less than one-half the single-particle gap Δ. Since the chemical potential is midgap for the undoped material, this result shows that a soliton is less costly to create than either an electron or a hole. It is for this reason that solitons are spontaneously generated when electrons and/or holes are injected by doping, by photoexcitation, or by thermal generation.

The electronic spectrum in the presence of a soliton is of particular interest. If we fix φ_n to be of the form given by Eq. (4.20), the electron spectrum is strongly altered in the vicinity of the soliton. In particular, a state ψ_0 of zero energy appears that is centered at the soliton and falls off on the scale of ξ. This can be seen by expanding ψ_0 in site basis states,

$$|\psi_0\rangle = \sum_n \psi_0(n)|n\rangle , \tag{4.21}$$

and requiring

$$\sum_m \langle n|H_{\rm el}|m\rangle \psi_0(m) = E_0 \psi_0(n) . \tag{4.22}$$

The matrix elements of $H_{\rm el}$ are

$$\langle n|H_{\rm el}|m\rangle = -[t_0 + (-1)^n \alpha(\varphi_n + \varphi_{n+1})] , \quad m = n+1 , \tag{4.23a}$$

$$\langle n|H_{\rm el}|m\rangle = -[t_0 - (-1)^n \alpha(\varphi_n + \varphi_{n+1})] , \quad m = n-1 , \tag{4.23b}$$

$$\langle n|H_{\rm el}|m\rangle = 0 \quad \text{otherwise} . \tag{4.23c}$$

Since $H_{\rm el}$ connects only nearest-neighbor states, the transformation

$$|n\rangle \rightarrow (-1)^n |n\rangle \tag{4.24}$$

sends $H_{\rm el} \rightarrow -H_{\rm el}$. However, the eigenvalue spectrum cannot be changed by a unitary transformation, so the spectrum of $H_{\rm el}$ is symmetric about $E=0$, and $H_{\rm el}$ exhibits particle-hole symmetry or charge-conjugation symmetry.

If there is a solution of $E_0 = 0$, then the $\psi_0(n)$ satisfy

$$\sum \langle n|H_{\rm el}|m\rangle \psi_0(n) = 0 \tag{4.25}$$

or

$$\psi_0(n+1) = -(\langle n|H_{\rm el}|n-1\rangle / \langle n|H_{\rm el}|n+1\rangle) \times \psi_0(n-1) \equiv -R_n \psi_0(n-1) . \tag{4.26}$$

As $n \rightarrow \infty$,

$$R_n \rightarrow [1-(-1)^n 2\alpha\varphi_n/t_0]/[1+(-1)^n 2\alpha\varphi_n/t_0] . \tag{4.27}$$

For a bounded solution, R must be <1 as $n \rightarrow \infty$ and >1 as $n \rightarrow -\infty$. This occurs if the $\psi_0(n)$ for odd n are nonzero, since $\varphi_n \rightarrow \pm u$ as $n \rightarrow \pm\infty$. The function for even n is unbounded and is not a solution for the soliton. However, if we interchange the A and B phases in Eq. (4.26), then

$$\varphi_n = -u_0 \tanh(na/\xi) \tag{4.28}$$

represents an antisoliton, and the even-n solution exists with $E_0 = 0$, but the odd-n solution is unbounded. Therefore, for each widely spaced soliton or antisoliton, there exists a normalized single-electron state in the gap center which can accommodate 0, 1, or 2 electrons due to spin degeneracy. This result is the analog of the Jackiw-Rebbi (Jackiw and Rebbi, 1976) zero mode for a spinless Dirac field coupled to a φ^4 kink. Indeed, the Atiyah-Singer (Atiyah, Patodi, and Singer, 1975) index theorem implies a state at $E_0 = 0$ for any shape of φ_n so long as φ_n satisfies the correct asymptotic form. The soliton shape is insensitive to the occupancy of ψ_0 within the above model. The electronic density of states $\rho(E)$, with and without a soliton present, is shown in Fig. 20.

As discussed below, $\psi_0(n)$ vanishes on even- (odd-) n sites for a soliton (antisoliton) regardless of the location of the center of the soliton. This property has been inferred (Heeger and Schrieffer, 1983) from electron-nuclear double resonance (ENDOR) experiments (see Sec. V.A) and gives strong added support for the model.

C. Continuum limit

The same soliton excitations can be studied in the TLM model. For given $\Delta(x)$, the $u \equiv \psi_{+1}$ and $v \equiv \psi_{-1}$ have c-number solutions $u_{m,s}(x)$ and $v_{m,s}(x)$, which correspond to the expansion coefficients for creating or destroying a quasiparticle. These amplitudes satisfy equations of the Bogoliubov–de Gennes form,

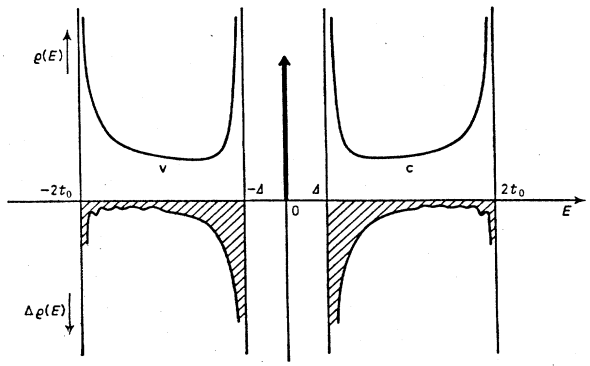

FIG. 20. Density of states $\rho(E)$ for pure *trans*-$(CH)_x$ and the change of density of states $\Delta\rho(E)$ when a soliton is created. The valence and conduction bands are each depleted by one-half of a state appearing at midgap (from Su, Schrieffer, and Heeger, 1980).

$$-iv_F\partial u_{ms}(x)/\partial x+\Delta(x)v_{ms}(x)=E_m u_{ms}(x)\ ,$$
$$iv_F\partial v_{ms}(x)/\partial x+\Delta(x)u_{ms}(x)=E_m v_{ms}(x)\ . \tag{4.29}$$

The variation of the system energy with respect to $\Delta(x)$ gives the self-consistency condition determining the stable mean-field states of the system,

$$\Delta(x)=-(4\alpha^2 a/K)\sum_{m,s}[u_{ms}(x)v_{ms}(x)+v_{ms}(x)u_{ms}(x)]\ . \tag{4.30}$$

The sum (over m,s) extends over occupied states. For the perfectly dimerized lattice $\Delta(x)=\Delta$, the electronic eigenstates correspond to a free Dirac spectrum with mass Δ:

$$\Delta=We^{-1/2\lambda}\ . \tag{4.31}$$

The self-consistency condition is the analog of the BCS gap equation determining Δ. Remarkably, the coupled nonlinear equations (4.29) and (4.30) can also be solved in closed form for a soliton with $\Delta(x)=\Delta\tanh(x/\xi)$, since the problem is analogous to the nonlinear Schrödinger equation. One finds that the energy to form a soliton at rest is

$$E_s=(2/\pi)\Delta\simeq 0.63\Delta\ . \tag{4.32}$$

This result is in reasonably good agreement with the SSH value, 0.61 Δ.

D. Soliton quantum numbers

A fascinating feature of the soliton solution is that, per spin direction, the total number of electrons or states in the filled valence band in the vicinity of the soliton decreases by precisely one-half when the soliton is formed. Of course, it is easily shown that the total number of states in the valence band must remain an integer in a large but finite ring. How is it possible to solve this apparent paradox?

Since $\varphi(x)$ must be single valued as we move around the ring, it is clear that a soliton S, $u_0\rightarrow u_0$, and an antisoliton, $\bar{S}$, $u_0\rightarrow u_0$, must be simultaneously created. However, one-half of a state is missing from the valence band in the vicinity of each excitation, S and $\bar{S}$, so that there is a total valence-band depletion of one state. From the charge-conjugation or particle-hole symmetry of $H_{\rm el}$ discussed above, it follows that a total of one state is also missing from the conduction band. These two states combine to form a pair of states on opposite sides of $E=0$, which approach midgap as S and $\bar{S}$ separate to distances d large compared to ξ. Asymptotically, one can view the situation as the mixing of a state centered on S and a state on $\bar{S}$, due to an exponentially weak overlap, so that the two become independent as $d\rightarrow\infty$. The actual mechanism by which this occurs is that the soliton causes a phase shift $\eta_k(x)$ of each of the valence-band scattering states ψ_k, which leads to a total local depletion near the soliton of one-half a state for each spin orientation near the soliton. The same happens near $\bar{S}$.

A more formal way to prove this result is to note that in the lattice model there is a sum rule satisfied by the local density of states $\rho_{nn}(E)$,

$$\int_{-\infty}^{\infty}\rho_{nn}(E)dE=1/\pi\int_{-\infty}^{\infty}|\,\mathrm{Im}G_{nn}(E)\,|\,DE\ , \tag{4.33}$$

where the one-electron Green's function is defined by

$$G_{nn}(E)=-i\int_{-\infty}^{\infty}\exp(iEt)\langle\,|\,Tc_{ns}^{\dagger}(t)c_{ns}(0)\rangle dt\ . \tag{4.34}$$

It follows that the change of $\rho_{nn}(E)$ due to the presence of a soliton is such that

$$\int_{-\infty}^{\infty}\rho_{nn}(E)dE=2\int_{0+}^{\infty}\Delta\rho_{nn}(E)dE+|\,\psi_0(n)\,|^2=0\ , \tag{4.35}$$

where we have used the invariance of H under charge conjugation and the fact that there is a state at $E_0=0$ with amplitude $\psi_0(n)$. Equation (4.33) shows that the missing electron number per spin is

$$\sum\int_{-\infty}^{\infty}\Delta\rho_{nn}(E)dE=-\tfrac{1}{2}\sum|\,\psi_0(n)\,|^2=-\tfrac{1}{2}\ . \tag{4.36}$$

Finally, for two spin states, the total valence-band electron deficit per soliton is -1. This type of argument was first used by Jackiw and Rebbi in their study of fermion fractionalization by kinks in relativistic field-theory models. In Fig. 21, the gap center state of a continuum-limit soliton centered on site n_0,

$$\psi_0(n)=(1/\xi)^{1/2}\mathrm{sech}[(n-n_0)a/\xi]\cos\pi n/2\ , \tag{4.37}$$

is plotted. Notice that $\psi_0(n)$ is zero on odd-n sites for an antisoliton, a property that is independent of the shape or the position of the soliton. Similarly, $\psi_0(n)$, which is given by Eq. (43.6) with cos→sin, vanishes on even sites for a soliton independent of its shape and location.

The charge and spin states of the soliton which follow from the above band-theoretic discussion are shown in

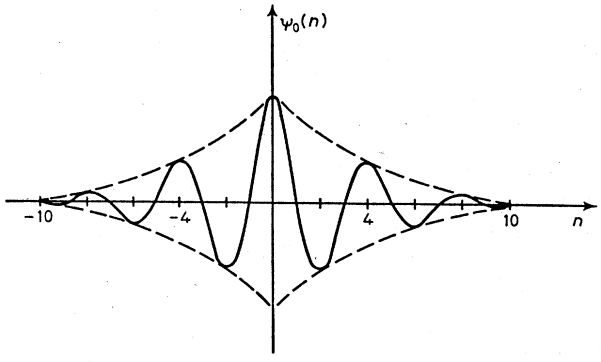

FIG. 21. The gap state ψ_0 plotted as a function of distance. Note that ψ_0 vanishes on the even (odd) sites for a soliton (antisoliton), regardless of the locations of these excitations.

Fig. 22 along with the localized chemical-bond representation. The neutral spin-$\frac{1}{2}$ soliton is analogous to a neutral free radical, and the charge species $S^{\pm}$ may be viewed as spinless "ions." However, the solitons move freely unless pinned, in contrast to the chemical analogs. From the physics point of view, an important fact is that the soliton has reverse spin-charge relations from conventional electron and hole carriers, i.e., charged solitons $S^{\pm}$ are spinless, while electrons and holes, of course, have spin $\frac{1}{2}$. Moreover, neutral solitons S^0 have spin $\frac{1}{2}$, in agreement with the magnetic experiments discussed in Sec. V.

The above discussion shows that a neutral soliton is electrically neutral on each site n, as follows from Eq. (4.34). Thus the charge and spin form factors of $S^{\pm}$ and S^0 are those of the gap center state,

$$\rho(n)|_{s^{\pm}}=\pm e\,|\psi_0(n)|^2\,, \tag{4.38}$$

$$S^z(n)|_{s^0}=\pm 1/2\,|\psi_0(n)|^2\,. \tag{4.39}$$

Another important property of a soliton is its mass M_s. If the soliton is slowly translating, φ_n is given by

$$\varphi(n,t)=u_0\tanh[(na-v_s t)/\xi]\,. \tag{4.40}$$

Then the increase of energy is given by

$$1/2M_s v_s^2=1/2M_s\sum_n(d\varphi_n/dt)^2=1/2M_s(u_0/\xi)^2 v_s^2\,, \tag{4.41a}$$

$$M_s=(4a/3\xi)(u_0/a)^2 M\approx 6m_e \tag{4.41b}$$

for the SSH parameters, with m_e the electron mass. The smallness of M_s arises from the width of the soliton ($2\xi\gg a$) and the smallness of the nuclear displacements (u_0 compared to the lattice spacing a), so that the nuclei gain little kinetic energy as a soliton passes. The small value of M_s alerts us to the possible importance of quantum effects in this system.

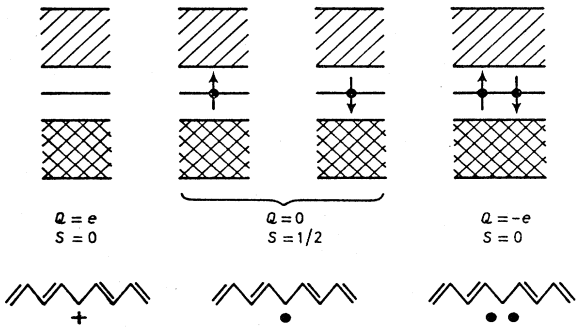

FIG. 22. Electronic structure leading to various charge and spin states of a soliton. The localized chemical shorthand for these delocalized structures is sketched.

E. Polaron excitations

While kinks or topological solitons are stable excitations of a *trans*-$(CH)_x$ chain, it was observed in early molecular dynamics studies (Su and Schrieffer, 1980) that the injection of a single electron or a single hole leads to the formation of a polaron. This nontopological excitation corresponds to the order parameter $\varphi_P(x)$ with a dip at its center but not changing sign [in contrast with the order parameter $\phi_S(x)$ of a kink or soliton], as shown in Fig. 23. Thus one has the symmetries

$$\varphi_P(-[x,x_0])=\varphi_P(x-x_0)\,, \tag{4.42a}$$

$$\varphi_S(-[x-x_0])=-\varphi_S(x-x_0)\,. \tag{4.42b}$$

Polarons are well known in polar insulators and in semiconducting materials (Ziman, 1960), acting as the quasiparticles arising from phonon dressing of an electron or a hole.

Independent of the molecular dynamics studies (Su and Schrieffer, 1980), polaron or baglike solutions (Brazovskii and Kirova, 1981; Campbell and Bishop, 1981, 1982) were discovered using the relation of the mean-field approximation to the continuum model and the Gross-Neveu (Gross and Neveu, 1974) model of quantum field theory. In the continuum limit, the order parameter $\varphi_P(x)$ describing a polaron centered at the origin is given by

$$\varphi_P(x)=u_0+(u_0/2^{1/2})\{\tanh[(x-x_0)/\sqrt{2}\xi]-\tanh[(x+x_0)/\sqrt{2}\xi]\}\,, \tag{4.43}$$

where $x_0=(\xi/\sqrt{2})\ln(1+\sqrt{2})\approx 0.623\xi$. Since a soliton located at y_0 is described by

$$\phi_S(x)=u_0\tanh(x-y_0)/\xi\,, \tag{4.44}$$

one can roughly describe the electron or hole polaron as a bound soliton-antisoliton pair (one charged and one neutral), with centers separated by $2x_0=\xi$. The factor $2^{-1/2}$ in Eq. (4.43) implies that, due to the interaction be-

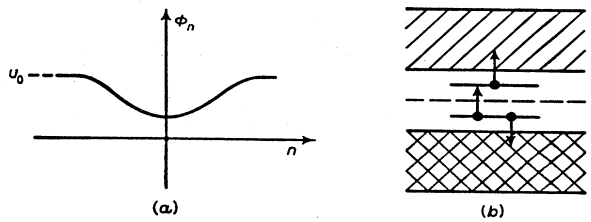

FIG. 23. Order parameter and band diagram for a polaron: the staggered order parameter ϕ_n as a function of n for a polaron; (b) two states symmetrically split off from the band edges for a polaron. An electron is missing from the upper state for an electron polaron, and only a single electron occupies the lower state for a hole polaron.

tween two solitons, their width is somewhat greater than at infinite separation.

While the soliton has a single bound state associated with it, the polaron has two bound states split off from the continuum, namely, a pair of states having energies

$$E_P = \pm\Delta/2^{1/2} , \tag{4.45}$$

as shown in Fig. 23. These two states are symmetric with respect to the gap center and can be thought of as the bonding and antibonding combinations of the two midgap states associated with the bound soliton-antisoliton pair that makes up the polaron; in effect, the lower state is split off from the top of the valence band and the upper state is split off from the bottom of the conduction band. Each of these states can accommodate one electron of each spin orientation. Starting from the charge-neutral case in which the lower state is filled, $n_- = 2$, and the upper state is empty, $n_+ = 0$, the conventional polarons are as follows:

electron polaron	$n_- = 2,\ n_+ = 1$
hole polaron	$n_- = 1,\ n_+ = 0$

The spin of the charge-neutral case is zero, since all states, both continuum and localized, are doubly filled. Therefore the electron and hole polarons each carry spin $\frac{1}{2}$, and the spin-charge relation is the conventional one.

Total energy calculations show that only the electron and the hole polarons are stable. If one adds, for example, a second electron to an electron polaron, the resulting "bipolaron" lowers its energy by increasing the soliton-soliton spacing $2x_0$ until a free kink-antikink pair evolves at large separation. Thus, on doping, the first injected electron forms a polaron; the second injected electron breaks apart the polaron to form two negatively charged kinks. Note, however, that when the precise ground-state degeneracy of the polymer is lifted, the resulting confinement of the solitons leads to stable bipolarons (see Sec. VI).

Since a polaron is stable only in the absence of another polaron, the role played by a polaron in *trans*-polyacetylene is rather limited. However, kinks can exist only in systems with exact ground-state degeneracy. Since most of the conducting polymers possess only near degeneracy, polarons and bipolarons take over the major role played by the kinks in such cases. In this sense, polarons and bipolarons are expected to be more generic.

F. Phonons and soliton-induced infrared-active vibrational modes

1. General formalism

We next examine the dynamics of small-amplitude excitations. We consider the situation in which the lattice configuration is nearly equal to one of the static lattice configurations that are local minima of the effective potential discussed in previous sections. We shall denote a static configuration by $\{\bar{u}_n\}$ [or by $\bar{\Delta}(x)$ for the continuum model]; an arbitrary configuration can be expressed as

$$u_n(t) = \bar{u}_n + \eta(n,t) \tag{4.46}$$

and, since $\eta(n,t)$ is assumed to be small, we can expand the Lagrangian to second order. Within the adiabatic approximation, the resulting linearized equations of motion are

$$d^2u_n/dt^2 = \tfrac{1}{2}\Omega_0^2[(u_{n+1}+u_{n-1}-2u_n) - D_{nm}u_m] , \tag{4.47}$$

where $\Omega_0 = 2\sqrt{K/M}$ is the zone-center optical-phonon frequency in the absence of electron-phonon coupling, and the dynamical matrix is

$$D_{nm} = \partial^2 E_{\rm el}(\{u\})/\partial u_n \partial u_m , \tag{4.48}$$

evaluated at $\{u\} = \{\bar{u}\}$, where $E_{\rm el}$ is the electronic energy; thus D_{nm} is a response function of the π-electron system. The normal modes and eigenfrequencies of the lattice motion,

$$\eta(n,t) = \eta_a(n)\cos(\omega_a t + \phi) , \tag{4.49}$$

are obtained by diagonalizing the dynamical matrix (this is nothing more than the standard method for calculating the phonon frequencies). The novel feature is that we include in Eq. (4.46) the possibility that the state we expand about, $\{\bar{u}\}$, is not the uniformly dimerized ground state. In Sec. IV.D.2 we shall apply the results we derive here to the case of the uniformly dimerized lattice, $\bar{u}_n = u_0(-1)^n$. In Sec. IV.D.3 we shall consider the phonon spectrum in the presence of a soliton.

Equations (4.45)–(4.48) are written in terms of the discrete model. Exactly the same considerations can be applied to the continuum model. For example, the linearized equations of motion are

$$[(\Omega_0^{-2})d^2/dt^2 + 1]\eta(x,t) = -\lambda\pi\hbar v_F \int dy\, D(x,y)\eta(y,t) , \tag{4.50}$$

where $\eta(x,t)$ plays the same role as $\eta(n,t)$, and

$$D(x,y) = \delta^2 E_{\rm el}(\Delta)/\delta\Delta(x)\delta\Delta(y) , \tag{4.51}$$

evaluated at $\Delta(x) = \bar{\Delta}(x)$. Once $D(x,y)$ is known, this equation can be solved to obtain the normal-mode frequencies $\omega(k)$ and the eigenvectors $\eta_k(x)$.

If we consider the continuum model as a field theory, then in the standard fashion the modes of Eq. (4.50) describe the particle excitations of the theory. The effect of the coupling to the π electrons described in Eq. (4.50) is simply the one-loop correction to the phonon energies. We shall discuss interchangeably results for the discrete and continuum models except where those results differ qualitatively or where some ambiguity arises.

Even in the perfectly dimerized case, evaluating the

dynamical matrix is somewhat complicated, since the variation of the electronic energy with respect to lattice displacement makes a significant contribution to the results (residual phonon softening from the Peierls instability). Because there is a gap in the electronic spectrum, this contribution is exponentially localized, $\partial^2 E_{\rm el}/\partial u_n \partial u_m \sim \exp(-|n-m|a/\xi)$, at large $|n-m|$. However, the decay length is of order ξ, so that the range of the dynamical matrix is the same as the interesting phonon wavelengths. Thus it is not justified to make a gradient expansion of the effective potential to obtain a Landau-Ginzburg-type energy functional. (The fact that there are strong similarities in the behavior of the φ^4 model field theory and the polyacetylene models must be viewed as a result of the common symmetries of the models and not of a deeper equivalence.)

Before proceeding to describe the solutions to these equations in the next two sections, we generalize to include multiple phonon branches. The actual C_{2h} symmetry of the polyacetylene does not admit an exact separation of the modes into transverse and longitudinal normal modes. There is no single physical phonon mode that corresponds to the single mode in the model. Thus, to permit direct comparison with experiment, one must include the four in-plane phonon branches of the carbon and hydrogen which correspond to the four branches at the Brillouin zone center of the undimerized polymer (one of these, the C-H stretch mode, is weakly coupled to the π electron and hence can be ignored).

The first calculations of this sort were carried out numerically (Mele and Rice, 1980b) by treating the electronic degrees of freedom in the SSH model. Similar results can be obtained (Horovitz, 1982) largely analytically for a multibranch version of the TLM model; the electrons are treated as in the TLM model, but the lattice order parameter $\Delta(x)$ is taken phenomenologically to be a sum of the contributions of N different phonon branches,

$$H=\sum\int dx\,\psi_s^\dagger(x)[-i\hbar v_F(\partial/\partial x)\sigma_z+\Delta(x)\sigma_x]\psi_s(x) + \sum(1/2\pi\hbar v_F\lambda_j)\int dx\{[\Delta_j(x)]^2+(\dot{\Delta}_j)^2/\Omega_j^2\}\ , \tag{4.52}$$

where

$$\Delta(x)=\sum_{j=1}^{N}\Delta_j(x)\ ,$$

λ_j is the dimensionless electron-phonon coupling constant for mode j, Ω_j is the nth bare optical-phonon frequency, and N is the number of phonon branches (we shall take $N=3$). As in the one-branch case (SSH$\rightarrow$TLM), this model can be derived as the continuum limit of a multibranch discrete model.

The static properties of the multibranch model are exactly the same as those of the TLM model. To see this, we derive the self-consistency condition for this model from the equation $\delta\langle H\rangle/\delta\Delta_j(x)=0$ for all n; hence

$$\Delta_j(x)=\pi\hbar v_F\lambda_j\langle\psi_s^+(x)\sigma_x\psi_s(x)\rangle\ . \tag{4.53}$$

Since $\langle\psi^+\sigma_x\psi\rangle$ depends only on $\Delta(x)$, Eq. (4.53) can be trivially summed over j to obtain the same self-consistency as in the TLM model, Eq. (4.31) above, where

$$\lambda=\sum\lambda_j$$

is the total electron-phonon coupling constant and $\Delta_j(x)=(\lambda_j/\lambda)\Delta(x)$.

The dynamics of the multibranch model are related to those of the TLM model but are somewhat richer. By using the spectral representation of $D(x,y)$ for the TLM model, it is easy to show that eigenfrequencies $\omega_j(k)$ of the multibranch model are related to the eigenfrequencies $\omega(k)$ of the TLM model as solutions to the equation

$$G[\omega_j(k)]=[\omega^2(k)/\Omega_0^2-1]^{-1}\ , \tag{4.54a}$$

where

$$G(\omega)=\sum_j(\lambda_j/\lambda)[(\Omega_j^2)/(\omega^2-\Omega_j^2)]\ . \tag{4.54b}$$

Note that the right-hand side of Eq. (4.54a) is independent of Ω_0, since $\omega(k)$ is proportional to Ω_0. From this it follows that to each phonon mode in the TLM model there are N corresponding modes of the multibranch model.

In the next two sections, we shall discuss the phonon spectrum of the perfectly dimerized model (Sec. IV.F.2) and the spectrum in the presence of a soliton or polaron (Sec. IV.F.3). In each case, we shall first do this for the one-phonon-branch model and then generalize the results to the multibranch model.

2. Phonons in the perfectly dimerized lattice

For the perfectly dimerized lattice, the phonon normal modes are Bloch waves with frequency determined by the Fourier transform of the response function D_{nm}. Figure 24 shows the results of such a calculation (Nakahara and Maki, 1986), in which D_{nm} has been approximated by its value for the continuum model.

Because there are two atoms per unit cell, there are two branches to the phonon spectrum: an acoustic branch and an optical branch. Because the acoustic phonons couple to the π electrons only in higher order in (a/ξ), the acoustic spectrum is little affected by the electron-phonon coupling. Indeed, in the long-wavelength limit, one finds [from Eq. (4.54)] that the dispersion relation for the acoustic phonons is

$$\omega_a(k)=c_a k\ , \tag{4.55a}$$

where the speed of sound is given by

$$c_a=\tfrac{1}{2}a\Omega_0(1-2\lambda)^{1/2} \tag{4.55b}$$

and $\Omega_0=(4K/M)^{1/2}$. For $\lambda\sim 0.14$, the speed of sound is decreased by 20% as a result of the electron-phonon cou-

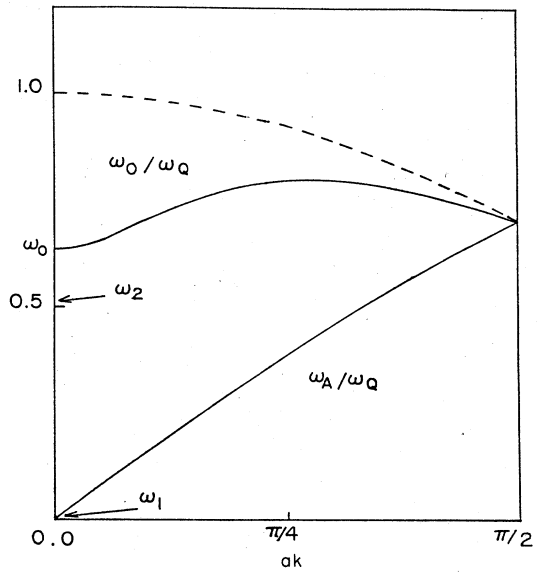

FIG. 24. Phonon spectrum of the continuum model of *trans*-polyacetylene with (dashed curve) and without (solid curve) the electron-phonon coupling taken into account (from Nakahara and Maki, 1986).

pling. On the other hand, the optical branch is expected to be strongly affected by the electron-phonon coupling so long as $\xi k \ll 1$. In this limit

$$\omega(k)^2=\omega_0^2+(c_0k)^2 \ , \tag{4.56}$$

where the zone-center optical-phonon frequency is proportional to the square root of the electron-phonon coupling constant

$$\omega_0=\Omega_0(2\lambda)^{1/2} \ , \tag{4.57}$$

and c_0 is

$$c_0=6^{-1/2}(\omega_0\xi) \ . \tag{4.58}$$

At first glance, the results in Eq. (4.57) seem very strange. In the limit of weak electron-phonon coupling, one might expect the effect of the electron-phonon coupling on the phonon spectrum to be small. Instead, we find that it is seemingly large. Indeed, it appears that the zone-center optical-phonon frequency tends to zero as λ tends to zero. This is as it should be. The zone-center phonon merely probes the curvature of the adiabatic potential shown in Fig. 18 near its minimum. The magnitude of the dimerization tends to zero as $\lambda \to 0$ and with it the curvature. However, note that for the same reason ξ gets exponentially large as λ gets small. Thus the region in k space that is strongly affected by the coupling ($|k\xi|<1$) is exponentially small. Moreover, since the depth of the adiabatic potential well gets to be quite small, anharmonic terms become important for $|k\xi|<1$ and $\lambda \ll 1$.

Finally, we note that the presence of structure in the phonon spectrum for $|k\xi| \sim 1$ is a reflection of the range of the interactions. This structure would be lost in a gradient expansion of the energy unless very-high-order terms were retained.

3. Phonons in the presence of a charged defect

The presence of a charged, localized structural defect such as a soliton, polaron, or bipolaron strongly modifies the local electronic states and the phonon spectrum. Treating the small-amplitude displacements of the lattice in the presence of a defect that spontaneously breaks the translational symmetry of the system is somewhat subtle. The problem involves the proper treatment of the translation modes (both uniform and nonuniform) of the soliton.

To be concrete, let us consider the small-amplitude phonon excitations of the TLM model in the presence of a soliton centered at position x_0,

$$\bar{\Delta}(x,x_0)=\Delta \tanh[(x-x_0)/\xi] \ . \tag{4.59}$$

Since the model is translationally invariant and the soliton breaks the translational symmetry, there must necessarily be a zero-frequency phonon mode, the Goldstone mode, associated with the broken symmetry. This is the soliton translation mode. The lowest-energy mode, $\eta_0(x,t)$, is thus proportional to the derivative of the soliton solution, $\bar{\Delta}(x,x_0)$, with respect to x_0,

$$\eta_0(x)=(\Delta/\xi)\mathrm{sech}^2[(x-x_0)/\xi] \ . \tag{4.60}$$

To see this, note that for small-amplitude A_0

$$\bar{\Delta}(x,x_0)+A_0\eta_0(x)=\bar{\Delta}(x,x_0+A_0)+O(A_0^2) \ . \tag{4.61}$$

This confirms that, for small amplitude A_0, $\eta_0(x)$ is the translational mode. Since the energy must be independent of x_0, this also implies that the energy of the mode is zero.

Because the soliton can freely translate, the amplitude of the Goldstone mode does not remain small. In order to treat the translational mode properly, one must promote the soliton position x_0 to the role of a dynamical variable, the collective coordinate $x_0(t)$ describing the position of the soliton at time t. Then $x_0(t)$ is determined from the condition that the amplitude of the Goldstone mode be zero at all times (Gervais and Sakita, 1975; Krumhansl and Schrieffer, 1975; Tomboulis, 1975; Wada and Schrieffer, 1978). The remaining normal modes of the system are defined relative to the field configuration corresponding to the soliton's instantaneous position. Note that the constraint that the amplitude of the Goldstone mode be zero eliminates one-phonon modes from the system and thus ensures that the total number of degrees of freedom is conserved. We return to this point in Sec. VIII.B, where the soliton diffusion constant is derived.

The remaining modes of the system are separated from

the Goldstone mode by a finite gap. They fall into two possible types. First, there is the possibility of a finite-frequency localized mode. For instance, in φ^4 field theory (Krumhansl and Schrieffer, 1975), there is a shape mode involving oscillations of the soliton width, which has frequency $\omega^2=\frac{3}{4}\omega_0^2$; such a mode exists in the TLM model as well, with similar frequency (Hicks and Blaisdell, 1985; Nakahara and Maki, 1986). This eigenmode is odd about the soliton center. It involves oscillations of the soliton width and, hence, is approximately proportional to the derivative of the soliton shape with respect to its width,

$$\eta_1(x)\approx(\Delta/\xi)[(x-x_0)/\xi]\mathrm{sech}^2[(x-x_0)/\xi] \ . \qquad (4.62)$$

Recently, a third very weakly bound mode (infrared-active) with frequency ω just below ω_0 has been predicted (Ito *et al.*, 1984; Ito and Ono, 1985). This mode has also been shown to be present in the SSH model (Sun *et al.*, 1985; Chao and Wang, 1987).

Second, there are the continuum optical modes which start at frequency ω_0. Because the soliton is a localized perturbation, the continuum density of states is only locally perturbed.

Finally, we go beyond the harmonic approximation to treat the translational motion of the soliton. Although the potential energy is independent of x_0, there is nonetheless kinetic energy associated with the soliton motion and hence a kinetic effective mass, $M\sim 6m_e$, computed previously [Su, Schrieffer, and Heeger, 1979, 1980; see Eq. (4.41)]. Notice that the model is not Lorentz invariant, and this mass is not related to the soliton creation energy. The effective mass is defined to be the coefficient of $\frac{1}{2}v^2$ in the soliton kinetic energy, where v is the soliton velocity.

To get a feeling for the implications of this light mass, we note that the equipartition theorem implies that the thermal velocity of the soliton at temperature T is $v\approx 4\times 10^5 T^{1/2}$ cm/s, where T is in degrees Kelvin. At $T=10$ K or above, the soliton velocity is of order the speed of sound, at which point we expect higher-order terms in v/c_0 to complicate the soliton dynamics.

Let us return now to a consideration of the possible differences between the discrete and continuum models in greater detail. The discrete model does not have translational symmetry, and so we expect that all the eigenmodes of the dynamical matrix have finite frequency (Mele and Rice, 1980a). This is an unphysical result. The soliton width is much larger than a lattice constant, $\xi/a\approx 7$, and hence the barrier height to soliton motion is less than 0.002 eV. Thus, within the harmonic approximation implicit in the small-vibration analysis, the lowest phonon mode consists of the translational mode of the soliton pinned by the lattice-discreteness potential. However, an estimate of the zero-point motion of a particle with effective mass $M_s\approx 6m_e$ moving in a quadratic potential with curvature (Su, Schrieffer, and Heeger, 1979, 1980) 0.002 eV/a^2 reveals that $(\Delta x)^2\approx(5a)^2$, i.e., the zero-point motion washes out any trace of the lattice discreteness. We conclude that even at temperatures low compared to the barrier height the soliton is not bound. The physically appropriate dynamical matrix to use in calculations of the phonon spectrum is obtained by averaging over soliton positions in a unit cell. The resulting phonon spectrum is expected to be similar to the continuum model spectrum.

The obvious experimental probe of the soliton-induced changes in the phonon spectrum is infrared (ir) spectroscopy (see Sec. V for a discussion of experimental results). In order to compare theory with experiment, it is necessary to consider the multiband model in which there are three modes (Mele and Rice, 1980a) corresponding to each of the three bound modes in the TLM model. The three modes corresponding to the translation mode are called T_0, T_1, and T_3. Goldstone's theorem implies that one of these modes (T_0) is still a zero-frequency mode, the true translation mode of the soliton. The other two modes occur at finite frequency. For a charged soliton, indeed for a charged defect of any kind, most of the infrared oscillator strength resides in these three modes (Horovitz, 1982). Thus the dominant ir features induced by any charged defect are almost identical, independent of the nature of the defect. Only the total oscillator strength in the T modes, which is inversely proportional to the soliton effective mass, depends at all on the nature of the charged defect. However, the other two localized phonon modes in the TLM model *are* characteristic of the soliton. In the multiphonon model, these correspond to three localized phonons for each mode of the perfectly dimerized system. Two of these are ir active, T_1 (strong) and T_3 (weak). The T_2 localized phonon, which comes from the soliton shape oscillation, is inversion symmetric and is not ir active. The remaining three corresponding to the most weakly bound mode in the TLM model are very weakly ir active. The experimental observation of soliton-induced localized phonon modes are discussed in Sec. V.

Finally, we comment briefly on the localized phonon spectrum induced by a polaron or bipolaron. As mentioned previously, most of the ir oscillator strength is associated with the uniform translation (T_1) modes and is rather insensitive to the nature of the defect, although the oscillator strength is a measure of the defect effective mass. However, there are a different number and distribution of other localized phonon modes around each type of defect.

G. Solitons in *trans*-$(CH)_x$: Photoexcitation

1. Molecular dynamics in the adiabatic approximation

Since the dynamical symmetry breaking leads to a gap in the electronic spectrum $E_g^{1D}\sim 1.8$ eV, compared to the φ_n optical-phonon energy $\hbar\omega_0\simeq 0.12$ eV, the Born-Oppenheimer approximation is valid for nuclear dynam-

ics in *trans*-$(CH)_x$; i.e., $\hbar\omega_0/2\Delta \simeq 0.08$. In this case, the electronic Hamiltonian is diagonalized for fixed nuclear coordinates at each instant of time, and one obtains an adiabatic potential V for the φ_n field given by

$$V(\{\varphi_n\})=(K/2)\sum(\varphi_n+\varphi_{n+1})^2+E_0(\{\varphi_n\}) , \quad (4.63)$$

where

$$E_0(\{\varphi_n\})=\sum_{j\alpha s} E_{j\alpha}(\{\varphi_n\})[n_{j\alpha s}] \quad (4.64)$$

is the sum over the one-electron energy eigenvalues labeled by j and α for given $\{\varphi_n\}$. In Eq. (4.64), $\alpha=\pm$ refers to positive and negative energy states (for a model such as that of SSH, which is charge-conjugation symmetric, $E_{j+}=-E_{j-}$). Thus the lattice dynamics is governed by an effective Hamiltonian of the form

$$H_{\rm ad}=\sum p_n^2/2M+V(\{\varphi_n\}) . \quad (4.65)$$

In this section, we shall discuss the lattice dynamics in terms of the solution of the classical Hamiltonian equations of motion.

From Ehrenfest's theorem, we know that the motion of the expectation values of the field variables obeys the classical equations of motion. In the limit of large ionic mass M, the important field configurations never differ much from the average field configuration. Thus the classical equations of motion provide a valid approximate description of the dynamics of the system. In Sec. VIII we shall return to a consideration of the effects of quantum fluctuations of the lattice.

The equations of motion that derive from $H_{\rm ad}$ are generally very complicated due to the nonlocal nature of the forces between ions mediated by the electron gas. However, the equations can be integrated numerically for rather long finite chain systems. Considerable information about many interesting nonlinear dynamical processes in $(CH)_x$ has resulted from such numerical solutions.

a. Uniform motion of a soliton

Subsequent to the initial numerical studies of the dynamics of a soliton emitted from the chain end of an odd-membered chain, the motion of isolated solitons has been studied extensively, with many interesting features emerging from the calculations (Bishop *et al.*, 1984a, 1984b; Guinea, 1984). At low velocities v, the moving soliton is a stable solution of the equations of motion. Although the equations of motion are not Lorentz invariant, as the soliton velocity gets to be of order the speed of sound, $c_a=\omega_0(a/2)$, a slight pseudo-Lorentz contraction of the soliton occurs, so that its width goes from $\xi\rightarrow\xi(v)<\xi$. However, this is never more than a 50% effect. There is apparently no stable solution of the equations of motion for a soliton with velocity above a maximum velocity v_m. The simulations showed that v_m depends somewhat on parameters; for $\xi/a=7$, $v_m=2.6c_a$ while for $\xi/a=2.75$, $v_m=0.6c_a$ (c_a is the sound velocity). If initial conditions are specified corresponding to a velocity greater than v_m, the soliton will emit a cloud of phonons, as shown in Fig. 25, so as to reduce its velocity below v_m. The cloud of phonons itself has interesting properties; it is the "breather" discussed below. Physically, the maximum soliton velocity originates from the inability of the ions to respond at rates substantially above their natural frequency ω_0. However, there does not appear to be a theoretical treatment that can predict the ratio of v_m to v_s. For a wide range of Δ, v_m is approximately determined by the condition that the maximum soliton kinetic energy is 0.1Δ (Bishop *et al.*, 1984a, 1984b).

b. Soliton pair production via electron-hole injection

The dynamical process that has had the most direct experimental verification is the formation of a soliton pair $S\bar{S}$ from an electron-hole pair. This process is directly relevant to the dynamics of a chain following absorption of a photon with energy greater than 2Δ. In the Franck-Condon approximation, the electronic transition occurs instantaneously. Thus, at time $t=0$, the lattice configuration corresponds to a perfectly dimerized lattice and an electron and hole are suddenly produced, each at a band edge. The fact that quantum (or thermal) fluctuations of the lattice in some sense produce a distribution of initial lattice configurations leads to important modifications of the present results, which we discuss in Sec. VIII.

The evolution of the lattice was studied (Su and Schrieffer, 1980) from this starting state; snapshots of the lattice order parameters are shown in Fig. 26 as a function of time. Initially ($t_A=0$) the lattice is at rest with $\varphi_n/u_0=1$, or perfect A phase. By time $t_c=0.4(2\pi/$

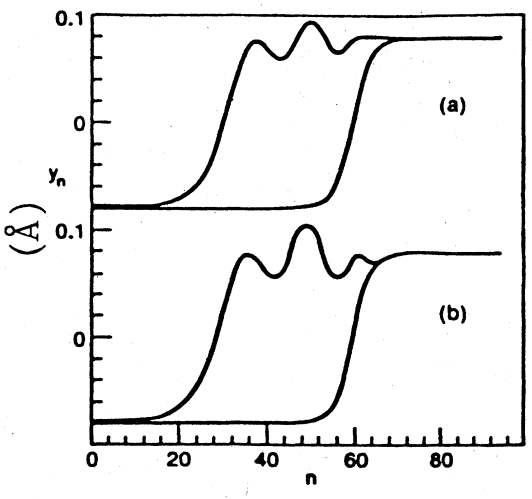

FIG. 25. Uniform velocity of a soliton: (a) $v_i=5.6\times10^6$ cm/s; (b) $v_i=8\times10^6$ cm/s (from Guinea, 1984).

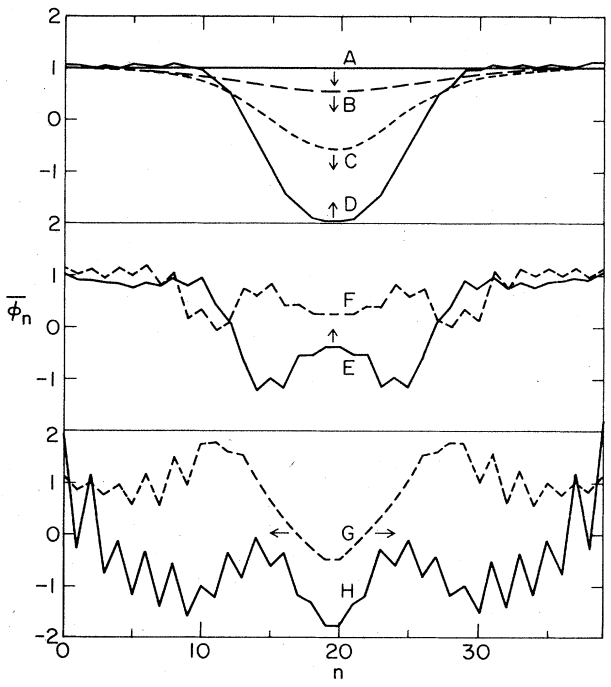

FIG. 26. The staggered lattice displacement parameter u_n vs lattice position for times $t=0$, 6, 12, 20, 30, 50, 60, and 130 in units of $\tau=1.25\times10^{-15}$ s after the injection of an electron-hole pair with energy 2Δ in *trans*-$(CH)_x$ (from Su and Schrieffer, 1980).

$\omega_0)\approx1.4\times10^{-14}$ s, the center of the chain has reversed the sense of its dimerization; the configuration already resembles a soliton-antisoliton pair $S\bar{S}$. Due to inertial effects, the lattice overshoots the B-phase configuration. By a time of order $(2\pi/\omega_0)=3.6\times10^{-14}$ s, there is a well-formed $S\bar{S}$ pair separating at a velocity comparable to the speed of sound and a cloud of phonons left behind in the middle. Subsequent calculations on longer chains have revealed that the solitons are, in fact, separating at the maximum soliton velocity v_m, and that the cloud of phonons is, in fact, a localized breather, as discussed below.

These results can be understood as follows: The creation energy of the electron-hole pair in the perfectly dimerized lattice is 2Δ. This state can be transformed by adiabatically distorting the lattice into a soliton-antisoliton pair with energy $2E_s=(4/\pi)\Delta<2\Delta$. The potential energy 0.73Δ that the system gains in this fashion must be converted into kinetic energy. Since a maximum of 0.1Δ can be converted into kinetic energy of the soliton, the remaining 0.5Δ must reside in the breather.

An initially surprising feature of the results is the extremely short time required to form the $S\bar{S}$ pair, $\approx10^{-13}$ s or roughly one or two optical-phonon periods. Because of the qualitative change of φ over many lattice sites involved in $S\bar{S}$ creation, one might think that a long nucleation period would be required. The rapid nucleation can be understood qualitatively by considering the adiabatic potential energy as a function of a collective coordinate R, which we think of as the soliton pair separation (see Fig. 27). At $R=0$, the lattice is by definition perfectly dimerized. The ground-state adiabatic energy we define to be 0, and hence the first-excited-state energy is 2Δ. As R is increased, the adiabatic potential for the ground electronic state V_0 (curve 1) increases, and for the first excited state V_1 decreases. Since these two states differ only by the occupancy of the two electronic states nearest the gap center, for nonzero R the splitting between these two potentials is simply the splitting between the bonding (ψ_+) and antibonding (ψ_-) combination of the midgap states associated with the two solitons. Thus, for $R>\xi$, where the lattice configuration begins to resemble a well-formed pair, both adiabatic potentials approach a common asymptotic value $2E_s$ exponentially fast. To estimate the speed with which the collective coordinate evolves to $R\sim\xi$, we estimate the force $F=-dV_1/dR\sim\Delta/\xi$ and the effective mass $M^*\sim1/2M_s=(2a/3\xi)(u_0/a)^2$ and hence $t\sim(\xi M^*/F)^{1/2}\sim(2\pi/\omega_0)$. Thus the short nucleation time is a consequence of the light soliton mass and of the strong repulsion between solitons in the first excited electronic state. Note also that in the SSH model the lowest-lying triplet state has the same adiabatic potential as the photogenerated singlet state. While electron-electron interactions will lift this degeneracy, we do not expect them to alter the qualitative shape of the adiabatic potential. Thus either a singlet or a triplet electron-hole pair will rapidly decay into an $S\bar{S}$ pair.

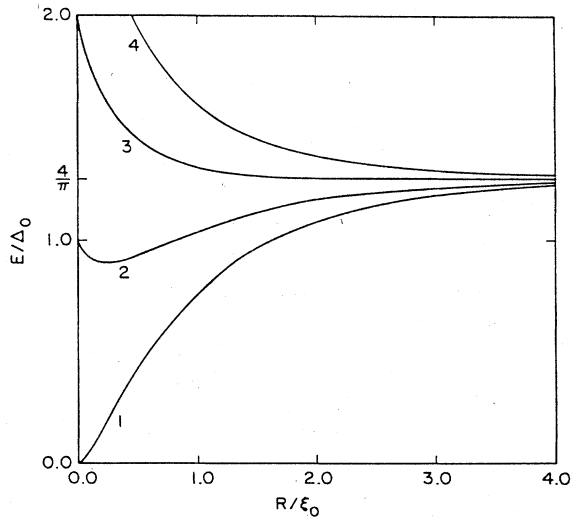

FIG. 27. Adiabatic potential energy curves as functions of the soliton pair separation R for different occupancies of the gap states (from Kivelson, 1986).

c. Polaron formation

As a third example (Su and Schrieffer, 1980), consider the addition of an electron to the bottom of the conducting band of a chain initially at rest in the A phase. As shown in Fig. 28, the electron drives a lattice distortion, which in turn localizes the electron in a self-consistent manner, emitting phonons to conserve energy. If the kinetic energy is removed, φ_n relaxes to the polaron form (see Sec. IV.F) except for discrete lattice effects.

d. Breathers

In all the molecular dynamics experiments we have discussed, whenever excess energy is released into the lattice, it does not dissipate into phonons as might be expected for a highly excited anharmonic lattice. Rather, a spatially localized dynamically bound state, or breather, is formed. This is a common occurrence in nonlinear one-dimensional field theories. For instance, in a sine-Gordon field theory, exact breather solutions to the equations of motion are known and can be shown to be stable (Dodd *et al.*, 1982). Molecular dynamics simulations have been carried out (Campbell *et al.*, 1983) to very long times on a φ^4 chain; the results confirmed the existence of breather solutions, which are at least highly persistent.

In all cases, the breather solution resembles a bound $S\bar{S}$ pair; in the case of $(CH)_x$, it is a neutral pair. Consider the ground-state adiabatic potential as a function of the soliton separation R shown in Fig. 27. One can imagine exciting oscillating bound states in this potential. As the soliton separation oscillates, one expects a pair of bound states, ψ_+ and ψ_-, to be pulled into the gap. Their energies should then oscillate periodically in time. To check this, more extensive molecular dynamics simulations were carried out (Bishop *et al.*, 1984a, 1984b) with results shown in Figs. 29–31. The bound-state electronic spectrum as a function of time after the production of an electron-hole pair is shown in Fig. 29. The corresponding lattice snapshots are shown in Figs. 30 and 31. The oscillating state near the band edge is localized on the breather and has an energy that oscillates with the breather frequency. (By particle-hole symmetry, there are two corresponding bound states in the upper half-gap.)

2. Charge branching ratio of photoproduced $S\bar{S}$ pairs

The branching ratio R for photoproduction of $S^0\bar{S}^0$ and $S^{\pm}\bar{S}^{\pm}$ in *trans*-$(CH)_x$ has been estimated (Flood *et al.*, 1982) by setting an upper limit on the number of $S^0\bar{S}^0$ pairs from the change of ESR signal and comparing that upper limit with the number of $S^{\pm}\bar{S}^{\pm}$ obtained from the strength of the infrared-active vibrational modes (calibrated against the strength observed on doping). One finds the surprisingly small value $R < 10^{-2}$.

A simple theorem (Ball *et al.*, 1983) has been proven concerning the branching ratio of photoproduced solitons. In the adiabatic approximation and to second order in the nonadiabaticity parameter, only charged solitons are produced by this mechanism. The proof has since been extended to all orders in the nonadiabaticity and to models including electron-electron interactions (Danielson and Ball, 1985; Kivelson and Wu, 1986b). These more general proofs rely on the charge-configuration symmetry of the model. The current operator has odd charge-conjugation parity. Hence the ground and photoexcited states have different symmetry; only when the effect of terms that break charge-conjugation symmetry (e.g., single-site phonons, next-nearest-neighbor hopping, or spatial disorder) are includ-

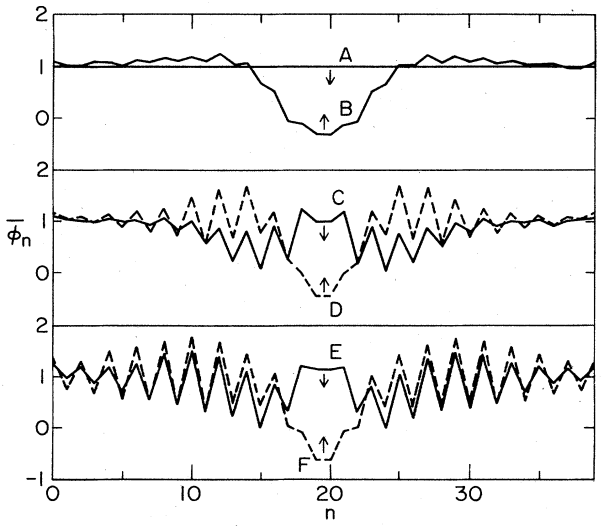

FIG. 28. Dynamical generation of a polaron from an injected electron (from Su and Schrieffer, 1980).

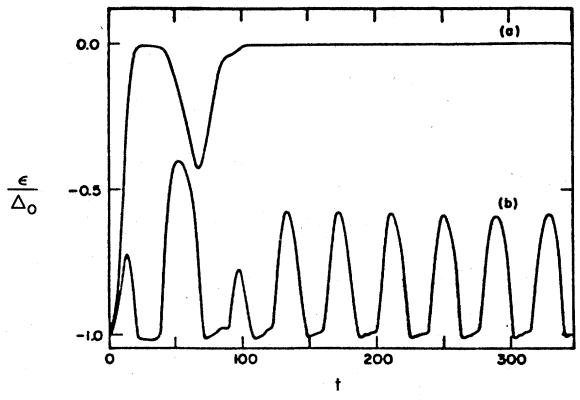

FIG. 29. Time dependence of the electronic levels: (a) state at top of valence band rapidly becoming a midgap state; (b) next state in valence band shifting into the gap and oscillating with breather frequency. Parameters are those of Fig. 30 (from Bishop *et al.*, 1984a, 1984b).

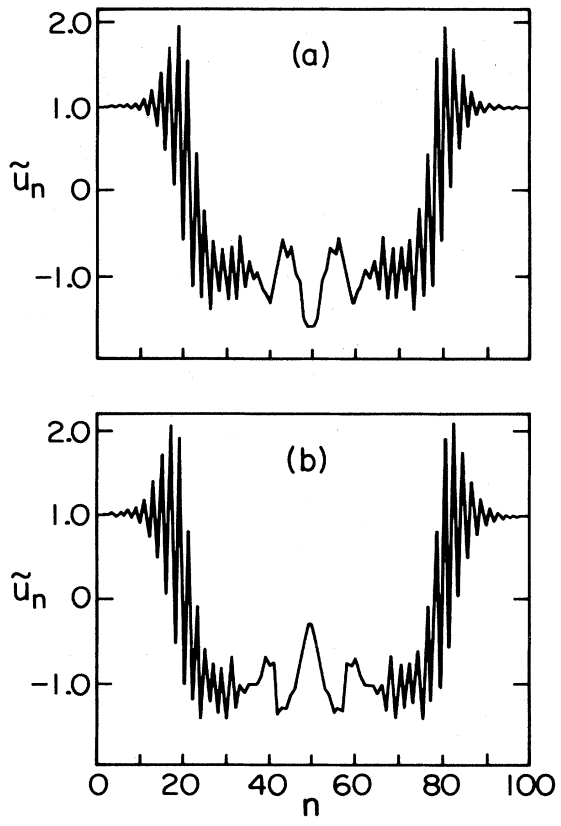

FIG. 30. The staggered lattice displacement parameter u_n vs lattice position for times (a) $t=279\times10^{-15}$ s and (b) $t=299\times10^{-15}$ s after the injection of an electron-hole pair with energy 2Δ in *trans*-$(CH)_x$.

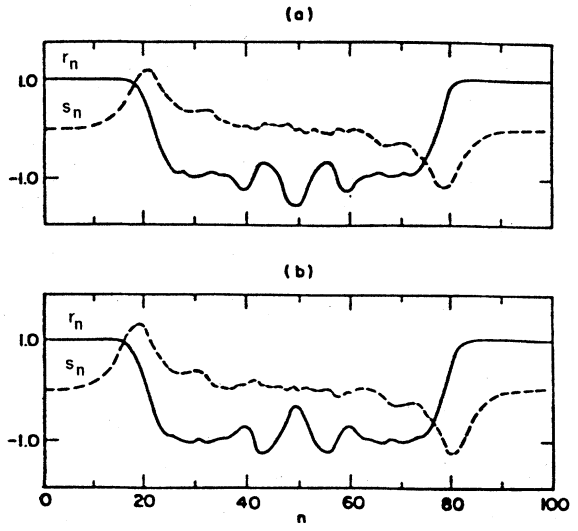

FIG. 31. The smoothed lattice displacement variables r_n, the optical-phonon coordinate, and s_n, the acoustic-phonon coordinate corresponding to the staggered displacements shown in Fig. 30. Both $r_n=1/4(-1)^n(2u_n-u_{n+1}-u_{n-1})/u_0$, and $s_n=1/4(2u_n+u_{n+1}+u_{n-1})/u_0$ are in units of the ground-state dimerization $u_0\approx0.10a$. Parameters (in units of 10^{-15} s) after photogeneration are (a) $t=279$, (b) $t=299$. The time difference of 20 units is 0.51 phonon periods or 0.51 breather periods (from Bishop *et al.*, 1984a, 1984b).

ed in the model can neutral solitons be produced. However, even rather weak symmetry-breaking interactions can lead to rapid conversion of charged-soliton pairs into neutral-soliton pairs (Kivelson and Wu, 1986b).

We shall not reproduce the more general proofs of the branching-ratio theorem here; the original argument in the adiabatic limit gives the most insight into the physics. As stated previously, at finite soliton separation $R>0$, there are two bound states $\psi_\pm$ with one electron in each. The states are labeled by their parity, with the lower (hole) state having even parity. This many-body state is consistent with the change of parity from the even-parity ground state through dipole absorption. Since the only states involved in determining the charge distribution of S and $\bar{S}$ are $\psi_\pm$, the entire electronic state is specified by the two-electron state

$$\psi(1,2)=(1/\sqrt{2})[\psi_-(1)\psi_+(2)+\psi\ (2)\psi_+(1)]\chi_{12}\ , \tag{4.66}$$

where χ is the singlet spin function. As the spacing D between S and $\bar{S}$ becomes large compared to ξ, $\psi_\mp$ can be represented as a linear combination of the states localized on S and on $\bar{S}$,

$$\psi_\mp=(\psi_s\pm\psi_s)/\sqrt{2}\ . \tag{4.67}$$

Inserting Eq. (4.66) into (4.65), one finds that terms having one electron on S and one on $\bar{S}$ exactly cancel, so that neutral S and $\bar{S}$ production is totally suppressed. It is readily seen that this result follows as a consequence of the Pauli principle and the invariance of H under parity. Thus the result is unaltered by the inclusion of electron-electron interactions. It is interesting to note that, in the analogous problem of photodissociation of H_2, there is zero probability for producing H^0+H^0 with each electron in the $1S$ state for the same reasons of symmetry. Note that the same argument applied to an initially spin-triplet electron-hole pair demonstrates that the resulting $S\bar{S}$ pair must also be neutral.

V. SOLITONS IN POLYACETYLENE: A SUMMARY OF EXPERIMENTAL RESULTS

A. Experimental studies of neutral solitons in *trans*-$(CH)_x$

The existence of neutral solitons formed during the isomerization process (from *cis* to *trans*) is a fortunate ac-

cident, since the thermodynamic number would be too small to detect ($E_S/k_BT \gg 1$). The unpaired spin makes possible magnetic resonance studies, which enable the determination of a number of important properties including the magnetic susceptibility and its temperature dependence, the spatial extent of the wave function, and the motion and dynamics of the neutral-soliton defects. On the other hand, since these neutral solitons are present only because of imperfections in the polymer chains, one must take care not to attempt to infer from their study properties of solitons (e.g., mobility) on perfect chains.

These spin-$\frac{1}{2}$ species were initially characterized as extended π-electron defects, approximately one per 3000 carbon atoms in a *trans*-$(CH)_x$ chain (Goldberg *et al.*, 1979; Weinberger *et al.*, 1980). The magnetic susceptibility followed Curie's law ($\chi \sim 1/T$), indicative of localized spins; the linewidth was narrow, implying motional narrowing of the hyperfine interaction.

A number of experiments were carried out to determine whether the spin-$\frac{1}{2}$ species are charged or neutral. In particular, after compensation with ammonia, the electrical conductivity decreased by many orders of magnitude, implying a corresponding decrease either in the number of charge carriers or in their mobility, but the number of spins did not change (Weinberger *et al.*, 1980). The narrow linewidth (implying a mobile species) both before and after compensation ruled out the possibility of trapping with an associated major change in mobility, thus indicating that the spin is associated with a neutral species. Moreover, the infrared-active vibrational modes characteristic of charged configurations (Fincher, Ozaki, Heeger, and MacDiarmid, 1979; Rabolt *et al.*, 1979; Etemad, Pron, *et al.*, 1981) are not observed in carefully prepared pristine samples. For example, the 1370-cm^{-1} mode would be detectable with 0.03 mol % charged defects. These data demonstrate that the spin-$\frac{1}{2}$ defects found in *trans*-$(CH)_x$ are neutral, consistent with the reversed spin-charge relations predicted for solitons (Su, Schrieffer, and Heeger, 1979, 1980).

Electron-nuclear double resonance (ENDOR) studies (Thomann *et al.*, 1983; Kuroda *et al.*, 1984, 1985; Grupp *et al.*, 1987; Kass *et al.*, 1987; Kuroda and Shirakawa, 1987) have been carried out with the goal of determining in detail the wave function of the spin-$\frac{1}{2}$ species. The delocalized spin distribution was directly observed from the distribution of ENDOR frequencies. A width consistent with $\xi \sim 7a$ was inferred directly from the maximum ENDOR shift (Kuroda *et al.*, 1984, 1985; Grupp *et al.*, 1987; Kass *et al.*, 1987; Kuroda and Shirakawa, 1987). A wide distribution of hyperfine fields (consistent with a smooth falloff of the midgap-state wave function, with a half-width of $7a-11a$, has been unambiguously established by two separate groups (Kuroda *et al.*, 1984, 1985; Grupp *et al.*, 1987; Kass *et al.*, 1987; Kuroda and Shirakawa, 1987). These results are not consistent with the delocalization over approximately 50 sites proposed earlier (Thomann *et al.*, 1983). The more careful control of the dilute *trans* content in the *cis*-rich oriented samples enabled the trapping of the neutral solitons more effectively, so that residual center-of-mass motion, with associated averaging (Heeger and Schrieffer, 1983), was minimized. The detailed ENDOR line shape was found to be consistent with the spin-density profile predicted by the soliton theory (Su, Schrieffer, and Heeger, 1979, 1980) supplemented to include a finite on-site Coulomb interaction (Subbaswamy and Grabowski, 1981; Heeger and Schrieffer, 1983). The width of the neutral solitons ($\xi \sim 8-11a$) found in the ENDOR experiments (Kuroda *et al.*, 1984, 1985; Grupp *et al.*, 1987; Kass *et al.*, 1987; Kuroda and Shirakawa, 1987) is in reasonable agreement with the value predicted theoretically (Su, Schrieffer, and Heeger, 1979, 1980) ($\sim 7a$) prior to the experiments and inferred from the electron-spin resonance linewidth (Goldberg *et al.*, 1979; Weinberger *et al.*, 1980), which is also due to hyperfine interactions with the many protons within ξ of the center of the kink.

That the neutral soliton was mobile was first inferred from the motionally narrowed ESR linewidth (Goldberg *et al.*, 1979; Weinberger *et al.*, 1980). This was subsequently confirmed through a series of nuclear-spin relaxation measurements, which were interpreted in terms of one-dimensional motion of the neutral solitons (Nechtschein *et al.*, 1983a, 1983b). Although nuclear spin-spin diffusion to static defects was suggested as an alternative explanation (Clark *et al.*, 1983; Clarke and Scott, 1986), proton NMR measurements as a function of ^1H concentration on partially deuterated *trans*-$(CH_fD_{(1-f)})_x$ showed (Zilcox *et al.*, 1985) that at high ^1H content the proton relaxation is homogeneous and thus truly reflects the dynamics of the electron spins.

Dynamic nuclear polarization (DNP) studies (Jeffries, 1963; Nechtschein *et al.*, 1980; Devreux *et al.*, 1981; Holczer *et al.*, 1981; Clark *et al.*, 1985) have provided definitive evidence of the mobility of the neutral solitons and have set a lower limit on the time needed for such a bond-alternation domain wall to diffuse a distance equal to its width. DNP has been used as a microscopic probe of soliton motion: if the solitons are fixed (trapped) or moving very slowly, the DNP occurs via the solid-state effect, whereas, if the mobility is high, DNP occurs via the Overhauser effect (Jeffries, 1963). The experimental results obtained from DNP studies of *trans*-$(CH)_x$ showed (Nechtschein *et al.*, 1980; Devreux *et al.*, 1981; Holczer *et al.*, 1981; Clark *et al.*, 1985) that the neutral solitons are trapped at low temperatures, and very mobile at high temperatures and that there is a gradual conversion from trapped to mobile populations over a temperature range $10 < T > 100$ K. The DNP data set an upper limit of $1.3 \times 10^{13} S^{-1}$ on the elementary jump rate, a value that is close to (but somewhat less than) the value inferred from analysis of the electron (Mizoguchi *et al.*, 1984) and nuclear-spin lattice relaxation measurements (Clark *et al.*, 1983; Nechtschein *et al.*, 1983a, 1983b; Zilcox *et al.*, 1985).

Multiple-quantum NMR coherence (Thomann *et al.*,

1987) has been used in an attempt to probe the motion of the neutral solitons in *trans*-$(CH)_x$. Although the results were interpreted as implying static neutral solitons, such a conclusion is inconsistent with all of the work listed above. Moreover, the observation of narrowing on electrochemical isomerization (Bernier, 1987) from *cis*- to *trans*-$(CH)_x$ with no change in the number of spins rules out exchange as the source of narrowing.

The magnetic resonance measurements have been extended to *trans*-$(CH)_x$ prepared using a modified synthesis (Thomann and Baker, 1987) that yields substantially fewer spins than typically found in material made with the Shirakawa technique (from about a factor of 3 smaller to about an order of magnitude smaller). The broader linewidth observed suggests that exchange plays some role in the spin dynamics. This conclusion is based on an assumption that the lower-spin material is in every other way identical to that made with the Shirakawa method. Although the lower-spin samples were characterized with a variety of standard techniques, there is no way of verifying whether or not trapping sites at the level of one per 10^4 carbons are the same. Nevertheless, by comparing not only the ESR linewidth but all aspects of the magnetic resonance, it was concluded (Thomann and Baker, 1987) that the spin dynamics are determined by a combination of one-dimensional diffusion of the solitons and soliton-soliton spin exchange. The latter is made possible by the one-dimensional diffusion; at the level of dilution involved, the exchange would be too small unless the spins diffused rapidly and approached one another over sufficiently short distances for exchange to occur.

B. Experimental studies of charged solitons in *trans*-$(CH)_x$

There are three specific signatures of charged-soliton formation for which detailed theoretical analysis exists and for which detailed experimental evidence exists.

(1) The formation of localized structural distortions with associated localized vibrational modes (localized phonons). These soliton-induced characteristic infrared-active vibrational modes (IRAV modes) can be observed in the mid-infrared frequency range typical for molecular vibrations.

(2) The generation of the midgap state and the associated electronic transitions at $\hbar\omega \sim \Delta$ (see Fig. 33 below). This soliton-induced transition can be observed in the near-infrared range.

(3) The reversed spin-charge relations, i.e., charge storage in *spinless* solitons. This can be directly verified through electron-spin resonance experiments. The key signature is that the ratio $N_s/N_{ch} \ll 1$ ($\Longrightarrow 0$), where N_s is the number of spins and N_{ch} is the number of charges.

As noted in the Introduction, solitons can be generated in two ways: charge transfer doping and photoexcitation. In the following two subsections, we briefly summarize the experimental evidence of the three signatures listed above for solitons induced by both of these two mechanisms.

1. Solitons in *trans*-$(CH)_x$: Charge transfer doping

a. Infrared-active vibrational modes

The characteristic doping-induced IRAV modes were discovered in the first infrared studies carried out on polyacetylene at dilute doping concentrations (Fincher, Ozaki, Heeger, and MacDiarmid, 1979; Rabolt *et al.*, 1979; Etemad, Pron, *et al.*, 1981). The principal doping-induced IRAV modes are at frequencies $\approx$900, 1260, and 1370 cm^{-1}, with a weaker mode at 1215 cm^{-1}. These doping-induced absorptions are remarkably intense (consistent with the large oscillator strength expected from moving charged domain walls); they are isotope sensitive (Rabolt *et al.*, 1979; Etemad, Pron, *et al.*, 1981), with corresponding shifts on going from $(CH)_x$ to $(CD)_x$. The doping-induced IRAV modes for $(CH)_x$ and $(CD)_x$ are shown in Fig. 32. The intensities of the observed IRAV modes are proportional to the dopant concentration (Fincher, Ozaki, Heeger, and MacDiarmid, 1979; Rabolt *et al.*, 1979; Etemad, Pron, *et al.*, 1981), but the frequencies are essentially independent of the dopant species.

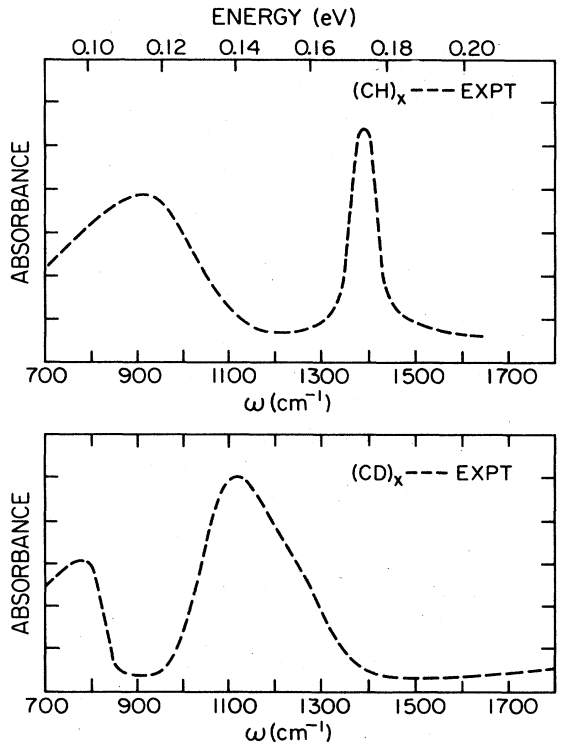

FIG. 32. Doping-induced infrared-active vibrational modes for *trans*-polyacetylene (from Etemad, Pron, *et al.*, 1981): (a) *trans*-$(CH)_x$; (b) *trans*-$(CD)_x$.

The absorption is polarized parallel to the polymer backbone [as verified by experiments on highly oriented samples (Fincher, Ozaki, Heeger, and MacDiarmid, 1979; Piaggio *et al.*, 1984; Leising *et al.*, 1985)]. Thus the doping-induced ir modes are characteristic of the doped polyacetylene chains.

The doping-induced IRAV modes are in excellent agreement with the predictions summarized in Sec. IV for the T_1 mode. The existence of these characteristic ir signatures demonstrates unambiguously that charged species with associated structural distortions are generated upon doping. As predicted, there is one localized phonon for each of the phonon branches of *trans*-$(CH)_x$ (as observed through Raman scattering). The oscillator strength is large (i.e., the dynamic mass is small) and of the order of magnitude predicted by theory.

The broad and intense absorption at 900 cm^{-1} is presumably the Goldstone mode, shifted up from zero frequency by pinning due to the Coulomb binding of the charged soliton to the (oppositely) charged counter ion. The breadth is indicative of nonuniformity of pinning. Because of the spatial extent of the soliton charge ($2\xi \approx 14a$), the pinning frequency is relatively insensitive to the detailed size and structure of the counter ion. The assignment of the 900 cm^{-1} as the pinned Goldstone mode is consistent with the observation that this mode appears at ≈ 550 cm^{-1} in photoexcitation measurements (see below); weaker pinning would be expected for photoexcitation, since the Coulomb field of the counter ion is absent.

Experimental evidence of the existence of the weak T_3 modes has not yet appeared for doped samples (the background problems are severe due to the many infrared-active modes of the pure polymer). Additional weak modes have been observed in photoinduced IRAV experiments (see Sec. V).

b. Electronic excitations: Visible and near-infrared absorption

Just as the soliton leads to new peaks in the ir absorption spectrum $\alpha(\omega)$, it is expected to lead to new peaks in the optical-absorption spectrum. From Fig. 33 we see that when solitons are introduced, a new absorption edge should onset at $\omega=\Delta_0$ corresponding to valence (v)$\rightarrow$gap center (0) excitation for S^+, and 0$\rightarrow$conduction (c) for S^-. Both processes are possible for S^0. Since the optical sum rule implies conservation of oscillator strength, we know that there will be bleaching (reduction of absorption) above the band edge to compensate for the extra edge at Δ, as shown in the following subsection.

The calculation of $\alpha(\omega)$ for a clamped lattice having one soliton has been studied (Suzuki *et al.*, 1980; Gammel and Krumhansl, 1981; Kivelson *et al.*, 1982); the one-soliton problem is meaningful even though S and $\bar{S}$ must be created in pairs, since a ring with an odd number of (CH) groups has an odd number of solitons, as does

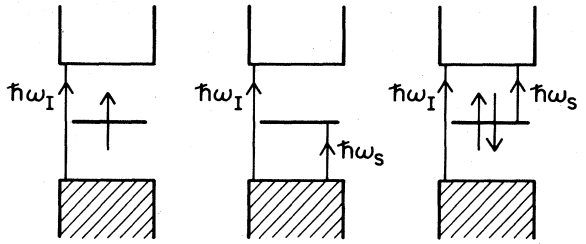

FIG. 33. Band diagram showing the midgap state associated with the soliton, and the interband ($\hbar\omega_I$) and midgap ($\hbar\omega_s$) transitions: left, neutral soliton; center, positively charged soliton; right, negatively charged soliton.

the ground state of a chain segment with odd N. Moreover, the single-soliton results should be applicable to experimental studies, so long as the soliton concentration (induced either by doping or by photoexcitation) is relatively dilute.

The calculations have been carried out in the continuum model in which the single-particle scattering states $\psi_k^{+,-}$ and ψ_0 are known analytically. The absorption to the soliton gap state is given by

$$\alpha_s(\omega)=\pi(e^2/\hbar c\,\varepsilon^{1/2})yN\xi^2[(\hbar\omega/\Delta)^2-1]^{-1/2} \times \mathrm{sech}^2\{\pi/2[(\hbar\omega/\Delta)^2-1]^{1/2}\}\ , \tag{5.1}$$

where N is the number of carbons per unit volume and y is the density of solitons per carbon. The interband contribution to $\alpha(\omega)$ is given by

$$\alpha_I(\hbar\omega)=(2/\omega)\sum_{kk'}|M_{kk'}|^2\delta(\hbar\omega-E_k^c-E_k^v)\ , \tag{5.2}$$

with $M_{kk'}$ given by a rather complicated expression. One finds that the soliton-induced change of interband absorption is given within 10% by scaling the absorption $\alpha_0(\omega)$ for the pure material as

$$\Delta\alpha_I(\omega)=-y(2\xi/a)\alpha_0(\omega)\ . \tag{5.3}$$

The total absorption satisfies a sum rule (Kivelson *et al.*, 1982)

$$\int_{-\infty}^{\infty}\alpha(\omega)d\omega=(2/\pi)(e^2/\hbar c\,\varepsilon^{1/2})Nav_F \tag{5.4}$$

independent of the lattice configuration or doping level. Thus the increase of absorption in the gap is compensated by a decrease of the interband absorption.

In Fig. 34 the experimental results for pure material as well as for 0.01%, 0.1%, and 0.5% AsF_5 are shown (Suzuki *et al.*, 1980). While the general features and scale of the curves are in qualitative agreement with theory, there is a considerable amount of rounding in the experimental data. While part of this comes from interchain hopping, band-structure calculations (Grant and Batra, 1979) show that the interchain hopping integral $t_\perp \simeq 0.025$ eV or $4t_\perp \sim 0.1$ eV, a width considerably small-

er than that required to account for the observed rounding. The nonlinear dynamics of *trans*-$(CH)_x$ leads to a strong broadening of the optical-absorption structure due to multiphonon emission (Su and Schrieffer, 1980; Mele and Rice, 1981) (as well as polaron formation) and due to $S\bar{S}$ creation for $(2/\pi)\Delta < \hbar\omega < 2\Delta$ (Brazovskii, 1980; Sethna and Kivelson, 1982; Su and Yu, 1983).

Although the corresponding subgap absorption has been calculated for polarons (Fesser *et al.*, 1983), this is of interest only at extremely low doping. Because the continuum and split-off states are known for a polaron in the continuum limit (Campbell and Bishop, 1981, 1982), $\alpha(\omega)$ can be directly calculated (Fesser *et al.*, 1983) from the golden rule. The reader is referred to Campbell and Bishop (1981, 1982) and Fesser *et al.* (1983) for details.

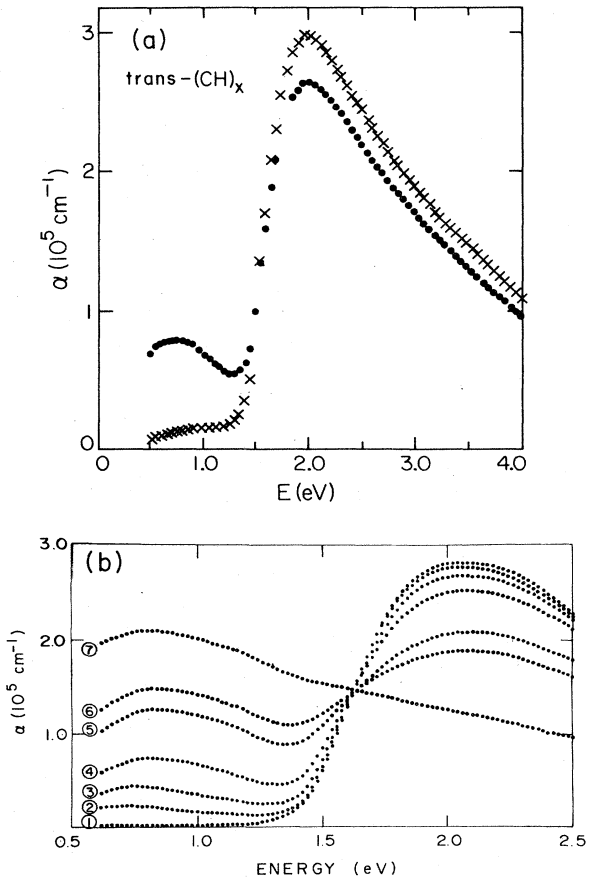

FIG. 34. Absorption spectra for neutral and doped *trans*-$(CH)_x$. (a) Absorption coefficient of *trans*-$(CH)_x$: ×, before doping; ●, after doping with a fraction of a percent by exposure to AsF_5 vapor (from Suzuki *et al.*, 1980). (b) *In situ* absorption curves for *trans*-$(CH)_x$ during electrochemical doping with $(ClO_4)^-$. The applied cell voltages (relative to Li) and corresponding concentrations are as follows: curve 1, 2.2 V ($y=0$); curve 2, 3.28 V ($y\sim0.003$); curve 3, 3.37 V ($y\sim0.0065$); curve 4, 3.46 V ($y\sim0.012$); curve 5, 3.57 V ($y\sim0.027$); curve 6, 3.64 V ($y\sim0.047$); curve 7, 3.73 V ($y\sim0.078$). From Feldblum *et al.*, 1982.

c. The midgap absorption

The midgap absorption (see Fig. 33) is a universal feature of doped polyacetylene (Tanaka *et al.*, 1980, Feldblum *et al.*, 1982; Chung *et al.*, 1984). This dopant-induced near-ir electronic transition has been observed to be independent of the dopant species and of whether that dopant is a donor (*n*-type doping) or an acceptor (*p*-type doping). For oriented samples, the midgap transition is polarized along the polymer chains. Thus this characteristic experimental feature is a property of the doped polyacetylene chain.

The results of *in situ* experiments [performed during electrochemical doping (Feldblum *et al.*, 1982)] on the visible-ir absorption in *trans*-$(CH)_x$ are shown in Fig. 34. As the doping proceeds, the midgap absorption appears, centered near 0.65–0.75 eV with an intensity that increases monotonically in proportion to the dopant concentration. At the same time, the strength of the interband transition decreases with an overall conservation of the oscillator strength. From the intensity of this absorption and from the magnitude of the associated bleaching of the interband transition, the width of the self-localized charged object can be inferred to be $\xi \approx 7a$, in good agreement with the theory.

The remarkable oscillator strength associated with the doping-induced spectroscopic features arises directly from the spatial extent of the charged soliton [see Eqs. (5.1)–(5.3)]. Whereas one might anticipate that the ratio of oscillator strengths (i.e., midgap to interband) would be equal to the dopant concentration, a detailed theoretical analysis shows that for dilute concentrations the midgap transition is enhanced by a factor of ξ/a, where 2ξ is the full width of the bond-alternation domain wall and a is the projection of the carbon-carbon distance along the chain. Because $\xi/a \sim 7$, this enhancement of the soliton transition makes it observable even at dilute dopant concentrations.

d. The reversed spin-charge relations: Charge storage in spinless solitons

The initial spin resonance experiments implying spinless carriers were carried out on *p*-type samples and utilized vapor-phase doping. The interpretation of these early experiments was controversial (Tomkiewicz *et al.*, 1979; Tomkiewicz, Schultz, *et al.*, 1981; Tomkiewicz, Shiren, *et al.*, 1981), with uncertainties arising because of the possibility of nonuniform doping, the use of thick films (thickness comparable to the microwave skin depth), and the complex chemistry of AsF_5 doping (Heeger and MacDiarmid, 1981). To avoid these problems, subsequent work utilized *in situ* ESR measurements on thin films (thickness of order 1 μm or less), carried out during either chemical (Chung *et al.*, 1984) or electrochemical (Chen *et al.*, 1985; Moraes *et al.*, 1985) doping. Since with the electrochemical technique the electrochemical potential (rather than the concentration)

is the controlled variable, the thin-film doped samples are at equilibrium. Both *n*-type (Chen *et al.*, 1985; Moraes *et al.*, 1985) doping $[Na^{+}_{y}(CH)^{-y}]_x$ and *p*-type (Chen and Heeger, 1986a, 1988) doping $[(CH)^{+y}(ClO_4^{-})_y]$ have been investigated.[1] The results of these measurements demonstrated unambiguously the spinless character of the doping-induced charge storage states at dilute concentrations and, thereby, established the reversed spin-charge relation for solitons in *trans*-$(CH)_x$.

The spin contribution to the magnetic susceptibility (χ) of Na-doped polyacetylene (from *in situ* measurements carried out during electrochemical doping; Chen *et al.*, 1985; Moraes *et al.*, 1985) is shown in Fig. 35, where χ is plotted as a function of the electrochemical potential μ (referenced to Na) of the doped polymer. The *n*-type injection threshold for *trans*-$(CH)_x$ was determined in earlier experiments (Kaufman *et al.*, 1983; Kaufman, Chung, and Heeger 1984) to be at about 1.75 V.

The initial susceptibility (due to neutral-soliton defects) decreases slightly; for voltages below about 1.5 V, the number of spins is independent of μ (and thus of y) with a value identical to that obtained in the analogous *in situ* *p*-type doping experiments (Chen and Heeger, 1986a, 1988). In this dilute-to-intermediate doping regime (where the temperature dependence indicates Curie law behavior), the number of spins remains fixed at $N_s \sim 2\times 10^{-4}$ per carbon for doping concentrations up to $y \sim 0.06$. The latter number was obtained from parallel electrochemical and optical measurements (Chen *et al.*, 1985; Moraes *et al.*, 1985). Assuming one charge per dopant, an upper limit was determined: $(N_s/N_{ch}) < 5\times 10^{-3}$. The results, therefore, demonstrate that for both *n*-type and *p*-type charge injection doping occurs via the formation of *spinless* charged solitons.

The small residual concentration-independent Curie contribution appears to arise from formation of one kinetically metastable spin-$\frac{1}{2}$ polaron per two $(CH)_x$ chains (Moraes *et al.*, 1985). This follows since solitons must be created in pairs, and for random doping at any significant dopant level (>1/chain length) approximately half the chains will have an odd number of charges.

A first-order phase transition signaled by the abrupt increase in χ (and in the linewidth) is observed (Chen *et al.*, 1985; Moraes *et al.*, 1985) at 0.8 V. For y less than the critical value, the susceptibility is small, and the temperature dependence is Curie-type. For y greater than the critical value, χ increases abruptly (to a concentration-independent value) and becomes temperature independent, indicative of a Pauli spin susceptibility characteristic of a metal. Note that in contrast to the early work (Tomkiewicz *et al.*, 1979; Epstein *et al.*, 1981; Ikehata *et al.*, 1981; Tomkiewicz, Schultz, *et al.*, 1981; Tomkiewicz, Shiren, *et al.*, 1981), in which the chemical potential was not controlled, there is no sign of any *T*-independent contribution for concentrations below the transition. A similar transition has been observed for *p*-type doping at very similar doping levels (Chen and Heeger, 1988).

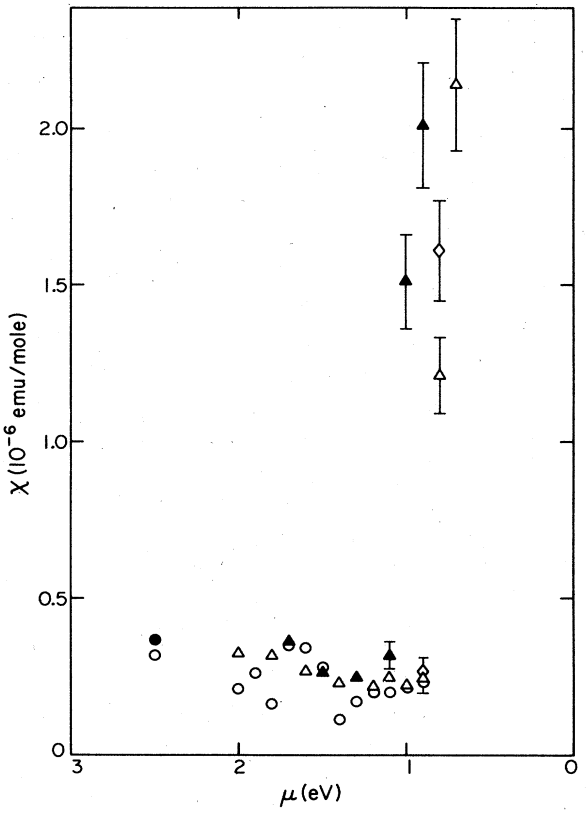

FIG. 35. Electron-spin contribution to the magnetic susceptibility for *n*-type $[Na^{+}_{y}(CH)^{-y}]_x$, plotted as a function of chemical potential μ (referenced to Na), of the polymer (Chen *et al.*, 1985; Moraes *et al.*, 1985).

Since the transition is first order, the susceptibility is discontinuous (and hysteretic) as a function of the chemical potential. As a function of the dopant concentration, however, the changes could be continuous due to an inhomogeneous mixture of the two phases ($y < y_c$ and $y > y_c$). This may be the origin of the smooth onset of χ_p found in samples doped without specifically controlling the chemical potential (Tomkiewicz *et al.*, 1979; Tomkiewicz, Schultz, *et al.*, 1981; Tomkiewicz, Shiren, *et al.*, 1981).

This remarkable abrupt increase in χ (and the associated change in temperature dependence) has been interpreted as a first-order phase transition from a soliton lat-

[1]The work of Chen and Heeger (1988) has shown the existence of the transition for *p*-type doping and it has extended the *n*-type doping range to ~ 16 mol %. The value for χ_p was found to be independent of dopant concentration (from ~ 6 to 15 mol %).

tice to a novel metallic state. The sharpness of the transition rules out disorder (due to doping) as the source of onset of metallic behavior.

2. Resonant Raman scattering

Raman spectroscopy has been extensively used together with infrared spectroscopy to study the vibrational modes of dimerized polyacetylene. The expected zone-center modes have been observed at frequencies that are in agreement with the calculated values (Harada *et al.*, 1980; Kuzmany, 1980; Lichtmann *et al.*, 1980; Etemad, Pron, *et al.*, 1981; Fitchen, 1982; Kuzmany *et al.*, 1982; Lefrant, 1983; Mulazzi *et al.*, 1985; see Sec. IV). The shift due to the electronic response is evident, as shown, for example, in Fig. 24.

Resonant Raman scattering has also been very useful for probing the electronic energy gap. For laser wavelength 676 nm ($\hbar\omega_L = 1.83$ eV), three phonon lines are observed, as shown in Fig. 36. As the excitation frequency increases, the Raman sidebands exhibit dramatic lineshape changes (Harada *et al.*, 1980; Kuzmany, 1980; Lichtmann *et al.*, 1980; Fitchen, 1982; Kuzmany *et al.*, 1982; Lefrant, 1983; Mulazzi *et al.*, 1985). Shoulders on the high-frequency side of the primary peaks eventually develop into secondary peaks at $\hbar\omega_L = 2.71$ eV. Several attempts have been made to explain the unusual features.

The first attempt involves a distribution of conjugation chain lengths in a real sample (Kuzmany, 1980; Fitchen, 1982; Kuzmany *et al.*, 1982; Lefrant, 1983; Mulazzi *et al.*, 1985). It is based on the well-known fact that both the optical excitation threshold and the Raman-active C=C stretching frequency decrease with increasing chain length in finite polyenes. In this approach, the line-shape dispersion is interpreted as a resonance process in which the Raman cross section for short *trans* segments of a given sample are selectively resonantly enhanced for exciting energies above the gap. In other words, it is possible to account for the experimental results in terms of the electronic and dynamical properties of long and short chains weighted by a bimodal distribution. Here, the short chains contain about 20 double bonds, and long chains have about 100 double bonds. The abundance of short chains in this distribution is difficult to reconcile with the observed high conductivities in doped samples (implying extensive delocalization or long conjugation lengths) and with the evidence of extremely mobile solitons obtained from analysis of the NMR and ESR data. Otherwise, the "short-chain" model seems to be capable of explaining the dopant, polarization, history, and sample quality dependences of the line shape.

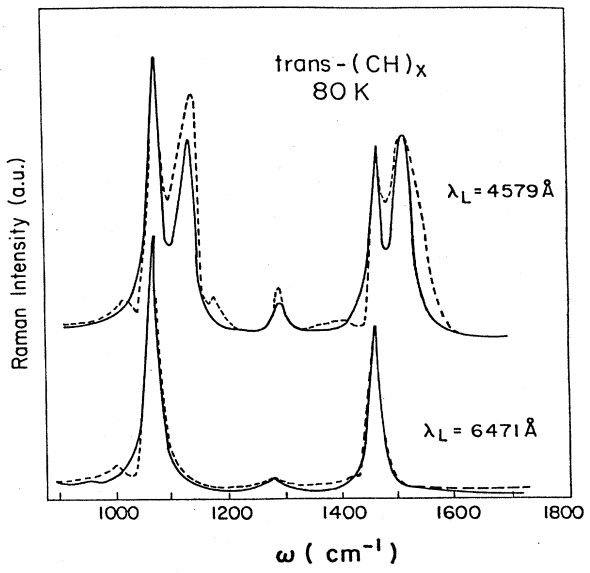

FIG. 36. Resonant Raman spectra from *trans*-$(CH)_x$: dashed line, experimental data; solid line, theoretical fit (from Mulazzi *et al.*, 1985).

A different origin of the Raman dispersion has been proposed: a distribution in the electron-phonon coupling constant λ, $p(\lambda)$, arising from disorder in the imperfect samples (Vardeny, Ehrenfreund, *et al.*, 1983, 1985; Horovitz *et al.*, 1984). Other parameters being fixed, λ uniquely determines the energy gap $2\Delta(\lambda) = W\exp(-1/2\lambda)$ and the phonon frequencies. In the analysis of Vardeny and co-workers, independent of the exciting frequency ω_L, the primary peaks correspond to the maximum of $p(\lambda)$ at $\lambda=\lambda_0$, whereas the satellite peak results from the resonance condition $\hbar\omega_L = 2\Delta(\lambda) > 2\Delta(\lambda_0)$. With a very narrow simple Lorentzian distribution (with width only about 6% of the peak value), it is possible to explain all aspects of the observed spectra in detail (Vardeny, Ehrenfreund, *et al.*, 1983, 1985; Horovitz *et al.*, 1984; see Fig. 36), including the sliced excitation profiles (Lauchlan *et al.*, 1983). The latter were inconsistent with the "short-chain" model (Harada *et al.*, 1980; Kuzmany, 1980; Lichtmann *et al.*, 1980; Fitchen, 1982; Kuzmany *et al.*, 1982; Lefrant, 1983; Mulazzi *et al.*, 1985). The distribution in λ arises from finite localization lengths, which in turn are due to disorder. Thus the $p(\lambda)$ model can be viewed as a somewhat more sophisticated attempt to include the "short-chain" effects. We note, however, that the particle-in-a-box picture of the "short-chain" model is certainly oversimplified. In reality, the localization lengths must be energy dependent, with more extensive delocalization in the band center than near the band edge. At present, there is no deeper theoretical understanding of the origin of $p(\lambda)$.

As a result of the $p(\lambda)$, one can experimentally probe the dependence of the energy gap on λ through an analysis of the Raman scattering data. When this was done (Vardeny, Ehrenfreund, *et al.*, 1983; Horovitz *et al.*, 1984), an exponential dependence was inferred, in excellent agreement with Eq. (4.31), as shown in Fig. 37.

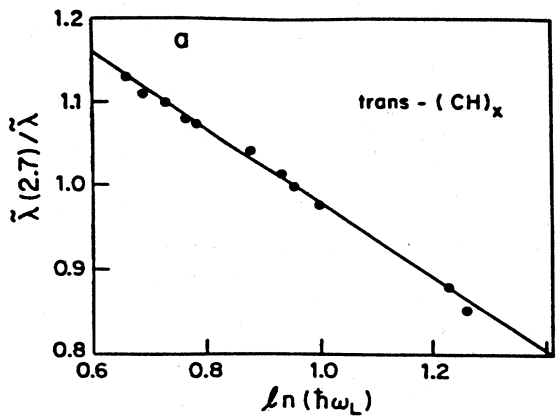

FIG. 37. The energy gap as a function of λ as inferred from analysis of the resonance Raman scattering data (from Vardeny, Ehrenfreund, *et al.*, 1983; Horovitz *et al.*, 1984).

There has also been a suggestion that the anomalous dispersion observed in the light scattering experiments was due to hot luminescence (rather than resonant Raman scattering; Mele, 1982). This interpretation was based on a numerical study of the lattice dynamics following the photoexcitation of an electron-hole pair above the band edge; it was found that a hot carrier tends to emit phonons with momentum specific to the carrier's energy. Since the phonon dispersion curves have a dip near the origin, $q \neq 0$ phonons have higher energies than the zero-momentum phonons. The satellite peaks were therefore identified with the phonons emitted by the hot carriers before the radiative recombinations take place. In contrast to the other two, this involves only intrinsic processes. However, since the importance of disorder has been established, it appears unlikely that hot luminescence is involved.

There is a common deficiency in the above approaches: a classical lattice is assumed. As we shall see, the quantum lattice fluctuations can give rise to subgap absorption even (as if from a distribution of gaps) for a fixed coupling constant in a fixed chain (see Sec. VIII.A). This intrinsic contribution to the energy-gap distribution is of fundamental interest, for it involves nonlinear ground-state fluctuations. The effect of such nonlinear ground-state fluctuations on the resonance Raman dispersion has not been calculated; it may be a source of "intrinsic disorder" and thus contribute to $p(\lambda)$.

3. Solitons in *trans*-$(CH)_x$: Photoexcitation experiments

Photoexcitation studies of conducting polymers were stimulated by the molecular dynamics calculations (summarized in the previous section), which demonstrated that in *trans*-$(CH)_x$ an electron-hole pair should evolve into a pair of solitons within an optical-phonon period, or about 10^{-13} s (Su and Schrieffer, 1980). Thus the absorption spectrum was predicted to change as oscillator strength shifts from $\hbar\omega_1$ to $\hbar\omega_s$ (see Fig. 38) on a time scale of 10^{-13} s after photoexcitation. Studies of the IRAV modes, midgap absorption, and electron-spin resonance following photoexcitation have confirmed the Su-Schrieffer mechanism (Su and Schrieffer, 1980) and provided detailed insight into the dynamics and subsequent recombination process.

a. Infrared-active vibrational modes

Photoinduced absorption has been reported arising from infrared-active vibrational modes (Blanchet, Fincher, Chung, and Heeger, 1983; Vardeny, Orenstein, and Baker, 1983a, 1983b). Three vibrational modes with large oscillator strength are observed. In the "amplitude mode" formalism (Horovitz, 1982), these correspond to the coupling of the three lattice degrees of freedom of the $(CH)_x$ chain (that modulate the dimerization amplitude and, thus, are resonantly enhanced in Raman scattering) to the zero-frequency uniform translational freedom of the charge. For a more general discussion, see Sec. IV.G. The existence of the photoinduced IRAV mode provides experimental proof that a localized lattice distortion is generated via photoexcitation. Moreover, the one-to-one correspondence between the principal IRAV modes, photoinduced (Blanchet, Fincher, Chung, and Heeger, 1983; Vardeny, Orenstein, and Baker, 1983a, 1983b) and doping-induced (Fincher, Ozaki, Heeger, and MacDiarmid, 1979; Rabolt *et al.*, 1979; Etemad, Pron, *et al.*, 1981) indicates that the same charged species is produced in both cases. The photoinduced IRAV spectrum is shown in Fig. 39.

The doping-induced IRAV mode at ~ 900 cm^{-1} was identified (Blanchet, Fincher, Chung, and Heeger, 1983) as the "pinned" uniform translation mode (or the Goldstone mode), the pinning being the result of the Coulomb attraction of the charged soliton to the charged counter ion. The large shift of the lowest-frequency IRAV mode upon photoexcitation, from ~ 900 cm^{-1} (Fincher, Ozaki, Heeger, and MacDiarmid, 1979) to ~ 540 cm^{-1} (Blanchet, Fincher, Chung, and Heeger, 1983), is consistent with more weakly pinned photogenerated charges. Re-

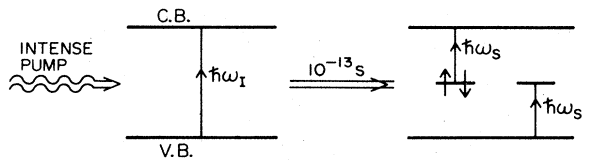

FIG. 38. A photopump makes electron-hole pairs, which evolve in 10^{-13} s to soliton pairs with states at midgap. The oscillator strength shifts accordingly. Analogous diagrams can be drawn for the case of polarons or bipolarons.

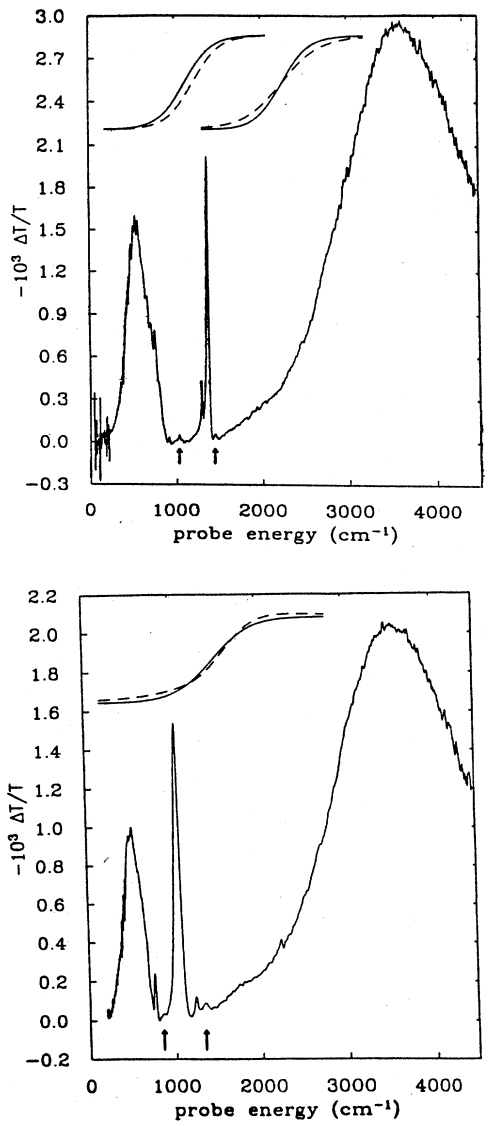

FIG. 39. Comparison of the infrared photoinduced absorption spectra for *trans*-$(CH)_x$ and *trans*-$(CD)_x$. (a) Photoinduced absorption of *trans*-$(CH)_x$ between 40 and 4500 cm^{-1}. The arrows indicate new absorptions at 1034 and 1438 cm^{-1}. The upper insets are schematic representations of the first (Goldstone) and second (breathing) modes of a soliton. (b) Photoinduced absorption of *trans*-$(CD)_x$ between 200 and 4500 cm^{-1}. The arrows indicate new absorptions at 858 and 1340 cm^{-1}. The upper inset is a schematic representation of the third bound mode of a soliton. From Schaffer *et al.* (1987).

cently, this frequency has been associated with the vibrational mode of a pair of oppositely charged solitons on separate chains. They are pinned to each other by mutual electrostatic attraction (Su, 1987).

A series of elegant calculations (Ito *et al.*, 1984; Ito and Ono, 1985; Mele and Hicks, 1985; Sun *et al.*, 1985; Terai *et al.*, 1985, 1986; Terai and Ono, 1986; Chao and Wang, 1987), based on the SSH Hamiltonian and its continuum version, predicted infrared activity due to the coupling of these same three lattice degrees to a soliton shape-modulation mode, i.e., one having nonuniform translation of the soliton (see Sec. IV.G). The observation of these extra absorptions in both $(CH)_x$ and its deuterated analog $(CD)_x$ has been reported (Schaffer *et al.*, 1987), with results in good agreement with the energies and weak oscillator strengths predicted.

Alternative explanations for these "weak modes" have been proposed (Vardeny, Ehrenfreund, Brafman, Horovitz, *et al.*, 1986). Weak absorptions have been independently reported (at energies slightly lower than those in Fig. 39) that disappear upon isomerization of samples. These absorptions were ascribed to the localization of charged solitons near structural defects such as chain ends or *cis* segments (Vardeny, Ehrenfreund, Brafman, Horovitz, *et al.*, 1986). In this case, the structural defect breaks the translational symmetry of the infinite polyacetylene chain; thus the selection rule preventing ir activity of the second (amplitude oscillation) mode of the soliton would be invalidated. However, detailed comparison of the weak modes as a function of isomerization for both Durham polyacetylene and Shirakawa polyacetylene indicates that the small absorptions are intrinsic to charged-soliton defects in *trans*-polyacetylene (Schaffer *et al.*, 1987).

The existence of these model-specific localized phonon modes (which couple to the nonuniform translation of the soliton) and the agreement with the predicted energies and weak oscillator strengths provide important confirmation of the accuracy of the electron-phonon coupling model for describing the nonlinear soliton excitation in polyacetylene.

b. Photoinduced absorption and photoconductivity

The photoexcitation of soliton-antisoliton pairs implies the photogeneration of charged carriers with the associated formation of states deep in the gap. Time-resolved spectroscopy (Orenstein and Baker, 1982) has been used to observe the predicted absorption due to photogenerated intrinsic gap states in *trans*-$(CH)_x$. Two photoinduced absorption features are observed (both in time-resolved and in steady-state measurements), one at $\hbar\omega \sim 0.5$ eV and one at $\hbar\omega \sim 1.34$ eV. Detailed studies have demonstrated (Vardeny, Orenstein, and Baker, 1983a, 1983b) that the 0.5-eV photoinduced absorption is associated with a charged excitation (presumably the charged solitons), whereas the 1.35 eV is associated with an unexpected neutral excitation. The 0.5-eV feature scales in every way with the characteristic IRAV mode (same temperature dependence, same dependence on laser pump intensity, etc.) (Blanchet, Fincher, Chung, and Heeger, 1983; Vardeny, Orenstein, and Baker, 1983a, 1983b).

The time scale for photogeneration of gap states has been investigated. Using subpicosecond resolution, these

studies demonstrated that the gap states and the associated interband bleaching are produced in less than 10^{-13} s, consistent with the theoretical predictions (Shank *et al.*, 1982; Vardeny *et al.*, 1982; Vardeny, 1984; Rothberg *et al.*, 1986). Data showing subpicosecond photoinduced bleaching (Vardeny *et al.*, 1982) of the interband transition are shown in Fig. 40. Using even better time resolution, Shank *et al.* (1982, 1983) demonstrated that the onset and initial decay occurred on the predicted time scale.

As a result of the existence of 1.35-eV photoinduced absorption, the importance of the Su-Schrieffer mechanism (Su and Schrieffer, 1980) was questioned (Orenstein *et al.*, 1984); the dominant initial response was claimed to be the formation of a neutral exciton. In this model (Orenstein *et al.*, 1984), charged solitons are formed only as a by-product after diffusion of a few charged polarons (which result from electrons and holes initially on different chains) to the neutral-soliton defects already present in the sample. Although the implied decrease in the number of spins was *not* observed in light-induced ESR experiments (Moraes *et al.*, 1986), there was a clear need for information on the charged versus neutral excitation branching ratio in the picosecond time regime; transient photoconductivity measurements (Sinclair *et al.*, 1986; Bleier *et al.*, 1987) demonstrated the fast photoproduction of charged excitations with a relatively high quantum efficiency.

Figure 41 shows the transient photoconductivity (Sinclair *et al.*, 1986) due to a 1-μJ pulse at 2.1 eV with a bias field of 1.5×10^5 V/cm. The rise time of the signal is $\sim$50 ps. The observed rise time represents a convolution of the sampling head response time (25 ps), the laser pulse rise time (15 ps), the trigger jitter (15 ps), the rise time of the transmission line, and the rise time of the photocurrent. Thus the charge carriers are produced within picoseconds of optical excitation. The fast rise is followed by (approximately exponential) decay with a time constant of $\sim$300 ps; the ratio of the photocurrent at 1500 ps to that at 50 ps is 0.03. The experimental demonstration that the photoconductivity and the photoinduced change in optical absorption, $\delta\alpha(t)$, decay on the same time scale implies that the photogenerated charge carriers involve a major shift in oscillator strength, consistent with the proposed photogeneration of charged solitons.

The relationship between the photocurrent and the incident photon flux is given by

$$\sigma_{\rm ph}=(E/\hbar\omega)e\eta\varphi\mu\ , \tag{5.5}$$

where $(E/\hbar\omega)$ is the number of absorbed photons per unit volume, η is the quantum efficiency, φ is the probability to escape geminate (or early time) recombination, and μ is the mobility. Although only the product $\eta\varphi\mu$ can be determined from photoconductivity alone, the pi-

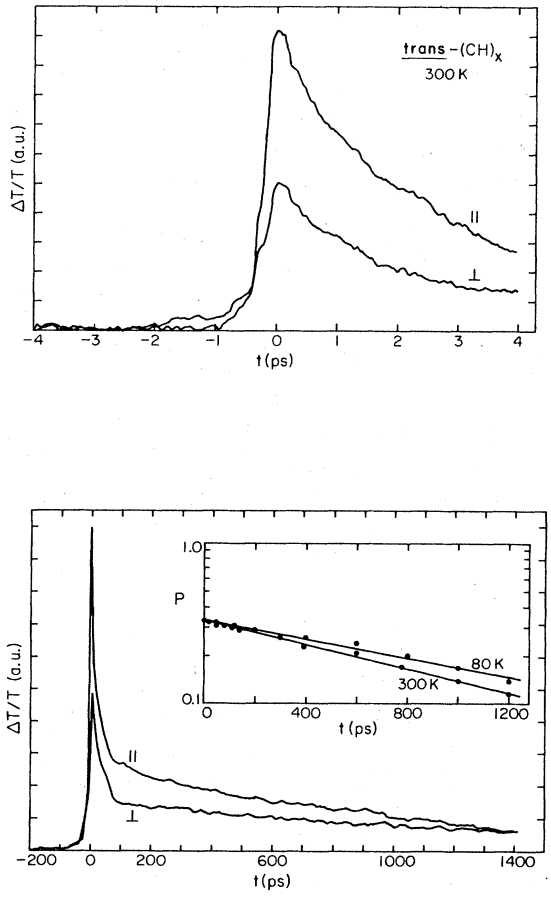

FIG. 40. Transient (picosecond) photoinduced bleaching of the interband transition in *trans*-$(CH)_x$: the oscillator strength shifts from the interband transition into the "midgap" transition (from Vardeny *et al.*, 1982).

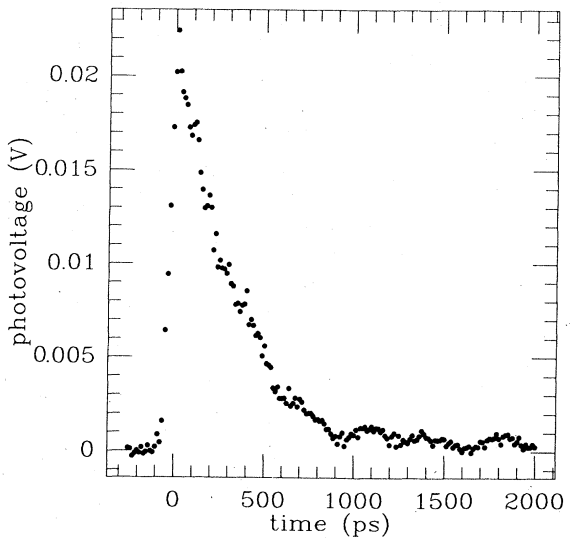

FIG. 41. Transient photovoltage across 50 Ω of *trans*-$(CH)_x$ in the Auston switch configuration. The peak value corresponds to a current density in excess of 10^3 A/cm^2 and a photoconductivity of $\approx$0.3 S/cm (from Sinclair *et al.*, 1986).

cosecond (Orenstein and Baker, 1982; Shank *et al.*, 1982; Vardeny *et al.*, 1982) and subpicosecond (Shank *et al.*, 1983; Shank, 1984) $\delta\alpha(t)$ data indicate that the number of photoexcitations has already decayed to less than 10^{-2} of the initial value at 50 ps. Thus the carrier yield at 50 ps is $\varphi \sim 0.01$. Using this value for φ together with $\sigma_{ph}(50\text{ ps}) = 0.3$ S/cm yields $\eta \sim 1$ and a mobility of approximately 1 $cm^2/V\,s$. With this value for the mobility, the net distance drifted in the measured decay time (300 ps) is about 400 Å, in good agreement with that inferred independently from the picosecond decay of photoinduced dichroism (Vardeny *et al.*, 1982).

The photoconductivity results, therefore, indicate a relatively high initial quantum efficiency for the fast photoproduction of charged nonlinear excitations, consistent with the Su-Schrieffer mechanism (Su and Schrieffer, 1980). The close agreement between the spectral onset of the absorption and high η photoconductivity is traditionally interpreted as ruling out the generation of neutral excitations as the *primary* excitations. Thus the photoconductivity data imply that the photoinduced absorption at 1.35 eV (due to neutral excitations) is generated as a *secondary process* during the rapid initial recombination of the photoinduced excitations.

The photoinduced absorption associated with the midgap transition has been time resolved (Rothberg *et al.*, 1986; pumping at 2.1 eV and probing the photoinduced absorption at 0.3–0.55 eV; see Fig. 42). In this experiment, the *intrachain* photogeneration of intrinsic charged solitons in *trans*-$(CH)_x$ was observed and information was obtained about their absorption spectrum and decay dynamics on a picosecond time scale. These intrachain soliton pairs, produced by the Su-Schrieffer mechanism (Su and Schrieffer, 1980), can be distinguished from charged solitons produced via an interchain absorption process (presumably leading initially to charged polarons on different chains); the latter are formed at later times either by neutral-to-charged soliton conversion or by the reaction

$$P^+ + P^+ \rightarrow 2S^+ \tag{5.6}$$

(or the negative counterpart) when two polarons of like charge diffuse onto a single chain. The direct study of charged-soliton dynamics complements the transient photoconductivity and the transient band-edge absorption and bleaching experiments.

A picture has been developed that is consistent with the results of all these experiments (Kivelson and Wu, 1986b; Sinclair *et al.*, 1986). The initial absorption is principally (>90%) intrachain. The midgap absorption due to charged solitons (0.45 eV), band-edge absorption (1.4 eV), and the bleaching of the interband absorption all decay on similar picosecond time scales with power-law decays. This fact and the large transient absorption strengths at both midgap and band edge (which demand quantum yields of order unity) suggest that these two absorptions are likely to arise from two different species in a single decay channel. A reasonable hypothesis is that charged soliton-antisoliton pairs are directly photogenerated within 10^{-13} s and begin to decay into neutral-soliton pairs (which must absorb at 1.4 eV) in several hundred femtoseconds. The neutrals in turn decay rapidly to phonons.

Thus there is clear and extensive evidence that charged solitons are produced both by charge transfer doping and by photoexcitation. There are two points of obvious importance which explicitly indicate the importance of electron-electron interactions: (i) The "midgap" transition peaks at about 0.75 eV for the doping-induced solitons and at about 0.5 eV for photogenerated solitons; (ii) in the case of photogenerated solitons, the relation $\hbar\omega_s = \Delta$ (as implied by Fig. 38) does not hold. Both of these result from electron-electron Coulomb repulsion. Since the relation $2\hbar\omega_s = E_g$ would hold in the absence of Coulomb interaction, the transition energies are shifted,

$$2\hbar\omega_s^{ph} = 2\Delta - U_s \ , \tag{5.7}$$

where U_s is an effective interaction describing the difference in Coulomb energy between initial state (charged soliton) and final state (neutral soliton plus band excitation). Note that $U_s \ll U$; see Eq. (7.22). From the experimental results for the interband and the photoinduced "midgap" absorptions (i.e., comparing either the onset of the two or the peaks), one finds 0.7 eV $< (2\Delta - 2\hbar\omega_s) = U_s < 0.9$ eV. For doping-induced solitons,

$$2\hbar\omega_s^{dop} = 2\Delta - (U_s - E_B) \ , \tag{5.8}$$

i.e., the shift of the transition by U_s is compensated by the Coulomb binding of the charged soliton to the dopant

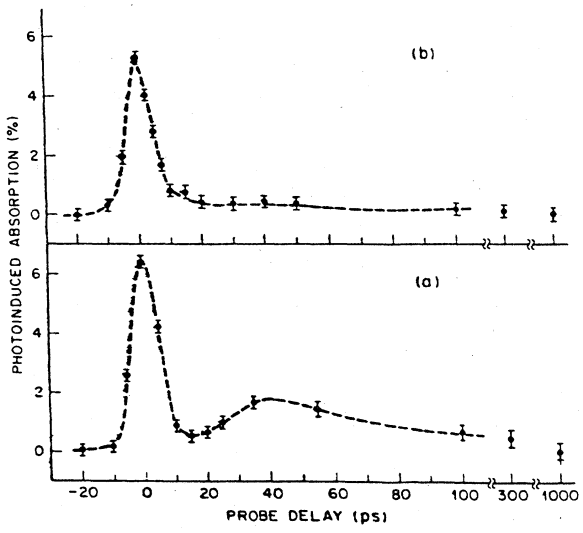

FIG. 42. Time-resolved photoinduced absorption of *trans*-$(CH)_x$ in the "midgap" spectral range: (a) 25 K, (b) 300 K. Dashed lines are to guide the eye (from Rothberg *et al.*, 1986).

counter ion (E_B). Since both U_s and E_B depend primarily on the spatial extent of the soliton, the two contributions approximately cancel.

The inferred value for U_s is consistent with the absence of a well-defined absorption below the gap in the case of neutral-soliton defects (Weinberger *et al.*, 1984). Since the transition energy for a neutral soliton would be

$$2\hbar\omega_s^N = 2\Delta + U_s \ , \tag{5.9}$$

the implied transition would be at about 1.35 eV, consistent with the value obtained experimentally from the photoinduced absorption associated with the decay-product neutral excitations.

c. The reversed spin-charge relations: Photogeneration of spinless charged solitons

Light-induced ESR experiments (i.e., electron-spin resonance experiments carried out during photoexcitation, LESR) have demonstrated that the photogenerated excitations are spinless (Flood and Heeger, 1983; Moraes *et al.*, 1986). The results confirm the reversed spin-charge relation of solitons.

The methodology is to determine the number of photogenerated spins ($N_s^{\rm ph}$) directly from quantitative ESR measurements (using an NBS Ruby standard) during photoexcitation and to determine the number of photogenerated charges ($N_{\rm ch}^{\rm ph}$) from the strength of the photoinduced IRAV mode and the photoinduced 0.45-eV "midgap" absorption, these photoinduced infrared features being calibrated through direct comparison with the corresponding doping-induced spectral features (where the dopant concentration is known).

LESR experiments have set an upper limit on the number of photogenerated spins. At a pump power of 20 mW/cm^2, any increase in the number of spins is less than or equal to 0.1% of the number of dark spins, corresponding to a concentration of $y_s^{\rm ph} < 3\times10^{-7}$ per carbon. Two independent calibrations have been carried out (Fincher, Ozaki, Heeger, and MacDiarmid, 1979; Hoffman, 1984) on the intensity of the IRAV mode as a function of doping concentration. In separate experiments, the midgap transition has been calibrated (Feldblum *et al.*, 1982). Using these data, the strength of the photoinduced infrared signatures (compared at the same pump power) set limits on the concentration of photogenerated charges: $10^{-4} < y_{\rm ch}^{\rm ph} < 5\times10^{-4}$. Thus, even using the smallest number for $y_{\rm ch}^{\rm ph}$, the ratio $y_s^{\rm ph}/y_{\rm ch}^{\rm ph} < 3\times10^{-3}$, indicating that the *photogenerated charge carriers are spinless.*

There appear to be two relevant time scales for the photoexcitation and decay processes in *trans*-$(CH)_x$: the picosecond regime during which the intrachain charged photoexcitations are produced (the Su-Schrieffer mechanism) and undergo initial rapid decay and the long-time behavior ($t > 10^{-9}$ s) during which the residual excitations are trapped and slowly decay. After 10^{-9} s, only a few percent of the initial photoexcitations remain. It is these trapped long-lived excitations that are observed in the steady-state photoinduced absorption and LESR experiments and that are responsible for the long-time tail in the photoconductivity.

In addition to the intrachain excitation processes, photoexcitation of electron-hole pairs on neighboring chains is expected to occur with a finite probability because of the finite interchange bandwidth. Such *interchain* pairs would form polarons and/or weakly bound excitons. Although the magnetic properties expected for photogenerated polarons are not observed (Moraes *et al.*, 1986), such interchain excitations may play a transient role in the formation of the charged solitons which are observed at long times. As these polarons diffuse along and between chains, they will form solitons in two ways: (a) two polarons with the same charge on a single chain will lead to a pair of metastable charged solitons; (b) a polaron on a chain with a preexisting neutral defect will convert the neutral soliton into a charged soliton. The first process appears to be the dominant one; it involves no change in the net number of spins and therefore is consistent with the LESR data (Flood and Heeger, 1983; Moraes *et al.*, 1986). This is also consistent with the observation of photoinduced bleaching only above the band edge (Colaneri *et al.*, 1988), as expected when the photogenerated soliton states are formed from band states [mechanism (a)] rather than by conversion of a neutral soliton [mechanism (b)].

We note that a soliton-antisoliton pair with like charge on a chain is metastable; the pair can only be annihilated by an oppositely charged pair on the same chain. This may account for the long lifetime of the residual charged solitons observed in the steady-state photoinduced absorption.

C. Transport

1. General comments

Although high electrical conductivity (as well as the ability to control the conductivity over many orders of magnitude through doping) has been a major stimulus to interest in the field of conducting polymers, progress toward understanding of the mechanisms involved has been slow. The difficulties rise principally from the complex morphology and the incomplete crystallinity (see Sec. II; Chroboczek and Summerfield, 1983; Chance *et al.*, 1984; Epstein *et al.*, 1984; Feldblum *et al.*, 1984; Conwell, 1985a, 1985b, 1987).

After heavy doping to the regime of highest conductivity (Basescu *et al.*, 1987, 1988; Naarmann, 1987a, 1987b; Naarmann and Theophilou, 1987), many of the properties of polyacetylene are clearly and unambiguously those of a metal (see the discussion in Sec. II). For example, there is a temperature-independent Pauli (spin) susceptibility (Epstein *et al.*, 1981; Moraes *et al.*, 1985), there is a term in the specific heat that is linear in tem-

perature (Moses *et al.*, 1980), the thermoelectric power is linear in temperature (Park *et al.*, 1979); analysis of these results leads to a value for the metallic density of states consistent with a broad-bandwidth metal. Nevertheless, in such samples, the temperature dependence of the resistivity is not metal-like; typically $\rho(T)$ *increases* as the temperature is lowered. This has been attributed to "series resistance" associated with the interfibrillar contacts, etc., which limit the flow of charge across a macroscopic sample. As better-quality samples have become available, the room-temperature conductivity has been increasingly higher ($\sigma \approx 1.5\times 10^5$ S/cm was reported for iodine-doped polyacetylene) (Naarmann, 1987a; 1987b; Naarmann and Theophilou, 1987). However, the absence of a "metallic" temperature dependence implies that the intrinsic value is still higher. For conductivity values in the range of $<10^3$ S/cm, the anomalous temperature dependence can be rationalized in terms of phonon-assisted transport through localized states and across the interfibrillar contacts in the complex morphology. On the other hand, for values greater than 10^5 S/cm, a phonon-assisted mechanism is more difficult to understand.

At dilute doping levels, the intrinsic resistivity of the material appears to dominate. In this regime significant progress has been made toward pinning down a precise mechanism. The dopant concentrations at which the crossover to morphology-limited behavior occurs are difficult to determine. This, for example, is one of the reasons why such a fundamental question as the possibility of a contribution to the dc transport by mobile charged solitons remains unsettled.

2. Intersoliton electron hopping

A specific soliton-related transport mechanism appropriate to the regime of dilute doping has been proposed: phonon-assisted electron hopping between soliton midgap bound states (Kivelson, 1981, 1982, 1983). The key feature of the intersoliton hopping theory (which distinguishes it from other hopping models that do not involve solitons) is that transport of charge occurs through *energetically equivalent levels that are at gap center.* This is in contrast, for example, with polaron hopping models which involve excitation from localized states near the band edge into band states. At light doping concentrations, moving a charged soliton far from the accompanying ion requires an activation energy, but a neutral soliton can always move freely along a chain without costing energy. If a neutral soliton moves past a charged soliton on a neighboring chain, there is a finite probability that the electron will hop from the neutral defect into the empty state of the neighboring charged (positive) soliton. At the time of the hopping, both solitons must be near (within a soliton width $\sim 7a$) at least one dopant ion; this maintains local charge neutrality and ensures that the states are energetically equivalent.

The intersoliton electron hopping mechanism predicts the following (Kivelson, 1981, 1982, 1983).

(1) The average dc conductivity is

$$\sigma_{\rm dc}(T,P)=(A/N)[e^2\gamma(T)/k_BT](\xi/R_0^2) \times[(y_n y_{\rm ch})/(y_n+y_{\rm ch})^2] \times\exp(-2BR_0)/(\xi)\ , \tag{5.10}$$

where $A=0.45$, $B=1.30$ are dimensionless numbers, $\xi=(\xi_\parallel\xi_\perp^2)^{1/3}$ is the dimensional average decay length ($\xi_\parallel$ and $\xi_\perp$ are the in-chain and out-of-chain wave-function decay lengths, respectively, $\xi_\parallel\sim 7a\sim 10$ Å, $\xi_\perp\sim 3$ Å), and the typical separation between impurities at concentration $c_{\rm im}$ is

$$R_0=[(4\pi/3)c_{\rm im}]^{-1/3}\ . \tag{5.11}$$

The variables y_n and $y_{\rm ch}$ are the concentrations of neutral and charged solitons, respectively. The factor $(y_n y_{\rm ch})/(y_n+y_{\rm ch})^2$ is needed to turn a quantum-mechanical transition rate into a net transition rate. The temperature dependence of $\gamma(T)$ arises from the difference in energy between the initial and final solitons between which the electron hops. In general, this temperature dependence can be quite complicated, depending on the dynamical nature of the states between which the solitons hop. However, since the initial and final soliton states are degenerate, one expects

$$-k_BT^2[\partial\ln\sigma(T,P)]/(\partial T)\to 0 \ \text{ as } T\to 0\ . \tag{5.12}$$

Since $\gamma(T)$ is not expected to be exponentially activated but should be strongly temperature dependent, a phenomenological fit to a high power law, $\hbar\gamma(T)\sim 500\,(T/300)^{n+1}$, was used (Kivelson, 1981, 1982, 1983).

The equation for $\sigma_{\rm dc}(T,P)$ can be rewritten in the following form:

$$\sigma_{\rm dc}(T,P)=\sigma(T)\sigma(P)\ , \tag{5.13}$$

where $\sigma(T)=\text{const}\times T^n$. The predicted dependence of $\sigma(T,P)$ on temperature (T) and pressure (P) is separated into T-dependent and P-dependent factors. This factorization is one of the unique features of the mechanism (Moses *et al.*, 1981).

(2) The thermopower is

$$S=\pm(k_B/e)[(n+2)/2+\ln(y_n/y_{\rm ch})]\ , \tag{5.14}$$

where the $+$ or $-$ sign designates p type or n type.

(3) The ac conductivity within this model is

$$\sigma_{\rm ac}=K'(\omega/T)[\ln(D'\omega/T^{n+1})]^4\ , \tag{5.15}$$

where K' and D' are constants. It shows a strong temperature and frequency dependence.

Measurements of electrical conductivity and thermoelectric power as a function of temperature and pres-

sure have shown (Moses *et al.*, 1981) that the electrical conductivity $\sigma(T,P)$ can be separated into T- and P-dependent factors. The T dependence is consistent with a power law ($\sigma \sim T^n$), and the value of n obtained from the conductivity agrees with that inferred from the magnitude of the thermopower of p-type *trans*-$(CH)_x$. Detailed analysis of the data demonstrated that both the magnitude and the pressure dependence of $\sigma(T,P)$ are inconsistent with the variable-range hopping model usually applied to disordered semiconductors. From measurements of n-type *trans*-$(CH)_x$ near the compensation point, the thermopower S of dilute n-type *trans*-$(CH)_x$ shows opposite sign but the same magnitude of p-type *trans*-$(CH)_x$.

The frequency-dependent conductivity of polyacetylene has been measured (Epstein, 1986). Neutral *trans*-$(CH)_x$ and lightly iodine-doped *trans*-$(CH)_x$ have a "weakly" T-dependent dc conductivity and a strongly T-dependent ac conductivity. The results differ from the usual expectations of variable-range hopping and polaronic hopping but are in good agreement with the predictions of the theory of charge transport via intersoliton electron hopping.

The electrochemical voltage spectroscopy (EVS) method has been used to determine the energies of charge injection and removal, as well as the kinetics of these processes. The electrochemical data demonstrate that ~ 300 ppm of charge [equal to the number of neutral solitons in undoped *trans*-$(CH)_x$] are removed in a narrow range of energy near the gap center (Kaufman *et al.*, 1983; Kaufman, Chung, and Heeger, 1984). These charges are, therefore, transported through the polyacetylene electrode via hopping among states at midgap, in agreement with theory (Kivelson, 1981, 1982, 1983). The specific demonstration of charge transport in a narrow energy range about midgap rules out other hopping models that would involve either states near the band edge or a broad range of localized states distributed through the gap.

In summary, the temperature and pressure dependences of the electrical conductivity of *trans*-$(CH)_x$, together with the frequency dependence of the hopping conductivity and the electrochemical measurements, are able to give strong evidence for the intersoliton hopping mechanism and to rule out other mechanisms (like variable-range hopping). In lightly doped *trans*-$(CH)_x$, charge is neither transported among a distribution of band-gap impurity states nor among localized (polaron) states near a band edge. The transport occurs at midgap. The agreement between theory and experimental results (the power-law temperature dependence of the conductivity, with power index $n=13$, the magnitude and sign of the temperature-independent thermopower, the pressure-independent power index n, the large dc and ac conductivity with a "weakly" temperature-dependent dc conductivity and a strongly temperature-dependent ac conductivity) indicates that the electrical properties of *trans*-$(CH)_x$ at dilute doping levels are intrinsic and not determined by the complex morphology.

VI. LIFTING THE DEGENERACY

A. Summary of theoretical results: Ground state and excitations

Lifting of the ground-state degeneracy leads to important changes in both the ground-state properties and the excitations.

(1) As a result of the one-electron crystal potential which lifts the degeneracy, the energy gap is not solely the result of the intrinsic Peierls instability (Δ_i) but also has a contribution (Δ_θ) from the one-electron crystal potential (Brazovskii and Kirova, 1981),

$$\Delta = \Delta_i + \Delta_e \ . \tag{6.1}$$

(2) Solitons are no longer proper excitations of the system. The nondegenerate ground state confines the soliton-antisoliton pairs into bipolarons. Polarons remain as possible excitations as well. The bipolaron can be thought of as a confined pair of charged solitons; the polaron can be thought of as a charged soliton bound (via confinement) to a neutral soliton (Brazovskii and Kirova, 1981; Heeger, 1981; Campbell and Bishop, 1982; Campbell *et al.*, 1986).

The fundamental origin of this "confinement" can be seen in simple terms (Heeger, 1981). Consider, for example, the structure of *cis*-polyacetylene shown in Fig. 1. In such a structure, the ground state is not degenerate [as shown schematically in Fig. 1(c)]. The energy difference between the two ground states ($\Delta E/l$) per bond would be finite. An obvious consequence of the lack of degeneracy is that such a structure cannot support stable, free-soliton excitations, since creating a soliton pair separated by a distance d would cost energy $\sim d(\Delta E/l)$, i.e., the system would be in the "high-energy" configuration over the distance between the two kinks. This linear "confinement" energy leads to bipolarons as the lowest-energy charge transfer configurations in such a chain, with creation energy somewhat greater than $(4\Delta/\pi)$ (the creation energy for a bipolaron goes to $4\Delta/\pi$ in the limit of zero confinement). The corresponding energy-level diagram (for a positive bipolaron) is sketched in Fig. 43. The two gap states are empty for a positive bipolaron (charge $2e$) and filled for a negative bipolaron (charge $-2e$) (Brazovskii and Kirova, 1981; Heeger, 1981; Campbell and Bishop, 1982; Fesser *et al.*, 1983).

Quantum chemical calculations of the electronic structure of the bipolaron have been carried out on specific polymers (e.g., polyparaphenylene, polypyrrole, and polythiophene; Brédas *et al.*, 1981a, 1981b, 1984; Epstein, 1986). The results provide insight into the origin of the bipolaron. Since pulling charge off a benzene ring favors the quinoid over the (aromatic) benzenoid structure, the polaron structure sketched for poly(paraphenylene) in Fig. 44(a) can be understood as a "quinoid-like" region induced onto a spatially localized region of the polymer by charge transfer.

An analogous diagram can be drawn for polythiophene

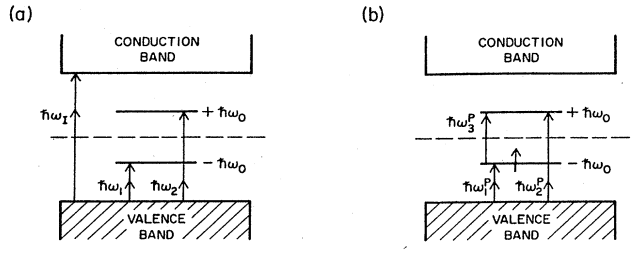

FIG. 43. Band diagrams for bipolarons and polarons, showing the localized gap states and their occupancy. (a) Bipolaron: the two gap states, the interband ($\hbar\omega_I$) and subgap ($\hbar\omega 1$ and $\hbar\omega_2$) transitions are shown; (b) polaron: the gap states are partially filled (e.g., one electron in the lower level for a positive polaron), leading to a third subgap absorption subsequent to polaron formation.

[Fig. 44(b)]. If one purposely leaves out the sulfur heteroatom, the resulting backbone structure is that of an sp^2p_z polyene chain consisting of four carbon all-*trans* segments linked through a *cis*-like unit. In such a structure, the ground state is not degenerate (see Fig. 45). However, the energy difference per bond, ($\Delta E/l$), might be expected to be small, i.e., greater than zero but perhaps comparable to that of *cis*-$(CH)_x$.

Polarons are known to be valid excitations both for degenerate-ground-state systems and for polymers in which the degeneracy has been lifted. In the degenerate-ground-state case, the energy for creation of a polaron E_p is given by (see Sec. IV.E)

$$E_p = 2^{1/2}(2\pi/\Delta) = 2^{1/2}E_s \ , \tag{6.2}$$

so that, for example,

$$P^+ + P^+ \Longrightarrow S^+ + \bar{S}^+ \ , \tag{6.3}$$

where P^+ denotes a positive polaron, and S^+ and $\bar{S}^+$ denote a positively charged soliton and antisoliton, respectively. Polaron excitations in such systems have

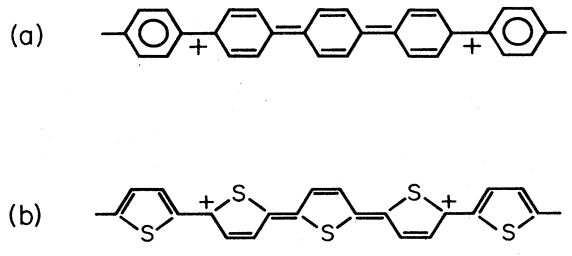

FIG. 44. Schematic structural diagrams of bipolarons: (a) a doubly charged bipolaron on a poly(paraphenylene) chain; (b) a doubly charged bipolaron on a polythiophene chain.

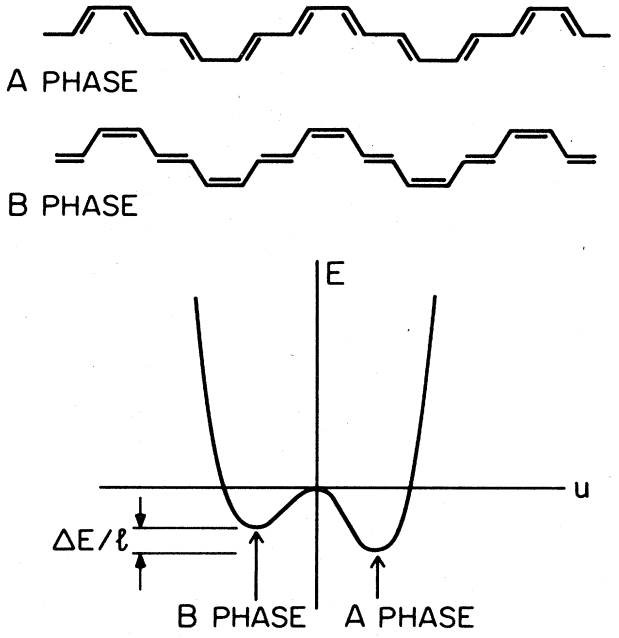

FIG. 45. The two schematic bond structures of a polyene analogous to *cis*-$(CH)_x$: *A* phase, the *cis*-transoid configuration; *B* phase, the higher-energy *trans*-cisoid configuration. The *B*-phase cinfiguration has greater energy per CH unit and thus in the infinite polymer is infinitely higher in energy than the *A* phase. The diagram below shows the two inequivalent minima associated with the two nondegenerate configurations.

energy-level diagrams similar to that sketched in Fig. 43(b). In the polaron case, however, the gap states are partially filled (e.g., one electron in the lower level for a positive polaron), leading to a third subgap absorption subsequent to polaron formation.

When the degeneracy is lifted, the confinement leads to the energy-level diagrams in Fig. 43(a). In this case, although the bipolaron energy is greater than that of two solitons (because of confinement), the energy for creation of a confined soliton pair (bipolaron) remains less than that for two polarons (Brazovskii and Kirova, 1981; Brédas *et al.*, 1981a, 1981b, 1984; Campbell and Bishop, 1982; Fesser *et al.*, 1983; Epstein, 1986):

$$E_B < 2E_p \ , \tag{6.4}$$

so that, for example,

$$P^+ + P^+ \Longrightarrow B^{2+} \ . \tag{6.5}$$

To model the explicit lifting of the ground-state degeneracy, the following term can be added to the SSH Hamiltonian (Brazovskii and Kirova, 1981):

$$\Delta H = t_e \sum_{n,s} (-1)^n (c^\dagger_{n,s} c_{n+1,s} + c^\dagger_{n+1,s} c_{n,s}) \ . \tag{6.6}$$

The effect of t_e is to modulate the one-electron potential,

thereby giving rise to a one-electron energy gap even in absence of a lattice distortion. The Brazovskii-Kirova (BK) continuum Hamiltonian then becomes (leaving out the kinetic energy term)

$$H_{\rm BK}=\int dx\ \psi(x)[-iv_F\sigma_y\partial/(\partial x)+\Delta(x)\sigma_x]\psi(x) + \int dx\,[\Delta(x)-\Delta_e]^2/\pi\lambda v_F\ . \quad (6.7)$$

The term Δ_e is a constant, which is proportional to t_e.

The fermion field ψ is a two-component spinor in which the upper (lower) component corresponds to amplitudes on the even (odd) sites. The notation here is related to that of the other sections by a rotation in the spinor space.

The Bogoliubov–de Gennes equations can be solved explicitly for the following family of solutions (Brazovskii and Kirova, 1981; Campbell and Bishop, 1982):

$$\Delta(x)=\Delta+k_0v_F\{\tanh[k_0(x-x_0)] -\tanh[k_0(x+x_0)]\}\ , \quad (6.8)$$

where k_0 and x_0 are related by

$$k_0v_F\coth(2k_0x_0)=\Delta\ . \quad (6.9)$$

The two discrete states are located at energies $\pm\varepsilon_0$, where

$$\varepsilon_0=(\Delta^2-k_0^2v_F^2)^{1/2}\ . \quad (6.10)$$

The total energy of the system in configuration (6.8) is given by

$$E_p=(4/\pi)[(1-\gamma)k_0v_F+2\gamma\Delta k_0x_0+\varepsilon_0\sin^{-1}(\varepsilon_0/\Delta)] +(n_+-n_-)\varepsilon_0\ , \quad (6.11)$$

where $\gamma=(\Delta_e/\lambda\Delta)$, which measures the relative weight of the extrinsic gap parameter, is called the confinement parameter, and n_+ (n_-) are the occupation numbers of the upper (lower) gap states. Minimizing the total energy with respect to ε_0 or x_0 leads to a configuration that can be shown to satisfy the self-consistent gap equation, which therefore represents the equilibrium configuration. The bipolaron configuration is similar to that of a polaron with a deeper depression in the middle. The two gap states are either both totally occupied or both totally empty [Fig. 43(a)]. Therefore the bipolaron is a doubly charged spinless carrier; it plays a major role in nondegenerate conjugated polymers.

From a bipolaron, we can construct a triplet polaron by taking one electron (with the same spin) out of each gap state. This does not affect the total energy, so the lattice configuration remains the same. The result of the operation is a neutral polaron in the triplet state, i.e., the lowest triplet excited state. Electron-electron repulsions tend to stabilize the neutral polaron, while they tend to destabilize the bipolaron (relative even to the charged polaron). The polaron solution in *trans*-polyacetylene is obtained by taking γ to be zero and (n_+-n_-) to be -1.

Because of the topological constraint, it is impossible for a soliton to hop from one chain to a nearby chain, whereas it is possible for a polaron or bipolaron. Therefore, polaron or bipolaron hopping may be especially important for three-dimensional charge transport.

B. Bipolarons in polythiophene: A summary of experimental results

As described above, lifting of the ground-state degeneracy leads to confinement of soliton-antisoliton pairs into bipolarons with an energy-level structure shown in Fig. 43(a). The inequality expressed by Eq. (6.4) and the associated "reaction" [Eq. (6.5)] are particularly important; bipolaron (and not polaron) formation can occur only if these are correct. Once again, there are three important experimental signatures of bipolaron formation. (1) The formation of localized structural distortions with associated localized vibrational modes (IRAV modes) in the midinfrared. (2) The generation of the symmetric gap states and the associated electronic transitions [see Fig. 43(b)]. These characteristic bipolaron-induced transitions can be observed in the near infrared.

(3) The reversed spin-charge relation, i.e., charge storage in *spinless* bipolarons. Each of these features has been verified in experiments carried out on polythiophene both after doping and during photoexcitation.

1. Bipolarons (and polarons) in polythiophene: Charge transfer doping

a. Infrared-active vibrational modes

Initial doping experiments (Hotta *et al.*, 1984/1985; Hayes *et al.*, 1985) showed the existence of four IRAV modes at 1020, 1120, 1200, and 1323 cm^{-1}, and additional weaker modes at 640, 680, and 730 cm^{-1}. As with polyacetylene, a comparison of the doping-induced IRAV modes with those produced by the cleaner technique of photogeneration is important. We defer the analysis of the IRAV modes until Sec. VI.B.2, where the results of the photoexcitation experiments are summarized. Once again, we emphasize that the existence of the IRAV modes is definitive evidence of the formation of structural distortions around the charge storage configuration(s) in polythiophene.

b. Symmetric gap states and associated electronic transitions

Figure 46 shows a series of absorption spectra taken *in situ* during electrochemical doping (Chung *et al.*, 1983). As the doping cycle proceeded via the reaction

$$(T)_x+xy\,\mathrm{LiClO_4}\rightarrow[T^{+y}(\mathrm{ClO_4})^-_y]_x+xy\,\mathrm{Li}\ , \quad (6.12)$$

the intensity of the interband transition decreased continuously and the absorption peak shifted toward higher energy. In addition, the two new absorption features appeared in the ir below the gap edge with intensities that

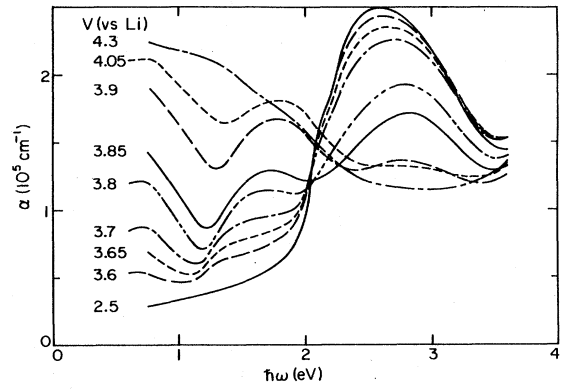

FIG. 46. *In situ* absorption curves for polythiophene during electrochemical doping with $(ClO_4)^-$. The applied voltages (vs Li) are shown on the left. The corresponding concentrations are as follows (in mol% per thiophene ring): 3.60 V ($y=0.028$), 3.65 V ($y=0.04$), 3.70 V ($y=0.054$), 3.80 V ($y=0.096$), 3.85 V ($y=0.12$), 3.90 V ($y=0.14$), 4.05 V ($y=0.20$); from Chung *et al.*, 1983.

increased as the dopant level increased.

The lower-energy ir peak remains at constant energy (~ 0.65 eV), while the higher-energy peak shifts upward in energy as the dopant level is increased. At the highest doping levels, the frequency-dependent absorption is characteristic of the free-carrier spectrum of the metallic state, similar to that found in heavily doped polyacetylene.

Better accuracy was obtained by analyzing the difference spectra (Chung *et al.*, 1983). Two examples are shown in Fig. 47 at dopant concentrations of $y=0.04$ (or 1% per carbon) and $y=0.12$ (or 3% per carbon). The two dopant-induced infrared bands are seen clearly with peaks at $\hbar\omega_1=0.65$ eV and $\hbar\omega_2=1.5$ eV.

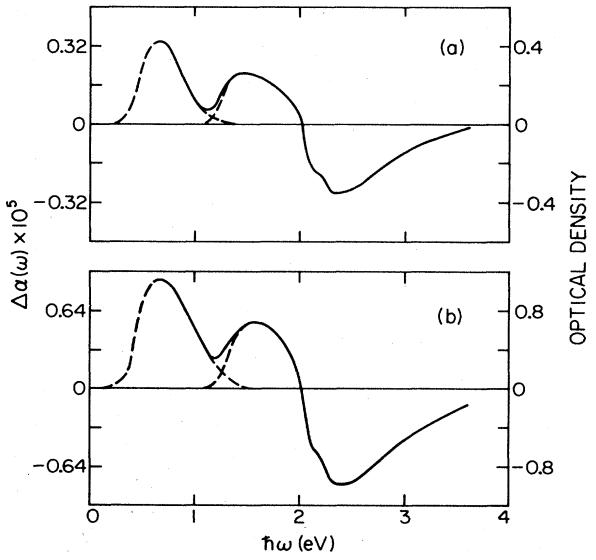

FIG. 47. Difference spectra obtained from Fig. 46: (a) $y=0.04$; (b) $y=0.12$. From Chung *et al.*, 1983.

Examination of Figs. 46 and 47 indicates that the oscillator strength of these two dopant-induced ir absorption bands is comparable to that of the midgap absorption in polyacetylene. We conclude, therefore, that these two absorption features arise from electronic transitions between the valence band and two localized levels that appear in the gap upon charge transfer doping, consistent with charge storage in bipolarons. The difference spectra also show clearly that the oscillator strength that appears below the gap edge comes primarily from the interband transition. In contrast to the case for *trans*-$(CH)_x$, the loss of interband oscillator strength is not uniform, but is greatest for frequencies near the band edge. This is in agreement with theoretical predictions for bipolaron doping (Campbell and Bishop, 1982; Fesser *et al.*, 1983).

The low-concentration regime (i.e., $y<0.01$) was studied in considerable detail in the case of poly(3-methylthiophene) (Harbeke *et al.*, 1985; Colaneri *et al.*, 1987). Evidence of a third absorption was presented, implying polaron formation (see Fig. 43) at these dilute concentrations. The existence of polarons at very dilute concentrations, going over to bipolarons at higher concentrations, means either that the inequality expressed in Eq. (6.4) is incorrect or that the reaction (6.5) is inhibited at very dilute concentrations (perhaps by disorder, finite chain length, etc.). In this context, note that injection of a single charge *must* always occur via the formation of polarons, with bipolarons resulting from the reaction expressed in Eq. (6.5). Thus, even in the case where the inequality (6.4) holds (or when the two energies are comparable), polarons can be expected at very dilute concentrations (Colaneri *et al.*, 1987), particularly in samples with a high degree of disorder and in samples with relatively low molecular weight (i.e., when the number of thiophene rings per chain is less than y^{-1}).

The absorption spectra of poly(3-methylthiophene), taken *in situ* during electrochemical doping (Harbeke *et al.*, 1985), are shown in Fig. 48. The spectrum of the neutral polymer (at 2.45 V vs Li) shows a band gap of about 2.1 eV, roughly comparable to that observed in polythiophene. At the higher doping levels (above ≈ 3 eV vs Li), two subgap absorptions are visible at ≈ 0.5 and ≈ 1.5 eV. Below about 3 eV a weak feature appears near 1.2 eV. Difference spectra on thicker films reproduce the earlier data (Chung *et al.*, 1981) on this system.

To determine whether or not the species introduced on doping carry spin, *in situ* ESR measurements were carried out during doping (Chen and Heeger, 1986b). The magnetic susceptibility was measured versus cell voltage (or chemical potential μ). At about the neutral point, a weak ESR signal is observed with $\chi<10^{-6}$ emu/mole. This corresponds to at most one spin per 10^3 backbone carbons, or <0.25 mol% per thiophene ring. If the cell is held at 2.5 V for several days, this value slowly decreases (eventually by an order of magnitude). On dop-

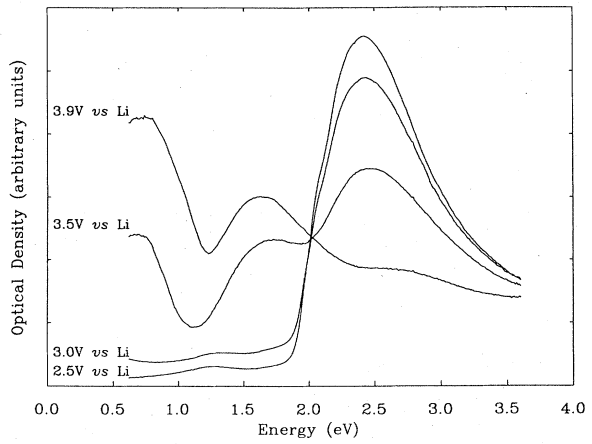

FIG. 48. Absorption spectra of poly(3-methylthiophene), taken *in situ* during electrochemical doping (from Harbeke *et al.*, 1985).

ing, a susceptibility maximum is observed (at about 3 V vs Li), corresponding to a value of $\approx 10^{-6}$ emu/mole; above 3.4 V vs Li, the susceptibility drops to a value less than 5×10^{-8} emu/mole. The conclusion is that the dominant charge storage configuration is the spinless bipolaron. Although polarons can be detected for μ in the gap (and below the principal injection threshold), the number of polarons never exceeds ≈ 0.2 mol%. Moreover, these polarons appear to be associated with localized defect states deep in the gap, and are therefore not the intrinsic self-localized charge storage configurations of the conjugated polymer chain. Above the injection threshold, the number of spins drops below one per 10^4 rings, consistent with charge storage in spinless bipolarons (see the following subsection; Colaneri *et al.*, 1987).

These concepts have been generalized and applied even to polymers in solution (Nowak *et al.*, 1987). The results of ESR and spectroscopic studies, *carried out in solution,* have been reported for the conducting polymer P3HT, poly(3-hexylthienylene), doped with ($NO^+PF_6^-$). The nature of the charge storage configurations were determined as a function of doping level and as a function of doped polymer concentration. The results indicate that the spinless bipolaron is the lowest-energy charge storage configuration on single P3HT macromolecules in dilute solution. Polarons are formed either as a result of an odd number of charges on a single polymer chain or as a result of interchain interactions (in the semidilute regime). The conclusion that the bipolaron is the lowest-energy charge storage configuration, together with the results of detailed analysis of the absorption spectra, indicates that electron-electron Coulomb correlations are relatively weak (compared with the difference in energy between a bipolaron and a pair of separated polarons), even for isolated conducting polymer chains in dilute solution. More generally, the results demonstrate that the novel concepts developed in the study of the solid-state properties of conducting polymers are directly applicable to such polymers in solution (Nowak *et al.*, 1987).

c. Electron-spin resonance measurements during electrochemical doping of polythiophene: Charge storage in spinless bipolarons

Electron-spin resonance measurements (Chen and Heeger, 1986b) have been carried out *in situ* during electrochemical doping of polythiophene with $(ClO_4)^-$, which we denote as $[T^{+y}(ClO_4^-)_y]_x$. The magnetic (spin) susceptibility is plotted in Fig. 49 as a function of ClO_4^- concentration. The susceptibility of the pristine sample was studied earlier (Kobayashi *et al.*, 1984) and shown to arise from a concentration of 250 ppm (per thiophene) defects with localized spins with a temperature dependence that followed Curie's law. The data of Fig. 49(a) show that χ *remains small throughout the dilute-to-intermediate doping regime,* increasing by only a

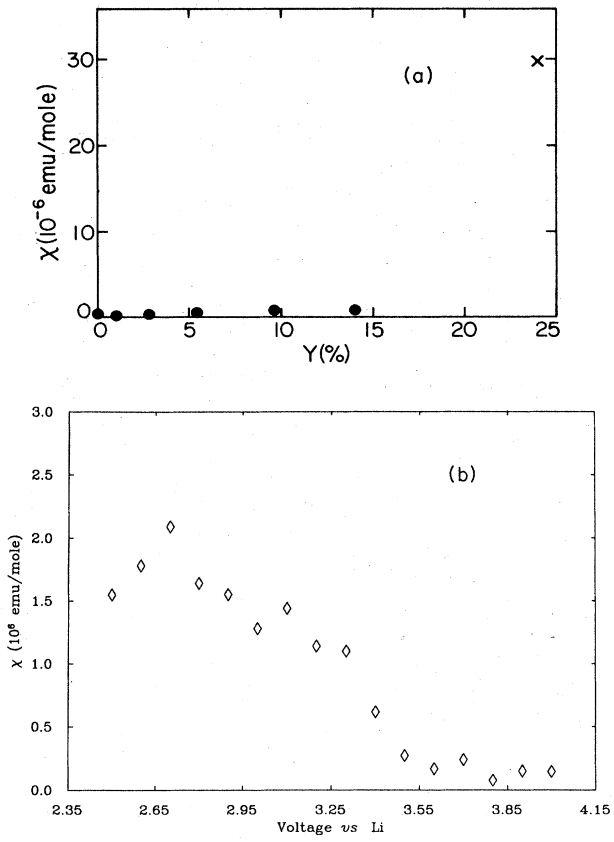

FIG. 49. Magnetic (spin) susceptibilities for polythiophenes: magnetic (spin) susceptibility χ of polythiophene as a function of dopant (ClO_4^-) concentration (from Chen and Heeger, 1986); (b) magnetic (spin) susceptibility χ of poly(3-methylthiophene as a function of dopant (ClO_4^-) concentration (from Colaneri *et al.*, 1987).

factor of 2 even at 14 mol %. As noted above, similar results were obtained from the 3-methyl derivative, as shown in Fig. 49(b).

A detailed study of the temperature dependence showed two contributions to χ: (1) the number of localized (Curie law) spins in $[T^{+y}(ClO_4)^-_y]_x$ remained constant at about 250 ppm (per thiophene), essentially unchanged from the neutral pristine sample, and (2) a small temperature-independent contribution was observed (e.g., $\chi_0 = 1.5 \times 10^{-7}$ emu per mole-thiophene at a dopant level of 5.4 mol %).

These susceptibility data indicate that charge is stored predominantly in a nonmagnetic configuration. At a molar concentration of 14%, $N_s/N_{ch} < 3 \times 10^{-3}$, where N_s is the number of localized spins as obtained from the Curie-law contribution to χ. No indication of polaron formation was observed, even at dilute concentrations. For example, a concentration of 1 mol % of polarons would correspond to a room-temperature susceptibility, a factor of 40 times greater than that of the pristine sample. *The spinless character of the charge storage configuration indicates that in polythiophene and in the P3AT derivatives, doping occurs via bipolarons.*

This clear evidence of bipolaron formation on doping is to be contrasted with the results reported for polypyrrole. From *in situ* ESR measurements, a major increase in the number of spins was observed on doping (Genoud *et al.*, 1985; Nechtschein *et al.*, 1986; Devreux *et al.*, 1987). At low doping concentrations, the data yielded a spin number comparable to the number of injected charges; at higher doping concentrations, the spin number decreased, extrapolating toward zero. Based upon these results, it appears that in polypyrrole the polaron and bipolaron energies are nearly degenerate. In that case, polarons would be favored at low concentrations because of increased entropy. As discussed in Sec. I, the proposed polaron-bipolaron degeneracy could arise if the Coulomb energy were sufficiently large. On the other hand, the data for polypyrrole are controversial; a decrease in spins on doping to a number below the level of detectibility has been reported in independent measurements. The differences in experimental results are evidently due to sample differences (Scott *et al.*, 1983; Kaufman, Colaneri, Scott, and Street, 1984; Devreux *et al.*, 1987).

We note once again that, since charge is initially injected as polarons, bipolarons can only be formed through the reaction defined in Eq. (6.5). Thus, even if the bipolaron configuration has the lowest energy, polarons can be kinetically metastable at dilute concentrations in low-molecular-weight samples in which defects and imperfections are sufficiently numerous to restrict polaron mobility and thereby inhibit the bipolaron formation reaction [Eq. (6.5)] (Colaneri *et al.*, 1987). Such effects may also be responsible for the initial increase in spins sometimes observed (Kaneto and Yoshino, 1984; Kaneto *et al.*, 1987) in studies of polythiophene.

The small temperature-independent Pauli susceptibility observed in polythiophene even at relatively dilute concentrations implies the existence of a finite density of localized states in the gap (due to disorder). Thus, although the charge is stored predominantly in nonmagnetic bipolarons, the transport may arise from a combination of bipolaron motion and electron hopping among the disorder-induced states in the gap (Epstein *et al.*, 1983; Kaneto and Yoshino, 1984; Kaneto *et al.*, 1987). In contrast to these results, the data obtained from carefully doped $[Na_y^+(CH)^{-y}]_x$ at concentrations below the first-order transition set an upper limit of $\chi_p < 10^{-8}$ emu/mole (Chen *et al.*, 1985; Moraes *et al.*, 1985; Chen and Heeger, 1986a). Therefore, in Na-doped polyacetylene, the analogous transport by electron hopping is ruled out by the absence of gap states. The implication is that in polyacetylene soliton transport makes a significant contribution to the electrical conductivity in the intermediate doping regime.

2. Bipolarons (and polarons) in polythiophene: Photoexcitation

The direct photogeneration of charged bipolarons is clearly impossible. After electron-hole photoinjection, the confinement resulting from the nondegenerate ground state will lead to rapid formation of a neutral "bipolaron," i.e., a neutral exciton with energy-level diagram analogous to Fig. 43 but with one electron in the upper and one electron in the lower gap state. Such neutral "bipolarons" can be expected to undergo rapid radiative decay. This is probably the dominant mechanism at early times. The observation of fast luminescence at $\hbar\omega$ just below the gap (1.9 eV) is consistent with this mechanism. Luminescence was observed in *cis*-$(CH)_x$ some time ago and attributed to the same mechanism (Lauchlan *et al.*, 1981; Hattori *et al.*, 1984). This recombination luminescence is rapidly quenched, however, by competing nonradiative processes leading to luminescence lifetimes in the picosecond regime (Danielson and Ball, 1985).

Because of the transverse bandwidth due to interchain coupling, some of the initial photoexcitations occur as electrons and holes on different chains. Chain distortions will quickly form around these single charges, leading to polaron formation. Bipolarons can then be generated (if energetically favorable) by the standard reaction [Eq. (6.5)].

a. Infrared-active vibrational modes

The photoinduced IRAV spectrum of PT (Moraes *et al.*, 1984; Schaffer and Heeger, 1986) is shown in Fig. 50(a). In addition to the strong T modes at 1020, 1120, 1200, and 1323 cm^{-1}, photoinduced absorptions (R modes) are observed at 690, 728, and 782 cm^{-1} with even weaker features at 900 and 1435 (possibly a doublet) cm^{-1}. As is the case in polyacetylene, the one-to-one correspondence between the principal IRAV mode ob-

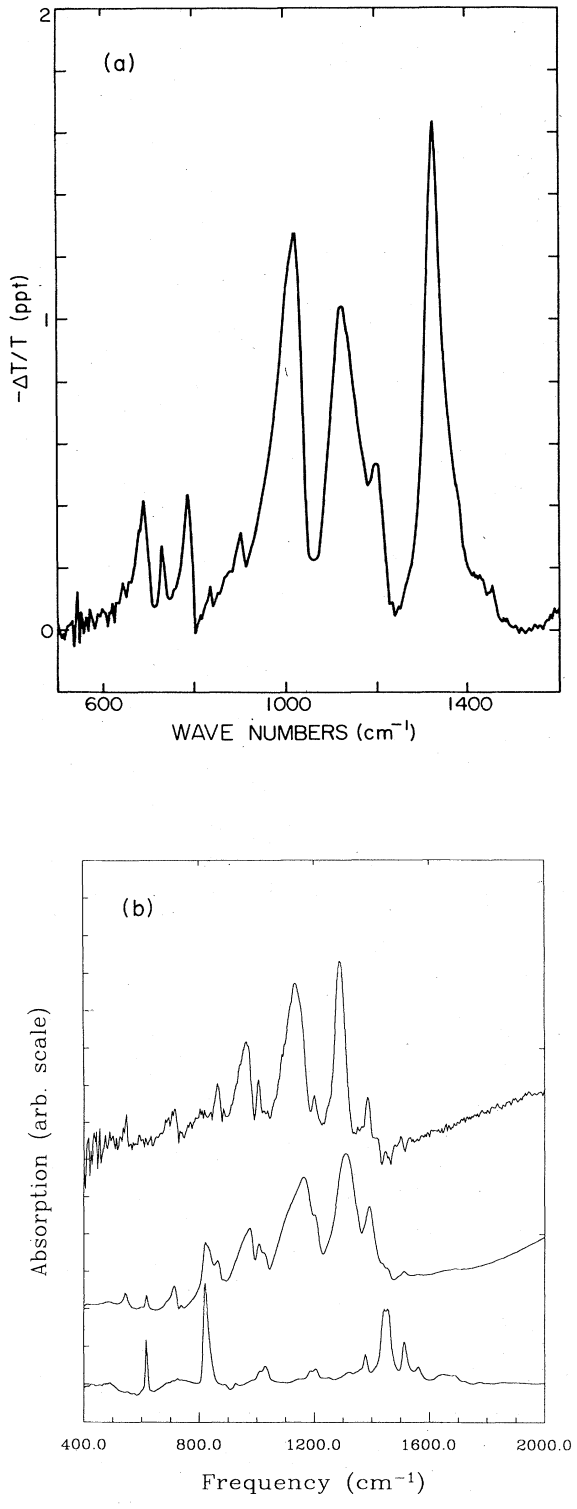

FIG. 50. Photoinduced infrared spectra for polythiophene and poly(3-methylthiophene): (a) photoinduced IRAV spectrum of polythiophene (Schaffer and Heeger, 1986); (b) detailed photoinduced (top), 4% PF_6^- doped (middle), and undoped (bottom) absorption of P3MT. Note the 1:1 correspondence of the photoinduced and the doping-induced data (Kim *et al.*, 1987).

served on photoexcitation and that after doping implies that the same charge storage configuration is involved in both cases.

The amplitude mode formalism (Horovitz, 1982; Horovitz *et al.*, 1984) considers the coupling of phonons to electronic excitations via a set of formal dimerization patterns which describe the Peierls distorted chain. Only those phonons that modulate the amplitude of the dimerization couple to the local fluctuations in the π-electron density. The resulting IRAV modes are then determined by the translational freedom of the charged defect (translational modes or T modes); see Sec. IV.D. Within the amplitude mode formalism, there is one localized phonon (one T mode) for each phonon branch, i.e., one for each principal Raman line of the pure polymer. The observed strong T modes (Fig. 50) are consistent with the principal Raman lines observed at 1047, 1175, 1220, and 1460 cm^{-1}. The amplitude mode formalism does not lead to infrared-active shape oscillations of the charged defect (Schaffer and Heeger, 1986) nor does it take into account the possibility of coupling to ring vibrations not directly associated with the dimerized backbone. The latter are of particular interest in polythiophene, for they provide quantitative information on the involvement of the sulfur atoms in the π-electron structure.

In thiophene, the four carbon p electrons and the two sulfur p electrons provide the six p electrons that satisfy the $(4n+2)$ condition necessary for aromatic stabilization. Localization of charge in a polaron or bipolaron after photoexcitation either adds an electron to an antibonding orbital or removes an electron from a bonding orbital, in either case decreasing the aromatic stabilization of the ring. This excess charge would induce changes in bond lengths and also distort the ring planarity. Photoexcitation can thus be expected to couple to all ring modes (R modes) of the thiophene unit. The photoinduced absorptions at 690, 728, 782, and 900 cm^{-1} have been interpreted (Schaffer and Heeger, 1986) as R modes (ir modes at 694 and 790 cm^{-1} in the pure polymer are known to be associated with ring vibrations). The relative strength of the R vs T modes provides a measure of the involvement of the coupling of the heteroatom to the π-electron excitations. That the R modes have oscillator strengths an order of magnitude below the strengths of the larger T modes, together with the success of the amplitude mode formalism in using the T modes and Raman data to provide a self-consistent picture, confirms the previous evidence that the involvement of the heteroatom in the electronic structure is weak. Thus, to a good first approximation, polythiophene may be considered as pseudopolyene, as sketched in Fig. 45 (Schaffer and Heeger, 1986).

Photoinduced and doping-induced IRAV spectra have been reported (Kim *et al.*, 1987) for poly(3-methylthiophene) as well. The four infrared-active T modes of bipolarons and the weak R modes were observed, similar to the parent polythiophene. The results are shown in Fig. 50(b). The 1:1 correspondence between

the IRAV modes induced through doping and by photoexcitation is quite evident.

Recent generalization of the theory (Mele and Hicks, 1985, 1986; Terai and Ono, 1986) beyond the amplitude mode formalism predicted the formation of additional localized phonons; the shape oscillations (A modes; see Sec. IV.D.3). The weak (but genuine) feature of 1435 cm^{-1} has been assigned (Schaffer and Heeger, 1986; Kim *et al.*, 1987) as the A_4^- mode.

b. Photogeneration of polarons and bipolarons in polythiophene: Photoinduced absorption and light-induced electron-spin resonance

The photoinduced absorption spectrum (Vardeny, Ehrenfreund, Brafman, Nowak, *et al.*, 1986) of polythiophene (at 20 K) is shown in Fig. 51. The spectrum consists of the four main IRAV lines (see previous subsection) below 0.2 eV and two asymmetric electronic bands with $\Delta\alpha > 0$. The low-energy band peaks at 0.45 eV and the higher-energy band peaks at 1.25 eV. These photoinduced absorption bands derive their strengths from states above 2 eV, where $\Delta\alpha$ changes sign and turns into photoinduced bleaching. Both the IRAV and the photoinduced electronic bands originate from the same charged species (same dependence on the excitation pump intensity, same temperature dependence, same excitation profile, etc.; Vardeny, Ehrenfreund, Brafman, Nowak, *et al.*, 1986).

LESR measurements were carried out under similar conditions (Vardeny, Ehrenfreund, Brafman, Nowak, *et al.*, 1986). The absolute value of N_s was determined from the relative strengths of the photoinduced and dark signals (the latter is known to be about 260×10^{-6} per thiophene monomer). Although a photoinduced signal was observed (indicative of photogeneration of polarons), the excitation profile for photogenerated spins is completely different from the excitation profile for photogenerated charges. In particular, for pump frequencies greater than E_g, $N_s/N_{ch} \ll 1$ (for example, at 3.1 eV, $N_s/N_{ch} < 10^{-2}$). Thus the dominant charge excitations photogenerated with $\hbar\omega > E_g$ are spinless bipolarons.

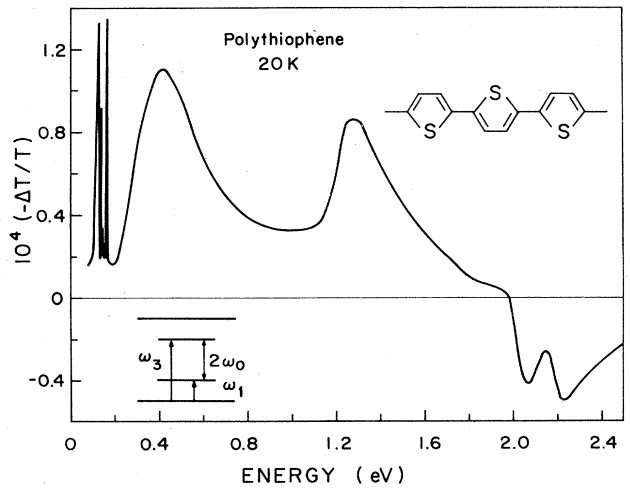

FIG. 51. Photoinduced absorption of polythiophene at 20 K (from Vardeny, Ehrenfreund, Brafman, Nowak, *et al.*, 1986).

A relatively small number of spin-$\frac{1}{2}$ polaron excitations are photogenerated in the as-synthesized samples (primarily by pumping into localized states in the gap) (Vardeny, Ehrenfreund, Brafman, Nowak, *et al.*, 1986). After improving the structural order and increasing the molecular weight by annealing the chemically synthesized samples at high temperature (Mo *et al.*, 1985), the photogenerated spins drop below the detectable limit, whereas the photoinduced absorption signal remains the same. Since the spin-$\frac{1}{2}$ excitation profile peaks deep in the gap and since the annealed samples show no photoinduced ESR, polaron excitation occurs via defect states deep in the gap (due to structural imperfection). These data provide insight into the reports from different laboratories of polaron formation by charge transfer doping. As argued in the previous subsection, polarons can be kinetically metastable at dilute concentrations in low-molecular-weight samples in which defects and imperfections are sufficiently numerous to restrict polaron mobility and thereby inhibit the bipolaron formation reaction. The annealing results described above prove this conjecture: removal of localized states due to chain imperfections, low molecular weight, and structural disorder quenches polaron formation. The conclusion, therefore, is that for polythiophene bipolarons are the lowest-energy charge storage configuration; polarons are formed only when the bipolaron formation reaction [Eq. (6.5)] is inhibited by sample imperfections.

The photoinduced absorption spectrum is consistent with bipolaron formation. The two subgap electronic absorptions shown in Fig. 51 are the two bipolaron transitions, $\hbar\omega_1$ and $\hbar\omega_2$, sketched in Fig. 43. The asymmetry of the 0.45-eV and the 1.25-eV bands indicates that transitions from (to) the continuum density of states at the band edge are involved, in agreement with predictions for bipolaron transitions. Since there is no splitting of either the 0.45-eV or the 1.25-eV bands, charge-conjugation symmetry holds for polythiophene. This is consistent with the weak coupling of the sulfur heteroatom to the π system demonstrated through the IRAV analysis (Schaffer and Heeger, 1986; Kim *et al.*, 1987).

The photoinduced absorption spectrum (Fig. 51) is similar to the doping-induced absorption spectrum (Fig. 47); the doping-induced absorption also shows two asymmetric bands, at 0.65 and 1.45 eV, identified with the bipolaron transitions, and both show bleaching of the interband transition above 2 eV. Moreover, the difference, $(\hbar\omega_1 - \hbar\omega_2) = 0.8$ eV, is the same in the two cases. If bipolarons are produced, the energy separation between the two gap states (see Fig. 43) should be the same and not depend on the generation process, since $(\hbar\omega_1 - \hbar\omega_2)$

is due to confinement and is a property of the bipolaron on a polythiophene chain.

Since the relation $(\hbar\omega_1^0+\hbar\omega_2^0)=E_g$ would hold in the absence of Coulomb repulsion, the transition energies are shifted (Vardeny, Ehrenfreund, Brafman, Nowak, *et al.*, 1986),

$$(\hbar\omega_1+\hbar\omega_2)^{\text{photo}}=E_g-2U_B\ , \tag{6.13}$$

where U_B is the difference in Coulomb energy between the initial state of the spatially extended bipolaron (double charge) and the final state (single charge) with fixed lattice coordinates. From Fig. 51, $(\hbar\omega_1+\hbar\omega_2)=1.7$ eV, while $E_g\sim 2.1-2.2$ eV was inferred from the absorption spectrum. A more accurate value for E_g^{1D} was obtained from analysis of the IRAV and resonance Raman data using the amplitude mode formalism, $E_g^{1D}=2.2$ eV. From Eq. (6.13), one finds $U_B\sim 0.25$ eV or $(U_B/E_g)\sim 0.12$. This small value for U_B (small even compared with the difference in energy between a bipolaron and a pair of polarons) is consistent with the existence of bipolarons rather than polarons as the dominant charged excitation. For doping-induced bipolarons, the shift of each transition by U_B is compensated by the Coulomb binding (E_B) to the dopant counter ion, so that

$$(\hbar\omega_1+\hbar\omega_2)^{\text{dop}}=E_g-2(U_B-E_B)\ . \tag{6.14}$$

As in the analogous argument for solitons [see Eqs. (5.7) and (5.8)], since U_B and E_B depend primarily on the spatial extent of the bipolaron, the two contributions approximately cancel.

Electronic correlations have been shown to stabilize the bipolaron excitations and to increase their absorption strength drastically (both the absolute strength and the relative strength of the two transitions; Sum *et al.*, 1987a, 1987b). However, the absence of additional splitting in the photoexcitation spectra (Vardeny *et al.*, 1984; Vardeny, Ehrenfreund, Brafman, Nowak, *et al.*, 1986) (where both positive and negative bipolarons are generated) sets implied upper limits on the strength of any interactions that would break the charge-conjugation symmetry.

VII. COULOMB INTERACTIONS

In the earlier sections of this review, we have ignored the explicit effect of electron-electron interactions on the properties of conducting polymers, although they have been included as effective interactions through the empirically determined values of the Fermi-liquid parameters that enter the "noninteracting" model. In this section, we consider the effects of the "residual" interactions that cannot be accounted for by a simple renormalization of the one-electron Hamiltonian. Since the residual interactions are also Fermi-liquid parameters, their magnitude is difficult to determine *a priori*; they must generally also be determined empirically. The fundamental question we address in this section is what is the range of interaction strength over which it is a valid zeroth-order approximation to ignore the explicit electron-electron interactions. Whether or not there is any range of interaction strength for which interactions have a small (perturbative) effect is a nontrivial question, since, in a one-dimensional (nondimerized) metal, arbitrarily weak interactions have a qualitative (nonperturbative) effect on the nature of the low-energy excitations (Solyom, 1979). We shall show, however, that in a conducting polymer the noninteracting model is a valid zeroth-order description up to fairly large interaction strengths (Kivelson *et al.*, 1985). Moreover, in this range, the corrections to the zeroth-order theory due to interactions can be computed to good accuracy using low-order perturbation theory (Wu and Kivelson, 1986).

There have been a number of other approaches used to investigate the effects of interactions that we shall not discuss in any detail. Among these are variational calculations based on the unrestricted Hartree-Fock approximation (Subbaswamy and Grabowski, 1981; Kivelson and Heim, 1982) or on Gutzwiller's ansatz (Horsch, 1981; Baeriswyl and Maki, 1985a, 1985b), Monte Carlo calculations (Hirsch, 1983; Hirsch and Grabowski, 1984), and direct numerical solutions of fully interacting models of small molecules (Zoos and Ramasesha, 1983; Campbell *et al.*, 1984; Tavan and Schulten, 1988). There have also been renormalization-group calculations which sum up the leading logarithmic terms in $\ln(2t_0/\Delta)$ to all orders in perturbation theory (Barisic, 1983; Fukatome and Sasai, 1983; Hayden and Mele, 1985, 1986; Horovitz and Solyom, 1985). While many of these calculations lead to similar conclusions concerning the role of electron-electron interactions in polyacetylene, some of the calculations, especially those based on intuitions derived from the chemistry of small polyenes, have reached the opposite conclusions about weakness of the interactions (Zoos and Ramasesha, 1983; Campbell *et al.*, 1984; Tavan and Schulten, 1988). It is our belief that these conclusions are based on a misunderstanding of the meaning of the Fermi-liquid parameters which enter the Hamiltonian and which already include, to a large extent, the effects of the certainly strong bare interactions. This conclusion is further supported by recent quantum chemical calculations; even on small polyenes and in the presence of strong electron-electron interactions, solitonlike configurations emerge (Tavan and Schulten, 1988). The advantages of the perturbative approach taken here are that it is a controlled approximate solution to the model Hamiltonian, it is analytically tractable, and it leads to a simple physical understanding of the role of interactions.

A. The model

Since the interactions are actually Fermi-liquid parameters whose magnitude and form depend in a very complicated way on the bare interactions, it is far from clear how the electron-electron interactions should be incor-

porated into the model. Moreover, the Coulomb interaction is long ranged and hence intrinsically three dimensional, so that it cannot be treated within the context of a one-dimensional model. A partial resolution (Barisic, 1983; Wu and Kivelson, 1986) of this second problem comes from an analysis of the effect of three-dimensional screening. Since $(CH)_x$ is an insulator, the dielectric function $\varepsilon(k,\omega)$ tends to a finite constant as k and $\omega \to 0$. Thus the static Coulomb interaction remains long ranged. However, at frequencies greater than the energy gap, $\omega > 2\Delta/\hbar$, and less than the plasma frequency, $\omega < \omega_p = (4\pi n e^2/m_e)^{1/2}$, the interaction is screened as in a metal, and hence the effective interaction has a short range. In a perturbative expression for a physical quantity, most of the interactions are integrated over momentum and energy transfer. Since in $(CH)_x$ the gap is small and $\hbar\omega_p \gg \Delta$, the integrals are dominated by the range of frequencies in which the interaction is screened. Thus, for many purposes, it is possible to use a one-dimensional model that mimics the screened Coulomb interaction by a short-ranged effective interaction between electrons on the same chain. For instance, the effective forward scattering matrix element

$$g_2 = \langle k_F, -k_F \mid V_{\rm int} \mid k_F, -k_F \rangle / 2t_0 ,$$

which is infinite in the absence of screening, is given by the expression (Kivelson *et al.*, 1985; Wu and Kivelson, 1986)

$$g_2 = g_2^{(0)} + [(e^2)/(\varepsilon_0 a 2t_0)] \ln[(2t_0)/\hbar\omega_p]$$

in the presence of screening so long as $2t_0 > \hbar\omega_p \gg \Delta$. Here $g_2^{(0)}$ is determined by the short-distance piece of the interaction, and ε_0 is the background dielectric constant.

It is important to note that the magnitude of the interaction that enters the one-dimensional model depends on the nature of the three-dimensional environment of the chain. Thus in $(CH)_x$ where $n \sim 10^{22}$ cm^{-3} and hence $\hbar\omega_p \sim 3.5$ eV, we expect the interactions to be largely screened, whereas in polydiacetylene where $n \sim 10^{21}$ cm^{-3}, and hence $\hbar\omega_p \sim 1.1$ eV $< 2\Delta$, the interactions should be unscreened. It is probably this difference that is responsible for the dramatic differences between polydiacetylene and most other denser conducting polymers, as mentioned in Sec. III.A.

We thus see that it is possible to consider a short-ranged one-dimensional model of the interactions in $(CH)_x$ to study any property of the system that does not depend especially on the low-frequency part of the effective interaction. We shall consider situations in which the long-range, low-frequency part of the interaction is crucial in Sec. VII.C.2. The model we study consists of the same noninteracting piece we have studied previously plus an interaction term.

To start, we consider the tight-binding model in which there is one electronic orbital (Wannier function) $\Phi_n(r)$ per site n (e.g., the carbon $2p_z$ orbital in the case of polyacetylene), and hence

$$H = H_{\rm SSH} + H_{\rm int} , \tag{7.1}$$

where $H_{\rm SSH}$ is the SSH Hamiltonian defined in Eqs. (3.4)–(3.6), and $H_{\rm int}$ is the electron-electron interaction, which can be written in its most general form as

$$H_{\rm int} = \sum_{\substack{n,m,l,p \\ s,s'}} V(n,m,l,p) c_{ns}^\dagger c_{ms'}^\dagger c_{ls'} c_{ps} + \delta\mu \sum_{n,s} c_{ns}^\dagger c_{ns} . \tag{7.2}$$

Here $c_{ns}^\dagger$ creates an electron of spin s on site n, and $V(n,m,l,p)$ is the appropriate matrix element of the electron-electron interaction potential $V(r)$,

$$V(n,m,l,p) = \int dr\, dr' \rho_{np}(r) \rho_{ml}(r') V(r-r') . \tag{7.3}$$

In Eq. (7.3), ρ_{np} denotes the matrix element of the electron-density operator $\hat{\rho}(r)$ in the Wannier representation

$$\rho_{np}(r) = \Phi_n^*(r)\Phi_p(r) = \langle n \mid \hat{\rho}(r) \mid p \rangle , \tag{7.4}$$

and $\delta\mu$ is an appropriate shift in the chemical potential so that the Fermi energy remains $E_F = 0$. Since the orbitals $\Phi_n(r)$ are typically exponentially localized, $\rho_{np}(r)$, $\rho_{ml}(r)$, and hence $V(n,l,m,p)$ will fall off exponentially with the separation $|n-p|$ and $|m-l|$. On the other hand, the dependence of $V(n,l,m,p)$ on $|n-m|$ reflects the range of the interaction. In a single-band model, the Wannier functions can be chosen to be real, and hence $\rho_{np}(r) = \rho_{pn}(r)$.

In previous treatments of the electron-electron interactions, only terms involving the diagonal matrix elements of $\hat{\rho}(r)$ were considered. A particularly well-studied example is the extended Hubbard model in which

$$H_{\rm int} = U \sum_n \hat{Q}_\uparrow(n)\hat{Q}_\downarrow(n) + \sum_{s,s'} \hat{Q}_s(n)\hat{Q}_{s'}(n+1) , \tag{7.5}$$

where $U = 2V(0,0,0,0)$, $V = 2V(0,1,1,0)$, and $\hat{Q}_s$ is the density of electrons of spin s on site n (minus the average density),

$$\hat{Q}_s(n) = (c_{ns}^\dagger c_{ns} - \tfrac{1}{2}) . \tag{7.6}$$

In addition to neglecting off-diagonal terms, this model assumes short-ranged electron-electron interactions. However, even for δ-function interactions, $V(r) = V_0\delta(r)$, this model neglects terms proportional to the off-diagonal matrix elements of $\hat{\rho}(r)$ that are larger (or at least as large) as those terms that are retained. Specifically, for reasonable forms of the Wannier function and $V(r) = V_0\delta(r)$, $U > X > V = W$ where $X = 2V(0,1,1,1)$ and $W = 2V(0,1,0,1)$.

Thus because $\hat{\rho}(r)$ is a function of the continuous spatial coordinate r (and not of a discrete lattice index, n), we are led to include off-diagonal matrix elements of $\hat{\rho}(r)$. Indeed, the same large overlap between orbitals on nearest-neighbor sites that is responsible for the large value of t_0 (i.e., the bandwidth) is responsible for the importance of the off-diagonal matrix elements of $\hat{\rho}(r)$. For

these fundamental reasons, one must explicitly include interactions (Kivelson *et al.*, 1987) that come from nearest-neighbor off-diagonal matrix elements of $\hat{\rho}(r)$ and hence that depend on the "bond charge density"

$$\hat{G}_s(n)=(c_{ns}^{\dagger}c_{n+1,s}+\text{H.c.}) . \tag{7.7}$$

Just as more-distant-neighbor hopping matrix elements can be ignored in computing the band structure [since $\Phi_n(r)$ falls off exponentially with distance], terms proportional to further-neighbor matrix elements of $\hat{\rho}(r)$ can be ignored to a first approximation. The resulting translationally invariant model can be expressed as

$$\begin{aligned} H_{\text{int}}=&\tfrac{1}{2}\sum_{n,m,s,s}\tilde{V}(n-m)\hat{Q}_s(n)\hat{Q}_{s'}(m) \\ &+\tfrac{1}{4}\sum_{n,m,s,s'}\tilde{X}(n-m)\{\hat{Q}_s(n),\hat{G}_{s'}(m)\} \\ &+\tfrac{1}{2}\sum_{n,m,s,s'}\tilde{W}(n-m)\hat{G}_s(n)\hat{G}_{s'}(m) , \end{aligned} \tag{7.8}$$

where $\tilde{V}(n-m)=2V(n,m,m,n)$, $\tilde{X}(n-m)=2V(n,m,m+1,n)$, and $\tilde{W}(n-m)=2V(n,m,m+1,n+1)$. In the spirit of the extended Hubbard model (and to help develop our physical intuition), we shall consider the simplified version in which we keep only nearest-neighbor interactions, and hence take $\tilde{V}(0)=U$, $\tilde{V}(1)=\tilde{V}(-1)=V$, $\tilde{X}(0)=X$, $\tilde{W}(0)=W$. All other matrix elements are assumed to be zero. While this simplified version of the model is not realistic for Coulomb interactions, it should be fairly accurate for short-range interactions. In this respect, it contrasts with the extended Hubbard model, which is unlikely to be reliable for any range of interactions.

The interactions can also be studied in terms of the continuum model, in which the matrix elements of V are evaluated between states at the Fermi surface. The resulting model is of the form

$$H=H_{\text{TLM}}+H_{\text{int}} ,$$

where H_{TLM} is the noninteracting continuum Hamiltonian defined in Eq. (3.8), and the electron-electron interaction term is

$$\begin{aligned} H_{\text{int}}=\sum_{ss'}\int dx\, \hbar v_F[&g_1\Psi_{s1}^{\dagger}\Psi_{s'1}^{\dagger}\Psi_{s'1}\Psi_{s2}+g_2\Psi_{s1}^{\dagger}\Psi_{s'2}^{\dagger}\Psi_{s'2}\Psi_{s1}+1/2g_3(\Psi_{s1}^{\dagger}\Psi_{s'1}^{\dagger}\Psi_{s'2}\Psi_{s2}+\text{H.c.}) \\ &+1/2g_4(\Psi_{s1}\Psi_{s'1}\Psi_{s'1}\Psi_{s1}+\Psi_{s2}\Psi_{s'2}\Psi_{s'2}\Psi_{s2})] , \end{aligned} \tag{7.9}$$

where $\Psi_{s1}(x)$ creates a right-moving electron of spin s, and $\Psi_{s2}(x)$ creates a left-moving electron. If the continuum model is obtained by taking the continuum limit of the discrete model defined in Eqs. (3.4)–(3.7), then the parameters defining Eq. (7.9) become the following:

$$\hbar v_F=2t_0a , \tag{7.10}$$

where a is the lattice constant and

$$g_1=(1/t_0N)\sum_{n,m,l,p}\{V(n,m,l,p)\times\exp[i\pi(n+p-m-l)/2]\} , \tag{7.11a}$$

$$g_2=(1/t_0N)\sum_{n,m,l,p}\{V(n,m,l,p)\times\exp[i\pi(n-p-m+l)/2]\} , \tag{7.11b}$$

$$g_3=-(1/t_0N)\sum_{n,m,l,p}\{V(n,m,l,p)\times\exp[i\pi(n+p+m+l)/2]\} , \tag{7.11c}$$

$$g_4=(1/t_0N)\sum_{n,m,l,p}\{V(n,m,l,p)\times\exp[i\pi(n-p+m-l)/2]\} , \tag{7.11d}$$

where g_1, g_2, and g_3 are the backward-scattering, forward-scattering, and umklapp-scattering matrix elements, respectively.

As before, the advantages of the continuum model are that it is very general, that calculations are simpler than with the discrete model, and that the full effects of the arbitrary interactions between electrons at the Fermi surface are embodied in the values of the four interaction parameters g_i. The disadvantage is that it is difficult to obtain physical insight into the relevant values of these coupling strengths. To obtain such an understanding, we have evaluated the expressions in Eq. (7.11) for the discrete model with nearest-neighbor interactions only. If one ignores the interaction between bond charges, then there are only two independent interactions, since $g_1=-g_3$ and $g_2=g_4$ [this result is independent of the range of $V(r)$]. Thus the quantities (g_1+g_3) and (g_2-g_4) measure the strength of the bond charge repulsion. In terms of the interactions in the nearest-neighbor model, the relations in Eq. (7.11) can be written as follows:

$$g_1=(U-2V+4W)/2t_0 , \tag{7.12a}$$

$$g_2=(U+2V)/2t_0 , \tag{7.12b}$$

$$g_3=-(U-2V-4W)/2t_0 , \tag{7.12c}$$

$$g_4=(U+2V)/2t_0 , \tag{7.12d}$$

and hence

$$g_1+g_3=2W/t_0\ , \tag{7.13a}$$

$$g_2-g_4=0\ . \tag{7.13b}$$

Note that the interactions at the Fermi surface are independent of X, so that there is no cross coupling between the bond and site charge densities. This is a specific feature of the half-filled band where $k_F a=\pi/2$. For other fillings, $g_3=g_4=0$, but g_1 and g_2 depend on X as well as U, V, and W.

B. Range of validity of perturbation theory

For a one-dimensional metal, the interactions are never a small perturbation. A perturbative expression (Kivelson *et al.*, 1985; Wu and Kivelson, 1986) for a physical quantity, such as an electron self-energy $\Sigma'(\omega)$, contains terms proportional to all powers of $(g/2\pi)\ln(\omega/2t_0)$. Thus, no matter how small g is, at low enough frequencies the effect of interactions is large. In a conducting polymer, there is a natural lower-frequency cutoff provided by the Peierls gap. Thus perturbation theory is well defined so long as

$$(g/\pi)\ln[(2t_0/\Delta)]\sim(U/2\pi t_0)\ln[(2t_0/\Delta)]\ll 1\ . \tag{7.14}$$

The validity of this result was confirmed (Kivelson *et al.*, 1985) by comparing perturbation theory with the Bethe ansatz solution of an integrable model in which only interactions between like-spin electrons $g_{\parallel}$ are retained ($g_{\perp}=0$). In fact, it turns out that, at least for this model, the perturbation series is convergent.

To get a more practical feeling for the range of validity of low-order perturbation theory, we have shown in Fig. 52 a comparison between the second-order perturbative expression (Kivelson and Heim, 1982; Kivelson *et al.*, 1985; Wu and Kivelson, 1986) and the Monte Carlo results (Hirsch, 1983; Hirsch and Grabowski, 1984) for the dimerization as a function of U in a model with only on-site (Hubbard) interactions between electrons. As can be seen, the perturbative result is quite accurate so long as $U<2t_0$. Since $(2t_0/\Delta)\approx 6.0$ in these calculations, they confirm that perturbation theory breaks down only when $(U/2\pi t_0)\ln(2t_0/\Delta)\approx 1$. [For large U, where perturbation theory is no longer valid, the dimerization can be computed analytically as well, since in this limit the Hubbard model is equivalent to a spin-$\frac{1}{2}$ Heisenberg model for which the dimerization follows from the spin-Peierls instability (Cross and Fisher, 1979). The dimerization in this limit is $(\Delta/2t_0)\approx(\alpha/KU)^{3/2}$.] As discussed below, the fact that the magnitude of the dimerization increases with increasing interaction strength U is an artifact of the Hubbard model. This figure is included simply to illustrate the range of validity and accuracy of perturbation theory.

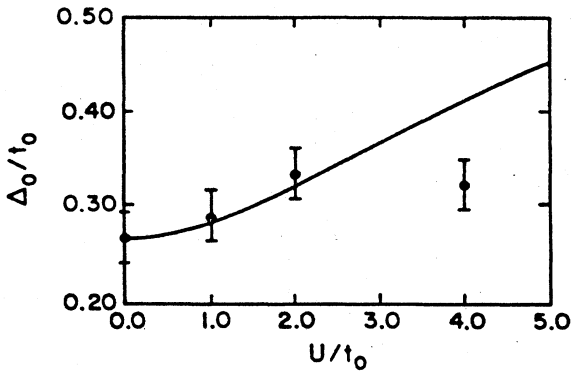

FIG. 52. A comparison between the second-order perturbative expression and the Monte Carlo results (Hirsch, 1983) for the dimerization as a function of U in a model with only on-site (Hubbard) interactions between electrons. From Wu and Kivelson, 1986.

C. Effect of weak interactions

To keep our discussion simple, we shall focus on the nearest-neighbor tight-binding model, although to compute second- and higher-order contributions it is generally easier to deal with the continuum model (see Wu and Kivelson, 1986, for an extensive treatment). To do this, we use Wick's theorem to factorize the expectation values of the products of four operators into products of the expectation values of $\hat{Q}_s(n)$ and $\hat{G}_s(n)$. Typically, $\langle\hat{Q}_s(n)\rangle$ can easily be computed explicitly. $\langle\hat{G}_s(n)\rangle$ can be readily computed by use of the Hellman-Feynman theorem, which implies that it can be determined from the derivative of the noninteracting electronic energy with respect to φ_n:

$$dE_{\rm el}/d(\varphi_n+\varphi_{n+1})=-\alpha\sum\langle\hat{G}_s(n)\rangle\ . \tag{7.15}$$

This expression is particularly useful for the states in which the lattice configuration minimizes the total energy,

$$dE_{\rm el}/d\varphi_n+dE_{\rm lat}/d\varphi_n=0\ . \tag{7.16}$$

Thus, so long as $\langle\hat{G}_s(n)\rangle$ is spin independent,

$$\langle G_s(n)\rangle=(2/\pi)+(-1)^n(K/2\alpha)(\varphi_n+\varphi_{n+1})\ . \tag{7.17}$$

For instance, in the case of a perfectly dimerized lattice, $\langle G_s(n)\rangle$ is independent of spin and is given by the expression (Kivelson *et al.*, 1987)

$$\begin{aligned}\langle G_s(n)\rangle&=-(2/\pi)[1+(-1)^n(z/1-z^2)-E(1-z^2)]\\&\approx(-2/\pi)\{1+(-1)^n z[\ln(4/z)-1]\}\ ,\end{aligned} \tag{7.18}$$

where $z=\Delta/2t_0$, $K(1-z^2)$ and $E(1-z^2)$ are complete elliptic integrals of the first and second kinds, and the second equality is valid for small z. The actual computations for more general lattice configurations are straightforward but can be somewhat tedious, so without further

elaboration we summarize the results of first-order perturbation theory.

1. The perfectly dimerized lattice

For all states of interest in the presence of a perfectly dimerized lattice, $\langle \hat{Q}_s(n) \rangle = 0$, and hence only terms proportional to $|\langle G_s(n) \rangle|^2$ contribute to the interaction energy. Since the ground-state energy as a function of dimerization is the effective potential that determines the self-consistent magnitude of the dimerization, the change in the ground-state energy,

$$\Delta E(z) = 2/\pi^2 (3W - V) z^2 \ln^2(4/ez) , \tag{7.19}$$

results in a change in the magnitude of the dimerization. For $3W > V$, ΔE is an increasing function of z (for $z \ll 1$); hence short-range interactions *oppose* dimerization. This occurs since the Coulomb repulsion between electrons provides additional stiffness against distortion away from the uniform structure and thereby opposes the dimerization induced by the electron-phonon interaction. For longer-range interactions, the dimerization is enhanced by Coulomb interactions (Wu *et al.*, 1987).

The effect of interactions on the one-particle gap for fixed dimerization can also be computed in a straightforward manner. The result is

$$\Delta = \Delta\{1 - [(3W - V)/\pi t_0] \ln(4/ez)\} . \tag{7.20}$$

For $3W > V$, interactions tend to decrease the gap. Since the electrons tend to screen the $2k_F$ potential caused by the dimerized lattice, the expected effect of electron-electron repulsion would be to reduce the single-particle gap (for fixed magnitude of dimerization), in agreement with Eq. (7.20). Note that, more generally, the same conclusions hold provided $(2g_1 + g_3 - g_2) > 0$. This condition, which in the absence of bond charge would require the (unphysical) condition that $V < 0$, is now seen to be satisfied for reasonable values of the bond charge repulsion.

By properly including Coulomb interactions between electrons located not only on the same site (Hubbard model) and on neighboring sites (extended Hubbard model), but also on bonds between sites, we obtain an increase in the effective stiffness constant leading to a decrease in the magnitude of the dimerization as a function of the Coulomb potential strength. While earlier results based on models that neglected the bond charge forces predict an initial increase in dimerization with increasing Coulomb strength (Horsch, 1981; Subbaswamy and Grabowski, 1981; Hirsch, 1983; Hirsch and Grabowski, 1984), the analysis outlined above shows that this apparent increase may be the result of overlooking the interactions involving bond charge. By including this bond charge interaction, one finds (at least for short-range interactions) that the dimerization monotonically decreases with increasing Coulomb strength (Kivelson *et al.*, 1987), as is reasonable from a physical point of view. The effect of Coulomb interactions on the dimerization was also considered in the context of the screened Coulomb interaction as a function of the screening length (Wu *et al.*, 1987). For short-ranged interaction, the dimerization decreases with increasing interaction strength; whereas for longer-range interaction there is an initial rise in dimerization before it begins to fall for large interactions

2. In the presence of a soliton

In the presence of a soliton,

$$\rho_s(n) = (f_s - \tfrac{1}{2}) \psi_0(n)^2 , \tag{7.21}$$

where $f_s = 0, 1$ is the number of electrons of spin s in the midgap state. Moreover, the midgap wave function $\psi_0(n)$ in Eq. (4.26), is zero on every other site. Thus, for a charged soliton (Kivelson and Heim, 1982),

$$\Delta E_{s\pm} = (U/4) \sum_n |\psi_0(n)|^4 \approx (U/6)(\Delta/2t_0) , \tag{7.22}$$

while for a neutral soliton

$$\Delta E_{s0} = -(U/4) \sum_n |\psi_0(n)|^4 . \tag{7.23}$$

It is interesting that exchange effects result in an actual reduction in the neutral-soliton creation energy; locally, the neutral soliton produces a spin-density wave which reduces the electron-electron repulsion.

The charged-soliton creation energy is an example of a quantity for which the short-ranged model is inadequate, since it involves the presence of a static charge which interacts via an unscreened interaction (Wu and Kivelson, 1986). Thus, to compute this energy, we should include the direct effect of the long-ranged part of the Coulomb interaction, which we can approximate as

$$E_{\rm LR} = \sum_n \sum_{m \geq 2} [e^2 f(m)/\varepsilon_0 ma] \left[\sum_s \rho_s(n)\right] \times \left[\sum_{s'} \rho_{s'}(n+m)\right] ,$$

where $f(m) = 0$ for ma less than the Thomas-Fermi screening length and $f(m) \to 1$ as $m \to \infty$. Since the perfectly dimerized state and the neutral soliton are both locally charged neutral, this term makes no contribution to either of these energies. However, it alters Eq. (7.22) for the charged-soliton creation energy to yield

$$\Delta E_{s\pm} = (U/4) \sum_n |\psi_0(n)|^4 + (e^2/\varepsilon_0 a) \sum_n{}' \sum_{m \geq 2} f(m) [|\psi_0(n)|^2 |\psi_0(n+m)|^2]/m$$
$$\sim (U/6)(\Delta/2t_0) + (e^2/\varepsilon_0 \xi) A_s , \tag{7.24}$$

where A_s is a number of order one that depends somewhat on the Thomas-Fermi screening length.

3. In the presence of a polaron or bipolaron

In the presence of a soliton pair configuration, there are two bound states, the negative-energy bonding state $\psi_b(n)$ and an antibonding state $\psi_a(n)$, but $|\psi_b(n)|^2=|\psi_a(n)|^2$. For the various polaron and bipolaron states discussed previously $\rho_s(n)=(f_{bs}-f_{as}-1)|\psi_b(n)|^2$, where f_{bs} (f_{as}) is the number of electrons of spin s in the bonding (antibonding) state. Again, since both the polaron $P^{\pm}$ and the bipolaron $B^{\pm}$ are charged, we must keep the direct term with unscreened interactions and hence

$$\Delta E_{p^{\pm}}=(V-3W)\sum_n |\psi_b(n)|^2|\psi_b(n+1)|^2+(e^2/\varepsilon_0 a)\sum_n\sum_{m\geq 2} f(m)[|\psi_b(n)|^2|\psi_b(n+m)|^2]/m$$
$$\approx(V-3W)[2\ln(1+2^{1/2})-2^{1/2}](a/\xi)+(e^2/\varepsilon_0\xi)A_p\ , \tag{7.25}$$

where A_p is a number of order l and

$$\Delta E_{B^{\pm}}=U\sum_n |\psi_b(n)|^4+4(V-2W)\sum_n |\psi_b(n)|^2|\psi_b(n+1)|^2$$
$$+(e^2/\varepsilon_0 a)\sum_n\sum_{m\geq 2} f(m)[|\psi_b(n)|^2|\psi_b(n+1)|^2]/m\ . \tag{7.26}$$

4. Spin density of a neutral soliton

Another quantity of considerable experimental importance is the spin density associated with a neutral soliton. Since this involves a change in the wave function, it involves a somewhat more involved computation. The result, derived in the continuum limit, is that for a soliton centered at the origin,

$$S(n)=\rho\downarrow(n)-\rho\uparrow(n)$$
$$=(1/\xi)\,\mathrm{sech}^2(na/\xi)[(1+X)\cos^2(n\pi/2)$$
$$-X\sin^2(n\pi/2)]+\delta S(n)\ , \tag{7.27}$$

where

$$X=(U/2\pi t_0)\ln[4t_0/(\Delta)] \tag{7.28}$$

and $\delta S(n)$ is a small term whose average over either even or odd sites is zero. Thus U leads to an enhancement of the spin density on even sites and a compensating negative spin density on odd-numbered sites.

The best experimental measure of the strength of the electron-electron repulsion is the ratio S_o/S_e of the spin on odd- and even-numbered sites in the presence of a neutral soliton [as obtained from ENDOR measurements (Kuroda *et al.*, 1984, 1985; Grupp *et al.*, 1987; Kass *et al.*, 1987; Kuroda and Shirakawa, 1987). This ratio is zero in the absence of interaction. From Eq. (7.27), it is clear that in the presence of interactions this ratio is $\rho_o/\rho_e=-X/(1+X)$. The electron-spin density using ENDOR (see Sec. V) is found to be $\frac{1}{3}<S_o/S_e<0.43$ and, thus, $1.25<U/t_0<2$. This is an equilibrium measurement and so its interpretation is straightforward.

Another experimental probe of the effects of correlation is photoinduced absorption. Two peaks have been observed in the photoinduced absorption: a low-energy peak that is associated with the process

$$S^{\pm}\rightarrow S^0+e^{\pm}$$

and hence is expected to have a threshold energy

$$\hbar\omega_L=\Delta+(E_{s0}-E_{s\pm})$$
$$=\Delta-(U/3)(a/\xi)-(e^2A_s/\varepsilon_0\xi) \tag{7.29}$$

and a high-energy peak that is associated with the process

$$S^0\rightarrow S^{\pm}+e^{\gg +}$$

and hence is expected to have a threshold energy

$$\hbar\omega_H=\Delta-(E_{s0}-E_{s\pm})$$
$$=\Delta+(U/3)(a/\xi)+(e^2A_s/\varepsilon_0\xi)\ . \tag{7.30}$$

The two energies have been found to be, respectively, $\hbar\omega_L=0.45$ eV and $\hbar\omega_H=1.40$ eV. As can be seen, the interpretation of these energies is complicated by the presence of long-ranged interactions. With the value of U deduced from the neutral-soliton spin density, these energies imply a value of $A_s\approx\frac{1}{2}$, which is consistent with a Thomas-Fermi screening length of a few angstroms.

D. Other features of electron-electron interactions

The long-ranged nature of the Coulomb interactions has important consequences for the dielectric response of solid $(CH)_x$. The dielectric function of polyacetylene at long wavelengths has been computed using the random-phase approximation (Lee and Kivelson, 1984). The static dielectric constant has the form

$$\varepsilon(k,0)=\varepsilon_0+\varepsilon_1(k_\parallel/k)^2[1+O(k_\parallel\xi)^2]+O(W_\perp/\Delta)^2\ ,$$

where ε_0 is the background dielectric constant and the π-electron contribution is

$$\varepsilon_1=(4e^2na^2/3t_0)[(2t_0/\Delta)]^2[1+O(\Delta/2t_0)^2]$$
$$\approx 10-12 .$$

At frequencies near the gap, local-field effects significantly alter the electromagnetic response of the material. In particular, since in the noninteracting model the optical absorption is divergent at the band edge, there is near-perfect screening. Thus, when local-field effects are taken into account, the $(\hbar\omega-2\Delta)^{1/2}$ singularity in $\alpha(\omega)$ is removed and $\alpha(\omega)$ is instead found to exhibit a broad peak at an energy somewhat above 2Δ. This effect brings gross agreement between the calculated and measured absorption (Neuman and van Boltz, 1988). Moreover, as discussed in Sec. II, the k- and ω-dependent dielectric function calculated in this way is in good quantitative agreement with the experimental values determined from electron energy-loss spectroscopy (see Fig. 6).

VIII. OTHER EFFECTS

A. Quantum fluctuations

In most of the theoretical calculations on the static properties of polyacetylene (discussed in earlier sections), the lattice field was treated in the classical mean-field approximation. When the Gaussian fluctuation around the classical configuration is estimated from the phonon spectrum, the zero-point motion of the lattice displacement, Δu, turns out to be comparable to u_0 itself, thereby casting some doubt on the validity of classical approximation (Su, Kivelson, and Schrieffer, 1980; Su, 1982). A related question is the tunneling between degenerate classical configurations. For a very small system, the tunneling rate would be rapid, and the ground-state symmetry would never be broken. Thus it is not clear whether in polyacetylene the broken symmetry survives the quantum tunneling.

In the following, we present results from various studies that show that the symmetry breaking does take place. We also discuss the effect of quantum fluctuations on excited states.

1. Ground state

Within the adiabatic approximation, the electronic degrees of freedom can be eliminated (at least implicitly) to give an effective Hamiltonian for the nuclear coordinates. That was the basis of the real-time dynamics calculations described in Sec. IV. The same effective Hamiltonian can also be used to study the quantum mechanics of the nuclear motion.

A very direct approach is to use the Monte Carlo functional integration technique (Su, 1982) to evaluate the ground-state probability distribution $|\Psi(\{\varphi_n\})|^2$, where Ψ is the wave function of the phonon field (Su, Kivelson, and Schrieffer, 1980). In this method, a large sequence of temporal configurations is sampled, each configuration $\{\varphi_n\}$ entering with a weight involving the associated classical action for the configuration (Metropolis *et al.*, 1953). In this way, one can estimate $|\Psi(\{\varphi_n\})|^2$.

Applied to a single particle moving in a harmonic potential $V(x)=1/2Kx^2$, the method yields a sequence $x_1,x_2,x_3,\ldots$ for the position x of the particle according to a Gaussian distribution (the ground-state distribution function). Alternatively, one can think of the sequence as a series of simulated measurements of the particle coordinate.

As an example of such simulation in a 16-site polyacetylene ring, the result of four "measurements" randomly picked out of the sequence is shown in Fig. 53. The staggered order parameter φ_n is normalized so that its average value is ± 1 for the classical ground states. As one can see from Fig. 53, it is rather easy for a *particular* CH group to go from the A phase ($\varphi>0$) to the B phase ($\varphi<0$). The tendency to tunnel from one potential-well minimum to another reduces the expectation value $\langle\varphi\rangle$. For a small system such as a single particle in a double-well potential, the tunneling is so frequent that the ground state is no longer degenerate and $\langle\varphi\rangle$ is zero. However, in a large system, it is possible that $\langle\varphi\rangle\neq 0$ (the broken-symmetry state). The average of $\langle\varphi\rangle$ over the ring ($n=0,1,\ldots,15$) and over thousands of configurations in the Monte Carlo sequence indeed gives a nonzero expectation value $\langle\varphi\rangle\approx 0.8$. Thus, despite the large mean-squared deviation caused by the quantum fluctuation (Fig. 53), the symmetry is broken (at least over long periods of time) and the ground state is still essentially degenerate.

The fluctuations due to quantum tunneling cause a renormalization (reduction) of the order parameter; it is this renormalized order parameter that should be compared to the x-ray experiment. Similarly, one expects the optical-absorption spectrum to peak at the correspondingly renormalized gap edge.

A more powerful fermion Monte Carlo method (Hirsch *et al.*, 1982; Hirsch and Fradkin, 1983), which does not invoke adiabatic approximation, was employed to study the quantum reduction on a larger ring (24 sites). It yielded a slightly smaller reduction (15%), so it is safe to conclude that bond alternation does survive quantum fluctuations in polyacetylene. A related interesting theoretical question is what would happen if the nuclei were massless so that the quantum effect was as large as it could be? It turns out that in this limiting case the lattice field can be integrated out to give an interacting fermion theory (Hirsch and Fradkin, 1983), the Gross-Neveu model (Gross and Neveu, 1974). The latter has been shown to possess dynamical symmetry breaking.

2. First-order corrections

Some quantum effects can be understood in terms of a straightforward expansion of the relevant quantities in powers of $(\hbar\omega_0/\Delta)$. Of these, the most important is the quantum correction to the soliton or polaron creation energy. To first order, this energy shift is just a result of the shift in the phonon zero-point energies (similar to a Casimir effect). The difference in the phonon zero-point energies in the presence and absence of a soliton appears as a correction to the soliton creation energy (Nakahara and Maki, 1982, 1986),

$$E_s=(2\Delta/\pi)+\frac{1}{2}\left[\sum_k(\hbar\bar{\omega}_k-\hbar\omega_k)+O(\hbar\omega_0)^2/\Delta\right]. \quad (8.1)$$

This correction is easily estimated. In the absence of the soliton, the phonon energies form a continuum starting at $\hbar\omega_0$ ($\hbar\omega_0=\hbar\Omega_0\sqrt{2\lambda}$). The density of states, as in all one-dimensional systems, has a $1/\sqrt{\omega-\omega_0}$ divergence near $\omega=\omega_0$. In the presence of a soliton, two states are pulled down from the continuum into the gap, the Goldstone mode to $\omega=0$ and the soliton shape mode to $\omega\approx 0.8\omega_0$, and the spectral density in the continuum is rearranged slightly. If we assume that the spectral weight stolen from the continuum comes predominantly from near $\omega=\omega_0$, then we can estimate that

$$E_s\approx(2\Delta/\pi)-1/2(0.0\hbar\omega_0+0.8\hbar\omega_0-2\hbar\omega_0) \quad (8.2a)$$

$$=(2\Delta/\pi)-0.6\hbar\omega_0\,. \quad (8.2b)$$

The quantum correction to E_s has been calculated (Nakahara and Maki, 1982, 1986) using the full phonon spectrum (see Sec. IV), with results in close agreement with Eq. (8.2). (This somewhat justifies our assumptions *a posteriori*.) Similar reasoning can be used to estimate the shift in the polaron creation energy using the energies of the localized phonon modes (Hicks and Blaisdell, 1985). Again, the result is in good agreement with an explicit calculation of the contribution from all modes:

$$E_p=(2^{3/2}/\pi)\Delta-0.85\hbar\omega_0+\cdots\,. \quad (8.3)$$

The direct calculation of the subgap optical-absorption constant is not straightforward. For $\hbar\omega$ substantially below 2Δ, the absorption involves high-order multiphonon processes, which precludes any sort of perturbative approach. The strongly nonlinear character of the phonon dynamics, which derives from the nonlocal and anharmonic nature of the adiabatic potential, renders the usual methods for summing over multiphonon processes inapplicable. For $\hbar\omega$ near $2E_s$, however, the optical-absorption problem can be mapped onto an equivalent multidimensional tunneling problem (Sethna and Kivelson, 1982), which can be solved using instanton methods, as discussed in the next subsection.

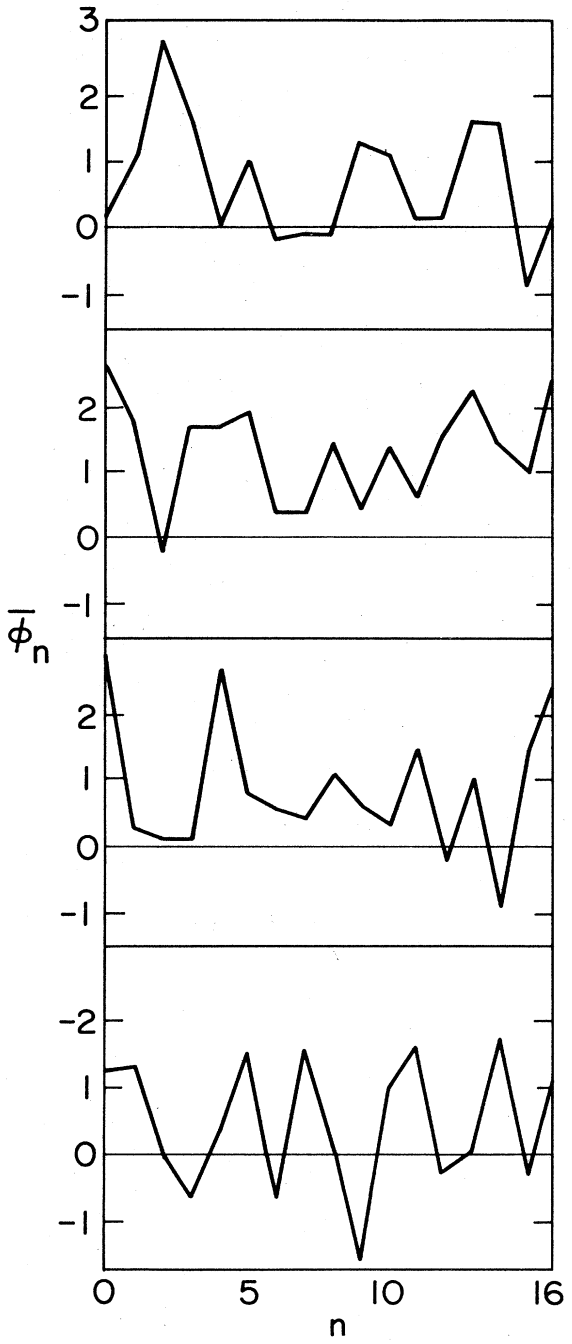

FIG. 53. Four typical configurations in the quantum ground state of a 16-site ring. The staggered order parameter ψ_n is normalized so that its average value is ± 1 for the classical ground states. From Su, 1981.

3. Excited states

A straightforward calculation of the absorption coefficient $\alpha(\omega)$ of a perfectly dimerized clamped lattice shows an inverse square-root singularity near the band gap 2Δ, $\alpha(\omega)\sim(\hbar\omega-2\Delta)^{-1/2}$ and nothing below it. Although a charged soliton-antisoliton pair has an energy lower than 2Δ, the optical transition to this state is for-

bidden by the Franck-Condon effect in the classical approximation. Once the quantum fluctuation is turned on, some virtual soliton-antisoliton pairs appear in the ground state and can lead to subgap optical absorption (Blanchet, Fincher, and Heeger, 1983; Weinberger *et al.*, 1984) and photoconductivity (Blanchet, Fincher, and Heeger, 1983). Moreover, the fact that an electron-hole pair decays into a soliton-antisoliton pair in such a short period of time means that there will certainly be a finite width in the absorption, thereby removing the singularity even in a strictly one-dimensional model.

There have been several attempts to understand the broadening mechanism more quantitatively. The absorption of a photon with energy $\hbar\omega < 2\Delta$ can be viewed as a tunneling process. For the tunneling path, a continuous family of soliton-antisoliton configurations was assumed, which are parametrized by the soliton-antisoliton separation R (Fig. 54) and for which analytical solutions for the electronic eigenstates are available. For simplicity, only the two gap states are considered. The total energy of the system in the electronic ground state as a function of R is the $V_0(R)$ curve in Fig. 55. $V_1(R)$ is the corresponding energy in the excited electronic state.

Starting at $R=0$, the system climbs up the potential energy hill described by $V_0(R)$ until a $S\bar{S}$ separation R_c is reached, where the energy difference between the upper

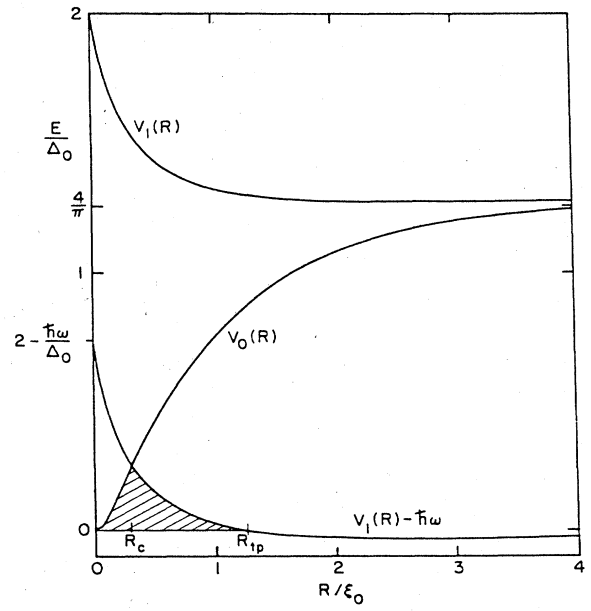

FIG. 55. Transition as a tunneling problem: adiabatic potential surfaces as a function of soliton separation R. Also shown is the upper surface shifted by a photon energy $\hbar\omega$. The shaded region is the tunneling barrier. Sethna and Kivelson, 1982.

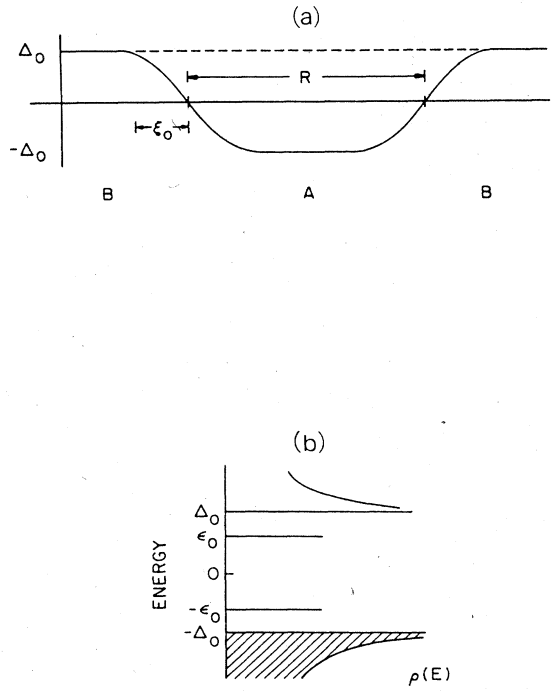

FIG. 54. Order parameter and level diagram for a soliton pair. (a) Schematic representation of a soliton-antisoliton pair. 2ξ is the soliton width, R is the separation between solitons; (b) electronic transition: density of electronic states in the presence of a soliton pair. The electronic transition is between the two localized gap states (at $\pm\varepsilon_0$).

and lower gap states is exactly $\hbar\omega$ so that optical transition can take place. From there, the system rolls down the other hill described by $V_1(R)-\hbar\omega$ until it hits the tunneling point R_{tp}. The WKB tunneling probability is proportional to $f(\omega)\exp[-S(\omega)]$ where

$$S(\omega)=2\int_0^{R_{tp}}\sqrt{2\mu V^*(R)}dR/\hbar\,. \tag{8.4}$$

More recently (Auerbach and Kivelson, 1986), the prefactor $f(\omega)$ was determined more accurately and found to be in good agreement with the experiment.

Alternatively, one can calculate the transition matrix elements connecting states with different lattice symmetry, using a formalism developed for treating the luminescence centers in solids (Su and Yu, 1983). Due to substantial change in the lattice geometry, the transition involves multiphonon emissions. As an example the nonradiative decay rate of a band electron into a polaron was calculated; a time scale consistent with the classical dynamical calculation was found. The rate of direct photoproduction of the $S\bar{S}$ pair was also calculated and shown to yield a broad absorption tail in the gap.

Third-harmonic generation has been used to probe the nonlinear optical susceptibility, $\chi_{\parallel}^{(3)}$, of polyacetylene (Sinclair, Moses, McBranch, *et al.*, 1988). Comparison of *cis*- and *trans*-$(CH)_x$ shows that $\chi_{\parallel}^{(3)}|_{\text{trans}}$ is 15–20 times larger than $\chi_{\parallel}^{(3)}|_{\text{cis}}$. The symmetry-specific aspect of $\chi_{\parallel}^{(3)}$ implies a mechanism that is sensitive to the existence of a degenerate ground state; it has been attribut-

ed to a mechanism that involves the generation of virtual solitons enabled by the nonlinear zero-point fluctuations in the ground state.

B. Soliton diffusion

Ideally, if a soliton behaved as a truly free particle, unscattered by other excitations or defects, its diffusion coefficient D would be infinite. In practice, a soliton is scattered both by thermally excited objects and by static defects. More generally, defects can pin a soliton, either charged or neutral, so that soliton motion is likely to be activated in the real system.

We restrict the discussion to scattering of a soliton by thermal excitations, the most important of which involves phonon-soliton scattering. As shown within the context of the φ^4 model, there are two fundamentally different mechanisms by which phonons influence D: center-of-mass motion and momentum exchange (Wada and Schrieffer, 1978).

Since low-amplitude sound waves (phonons) pass through a soliton without change of their momentum or energy, it would appear that this process cannot influence soliton motion. On closer inspection (Ogata and Wada, 1988), the phonon undergoes a phase shift such that, after the phonon has passed, the soliton's center of mass is displaced either to the left or to the right, depending on the phonon's wavelength compared to the soliton width 2ξ. This process leads to a random walk driven by the thermal population of phonons. One finds that the center-of-mass displacement mechanism leads to

$$D_{\text{c.m.}} = 2.06 T_s^2 c_0^2 \omega_0^{-1} , \tag{8.5}$$

where the scaled temperature is

$$T_s = k_B T / m l c_0 \omega_0 \varphi_0^2 . \tag{8.6}$$

Thus $D_{\text{c.m.}}$ varies as T^2.

The standard momentum exchange mechanism for this model was worked out with the following result:

$$D_{\text{mom}} = 12.25 c_0^2 / T_s \omega_0 , \tag{8.7}$$

so that D_{mom} varies as $1/T$. Combining Eqs. (8.6) and (8.7), one finds the total diffusion constant shown in Fig. 56 for zero frequency and frequencies $\omega/\omega_0 = 10^n$, $n = 1, 2, \ldots, 6$. One sees that D increases quadratically with T up to a crossover temperature $\tilde{T}$ representing the ratio of the energy of the thermally excited phonon to that of the soliton. Above $\tilde{T}$, soliton diffusion is limited by momentum exchange with phonons.

There are very little experimental data available relevant to the above calculations of soliton diffusion. Although neutral-soliton diffusion has been observed (see Sec. VI), the temperature dependence appears to be dominated by trapping. Charged solitons induced by doping are also pinned. The soliton diffusion may play an important role in the motion of the photoexcitations. In particular, the short-time transient photoconductivity (Sinclair *et al.*, 1986; Jeyadev and Conwell, 1987a, 1987b) and the decay of the photoinduced dichroism (Vardeny *et al.*, 1982) imply charged-soliton motion over relatively large distances.

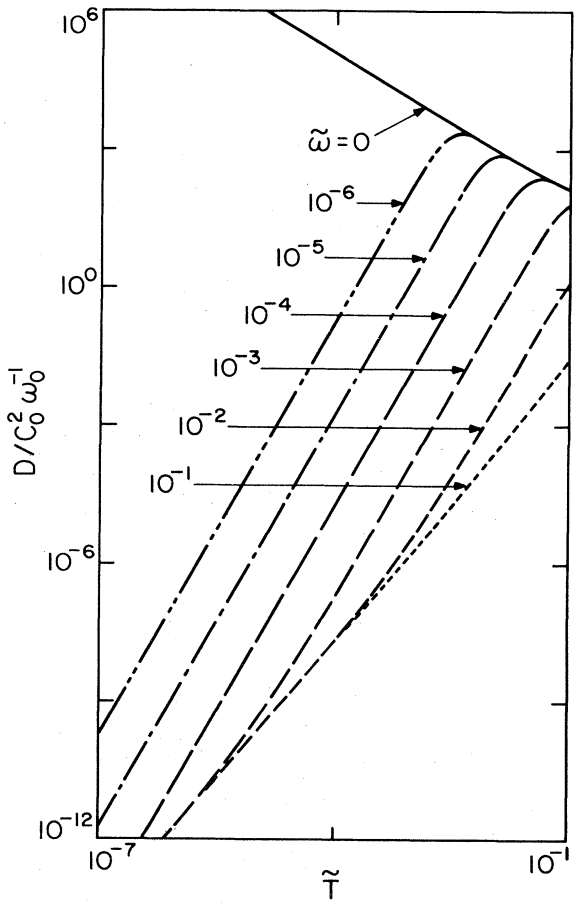

FIG. 56. The total diffusion cosntant, $D_{\text{c.m.}} + D_{\text{mom}}$.

C. Fractional charge

Solitons in $(CH)_x$ exhibit reverse charge-spin relations compared to electrons and holes. This is an example of a more general situation; namely, that topological excitations in broken-symmetry systems carry fractional quantum numbers.

The existence of stable excitations that carry fractional fermion numbers was first discovered in the Jackiw-Rebbi theory (Jackiw and Rebbi, 1976) of a spinless Dirac field coupled to a φ^4 Bose field in $1+1$ dimensions. Taking φ to be a static tanh kink, Jackiw and Rebbi found one zero-energy fermion state for each kink. In addition, the change of fermion number in the vicinity of the kink was either $\pm\frac{1}{2}$ depending upon whether the zero

mode was full or empty. Their proof of fractional charge relies on the charge-conjugation symmetry of their model.

While we are interested in quantum systems, the essence of the problem can be understood by the following simple classical model (Schrieffer, 1985). Consider an infinite line with the integers marked off as in Fig. 57. We place particles, each of charge q, on the odd sites starting at $-\infty$, leaving the even sites vacant. Having filled a given site, say number 1, we make an error and place the next particle at 2 instead of 3. We continue placing charges on every other site, i.e., the even sites to $+\infty$. Note that we have made two domains, one from $-\infty$ to 1 with odd sites occupied, even sites empty (termed the A phase), and another from 2 to $+\infty$ with the reverse occupancy (termed the B phase). A domain wall separates the two phases and is located at the midpoint $x=\frac{3}{2}$ between the two adjacent occupied sites. The width of the domain wall is irrelevant in determining the effective charge of the wall, as is easily seen.

Suppose we move the particle initially located on site 2 to site 3, as shown in the figure. Notice that the midpoint between the two adjacent occupied sites has moved to $x'=\frac{3}{2}+2$; that is, the domain wall moves *two units* even though we moved the particle only *one unit.*

Let us now determine the effective charge Q associated with the domain wall, i.e., the charge that will be observed in long-wavelength experiments. We do this by equating the change in electric dipole moment Δp of the system calculated in two ways, namely, through the particle motion $q\,(+1)$ and through the domain-wall motion $Q\,(+2)$. Since Δp must be independent of how we describe the system, we have $q=2Q$ or $Q=q/2$. Thus, from integer charges q, we have discovered an "excitation" whose charge Q is fractional, $Q/q=1/2$.

While this example appears to be trivial, it illustrates one mechanism for the occurrence of fractional charge, namely the existence of domain walls or, more generally, topological solitons separating degenerate ground states that have different negative-energy fermion wave functions. The charge-conjugate wall with $Q/q=-1/2$ is given by leaving two vacant spaces rather than no spaces between particles at the wall.

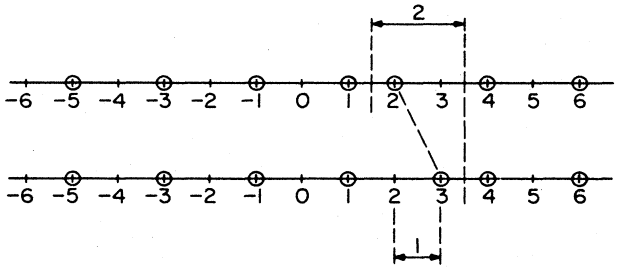

FIG. 57. A classical example of a fractionally charged excitation, illustrating the difference between the particle and domain-wall interpretation of the configuration changes.

Clearly, we could generalize the model to charge $Q/q=1/3$ by placing charges on every third site, with one rather than two spaces between particles at the wall, etc. Below, we discuss fractionalization in the quantum systems.

A simple general proof of particle or charge fractionalization, which holds for quantum and classical systems, is as follows (Kivelson and Schrieffer, 1982; Schrieffer, 1985). Suppose one has a one-dimensional charge-density (particle-density) wave system with the density described in terms of a charge-density wave (CDW) phase angle θ,

$$\rho(x)=\rho_0\cos[Kx+\theta(x)]. \tag{8.8}$$

We assume that the amplitude ρ_0 of the CDW is unaffected by spatial variations of θ. Let the ground state be n-fold degenerate. Then the system energy $E(\theta)$ has n degenerate minima at $\theta=2\pi\eta/n$, $\eta=0,1,2,\ldots,n$. In keeping with the above notation, we call these minima the $A,B,C,\ldots$ phases. Suppose $\theta\to 0$ as $x\to-\infty$ and θ increases to $(2\pi/n)$ as x passes x_1, to $2(2\pi/n)$ as x passes x_2, etc. until θ increases to $n(2\pi/n)=2\pi$ as x passes x_n.

The n domain walls or solitons are taken to be widely spaced compared to the width of the soliton. Assuming that the soliton charge is localized in the vicinity of each soliton, it follows from the translational invariance of the system that each soliton has the same charge Q. Thus the total charge of n solitons is nQ. However, the amount of charge passing to $+\infty$ as θ is deformed from $\theta(x)=0$ to the form shown in Fig. 57 is just the charge q per wavelength of the CDW, since a 2π phase shift corresponds to one wavelength of a CDW passing a given point. From charge conservation, we find

$$Q=-q/n\ . \tag{8.9}$$

For $n=2$ and two spin directions occupied, as in $(CH)_x$, $q=-2e$ (two π electrons per two carbon atoms in the dimerized structure). Thus $Q=e$, as discussed above. If, in Fig. 57, the phase shift at ∞ is -2π, $Q=-e$.

However, for $n=3$ ($\frac{1}{3}$-filled band) and two spin directions occupied, one still has $q=-2e$ but $Q=(2e)/(3)$ a fractional value. The fractional charge can be changed by integers by adding electrons or holes, i.e.,

$$Q=\begin{cases}\frac{2}{3}e,-\frac{1}{3}e,-\frac{4}{3}e\ ,\\ -\frac{2}{3}e,\frac{1}{3}e,\frac{4}{3}e\ ,\end{cases} \tag{8.10}$$

where the $\pm\frac{1}{3}e$ objects carry spin $\frac{1}{2}$, since the fundamental states $\pm\frac{2}{3}e$ are spinless, recognizing that both spin states have the same phase shift.

It has been proven that in the limit of a sampling region of size $L\gg\xi$, the fractional charge is quantum-mechanically sharp; i.e., it does not fluctuate about its mean value (Kivelson and Schrieffer, 1982). Thus, in this limit, a soliton is an eigenstate of the charge operator with fractional quantum number. These results are clearly related to those for the fractionally charged excitations present in the two-dimensional fractional quantum Hall

effect. Furthermore, these excitations exhibit fractional statistics in two dimensions (Arovas *et al.*, 1984).

D. High dopant concentration

When polyacetylene is doped to concentrations in excess of a critical concentration, $y_c \approx 6\%$, the system undergoes a rapid transition (Chen *et al.*, 1985; Moraes *et al.*, 1985) from the spinless soliton lattice state to a "metallic" state in which the spin susceptibility is roughly what one would expect from a nearly half-filled π band in the absence of any Peierls distortion. Nonetheless, there is indirect evidence from the infrared conductivity that the bond alternation, characteristic of the Peierls state, persists to the highest dopant levels (Rabolt *et al.*, 1979; Benoit *et al.*, 1983; Yang *et al.*, 1987). The transition between the soliton lattice and metallic states is always observed to be rapid as a function of y; for relatively more disordered arrangements of the dopant ions, it is more rounded (Epstein *et al.*, 1981), while for more ordered dopant lattices, in particular for Na-doped material (Chen *et al.*, 1985; Moraes *et al.*, 1985), the transition is sharp and hysteretic and, hence, probably first order.

The metallic state is fundamentally different from the low doping regime (where solitons are the important excitations); the charged excitations in the metallic state apparently carry spin as well. Since for any simple model of the Peierls state (such as the SSH or TLM models) the soliton lattice is always the lowest-energy state at any doping level, additional interactions that are not included explicitly in those models must play a role in driving the system to the metallic state. Since the nature of the metallic state is not yet well established, we summarize (Kivelson and Heeger, 1987) which interactions may play a role in driving this transition and summarize the current (incomplete) understanding of that transition. There are three important points.

(1) While in lightly doped $(CH)_x$ it is reasonable to expect that a simple model, in which to zeroth order only the dominant Peierls interaction is taken into account, will give an accurate description of the properties of the system for $y < y_c$, for $y > y_c$, many other interactions, notably electron-electron interactions, interchain coupling, dynamical phonon exchange, and disorder all are potentially of comparable importance to the static electron-phonon interaction considered by SSH. This greatly complicates the analysis of the metallic state.

(2) The critical concentration y_c at which this crossover occurs can be determined very simply from considerations independent of the nature of the metallic state to be $y_c = \text{const} \times (\Delta / W)$, where W is the π-band width, 2Δ is the Peierls gap, and const is a number of order unity.

(3) It is possible to show that if disorder is the dominant effect the system will make a transition to a gapless Peierls state (Mele and Rice, 1981; Yang *et al.*, 1987), whereas, if interchain coupling or electron-electron repulsion are the most important additional interactions, the system can have a transition to a polaron lattice (Kivelson and Heeger, 1985, 1987). This latter scenario is easily generalized to the case of nondegenerate ground states, where it leads to a transition from bipolaron lattice to polaron lattice.

Consider the evolution of the ground state as a function of y for the pure SSH model. For $y \neq 0$, the system is incommensurate with the underlying lattice, with the result that an incommensurate charge-density wave is set up with spatial period determined by the new value of the Fermi momentum,

$$\lambda_{SL} = (k_F - \pi/2a)^{-1} = (2a)y^{-1} . \tag{8.11}$$

At small values of y, this state is not at all sinusoidal but is rather a periodic array of solitons [a soliton lattice (SL) with one soliton and one antisoliton per unit cell]. Its properties are those of a collection of almost noninteracting solitons, so there is a narrow full band at midgap which derives from the midgap bound state associated with each soliton (see Fig. 58). The gap between occupied and unoccupied states remains $\approx \Delta$. The bandwidth of the midgap band is exponentially small, as are the interactions between solitons. Since both $\hbar\omega$ and V_d are large compared to the soliton-soliton interactions, either one of them will strongly perturb the ordered array of solitons. However, the properties of interest of the dilute, disordered array of solitons are similar to those of the ordered array, namely those of a dilute gas of noninteracting solitons.

New physics occurs when the separation between solitons becomes comparable to their width 2ξ, so that interactions between solitons become important. Because the soliton interactions fall off exponentially with distance at separation larger than ξ, the interactions turn on rather rapidly as a function of concentration even in the absence of any phase transition. Thus, on dimensional grounds alone, we can define a characteristic dopant con-

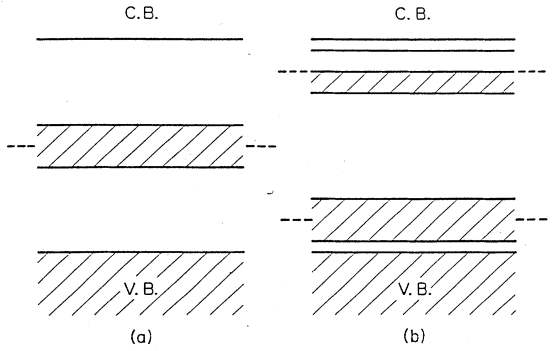

FIG. 58. Band diagrams comparing the soliton lattice and the polaron lattice: (a) soliton lattice—the midgap band is full (n-type doping); (b) polaron lattice—the upper polaron band is half-full (n-type doping).

centration y_c that is determined *solely* by the $y \to 0$ coherence length ξ at which the crossover from weakly interacting solitons to a new interacting state occurs:

$$y_c \approx (a/2\xi) . \tag{8.12}$$

In the SSH model, this new state is well approximated (Kotani, 1977) by a simple sinusoidal incommensurate CDW. The corresponding density of states is shown in Fig. 58(b). The incommensurate (Ic) state is still semiconducting. Note, however, that the gap, $2\Delta_{Ic}$, between the full midgap band and the conduction band is very much reduced; its new value is

$$\Delta_{Ic} \approx \Delta(2\Delta/W) \approx 0.2 \text{ eV} . \tag{8.13}$$

This energy may be small compared to the disorder potential, the effective electron-electron interactions, and the interchain bandwidth, and it is comparable to the phonon energy $\hbar\omega_0$. Thus a large fraction of the elements that gave us confidence in using the simple SSH model for the noninteracting system no longer pertain for $y > y_c$. We must seriously examine the effects of other interactions in producing the "metallic" state.

Disorder can easily turn the incommensurate state into a gapless Peierls state (Mele and Rice, 1981). Indeed, many of the features of the metallic state can be explained from this model (Yang *et al.*, 1987). However, in this model the transition to the metallic state is not a true phase transition, but rather a rapid crossover between two limiting results.

The possibility of a genuine phase transition has been demonstrated theoretically (Kivelson and Heeger, 1985, 1987). As a function of y the difference in energy per charge $\Delta E(y)$ of a soliton lattice and a polaron lattice falls in the SSH model from

$$\Delta E(0) = (2^{1/2} - 1)2\Delta/\pi \approx 0.41 E_S ,$$

where $E_S = 2\Delta/\pi$ is the soliton creation energy, to less than 10% of E_S for $y > y_c = (2\Delta/3W)$. The source of this reduction is the effective attraction between polarons (Onadera, 1980; Vardeny, Ehrenfreund, *et al.*, 1983) due to the formation of a half-filled band of delocalized electrons from the upper (antibonding) bound state of the isolated polaron (see Fig. 58). In the SSH model the energy of the polaron lattice is always greater than that of the soliton lattice, and the polaron lattice is not even locally metastable but is rather differentially unstable toward the formation of a soliton lattice (Kivelson and Heeger, 1985). However, because the polaron lattice is metallic, there are low-lying excitations which allow the system to develop the correlations necessary to take advantage of additional interactions. For instance, in the presence of interchain coupling, the polaron band develops a transverse bandwidth, and hence the polaron lattice gains an energy of order $-W_\perp$ per polaron. In the presence of electron-electron repulsion, the polaron lattice gains an energy of order $-(0.05)(U^{\text{eff}})^2/\Delta$, where U^{eff} is the repulsion between two electrons on the same polaron. In contrast, all the bands are filled for the soliton lattice, and hence its energy is not similarly reduced. It has been proved that for certain simplified models (Kivelson and Heeger, 1987) either of these interactions will actually drive the transition.

In trying to compare these theoretical considerations with experiment, one is confronted with the question of whether the observed first-order transition is of electronic origin (as implied by the above arguments), or whether it originates from a structural transition driven by the need for the polyacetylene lattice to accommodate the dopant ions during the doping process. This has been resolved for Na-doped polyacetylene through the *in situ* monitoring of the structural changes during electrochemical doping (Winokur *et al.*, 1987). The abrupt first-order increase in the magnetic susceptibility near 6 mol % appears to be the signature of a genuine *electronic* phase transition: it occurs without a change in structure (only the discommensuration density is changing in this regime).

Although the origin of the first-order transition and the nature of the metallic state remain important unresolved issues, from the considerations outlined above and in Kivelson and Heeger (1987), there is experimental evidence in favor of a soliton-lattice to polaron-lattice transition.

(i) The transition is first order; this has a number of consequences. As a function of dopant chemical potential, various quantities such as the susceptibility should be discontinuous and hysteretic. As a function of dopant concentration, the changes may be continuous, since for $y < y_c$ there may be coexistence of an inhomogeneously doped phase with regions of low dopant density and regions of density $> y_c$. Disorder does not drive the first-order transition; it would smear the transition out over a range of dopant concentrations.

(ii) The density of states at the Fermi surface for $y = y_c$ is easily seen to be approximately that of the undimerized chain:

$$\rho(E_F, y_c) = [(\pi/2)\hbar v_F^*]^{-1} = A\rho_0 ,$$

where $\rho_0 = (\pi t_0 a)^{-1} = [(\pi/2)\hbar v_F]^{-1}$ is the density of states at the Fermi surface and A was estimated (Kivelson and Heeger, 1985) for the noninteracting model to be 0.9. Here v_F and v_F^* are, respectively, the bare and effective Fermi velocities. The fact that $v_F^* \approx v_F$ also implies that most of the oscillator strength for optical absorption is exhausted by the intraband absorption. Similarly, the Pauli susceptibility should be comparable to that of the undimerized lattice.

(iii) The metallic state is strongly correlated and hence not obviously describable in terms of the noninteracting model. Both the repulsive interaction between two electrons on the same polaron, U^{eff}, and the induced attractive interaction due to the exchange of phonons are comparable to each other and to the polaron bandwidth (Kivelson and Heeger, 1985). In addition, there is the possibility of a further Peierls instability of the polaron

lattice. Thus the question of whether the state is truly metallic or whether there is a small remaining Coulomb or Peierls gap remains unanswered.

The strongest circumstantial evidence for this model comes from the observation of a first-order phase transition to a metallic state in Na^+-doped $(CH)_x$ at a dopant concentration of about $y_c \approx 6\%$, where the fact that $y_c \approx (2\Delta/3W)$ suggests that the transition is, in fact, driven by interactions in the π-electron band (soliton-soliton interactions). More generally, most of the existing experimental data seem to be roughly consistent with the present description of the transition but not uniquely so. On the other hand, the intensity of the IRAV modes in the metallic regime is difficult to understand within the context of a polaron metal (Rabolt *et al.*, 1979; Benoit *et al.*, 1983; Hicks *et al.*, 1987; Tanner *et al.*, 1987). More detailed theoretical and experimental studies are necessary to test the model critically.

IX. APPLICATIONS

With the discovery of conducting polymers about ten years ago, there was genuine excitement at the possibility of combining the important electronic properties of semiconductors and metals with the attractive mechanical properties and processing advantages of polymers. Without exception, however, the initial conducting polymer systems were insoluble, intractable, and nonmelting (and thus not processible), with relatively poor mechanical properties. In addition, the environmental sensitivity of the initial systems proved to be discouraging.

Remarkable progress has been made. The class of conducting polymers has been greatly enlarged, and a good underlying understanding of the fundamental molecular features necessary to achieve and control the electronic properties has begun to develop. Soluble conducting polymers have been developed (soluble either in water or in common organic solvents), and initial attempts at processing from solution (Nowak *et al.*, 1987), from the melt (Yoshino *et al.*, 1987), and from preformed gels as reaction media (Chiang *et al.*, 1988) have proven successful. Major improvements have been made in material quality, environmental stability, and in the achievement of highly oriented (chain-aligned) materials. Based on this excellent progress, there is every reason to believe that these materials will continue to evolve to the point where they can be used in a wide variety of technological applications.

In parallel with these efforts toward materials improvement, a number of potentially important application areas have been identified, including anisotropic electrical conductors, novel electrochemistry, and nonlinear optical phenomena.

The initial ideas were focused on the possible use of conducting polymers as conductors; i.e., as substitutes for known conductors. Although at earlier times this appeared remote, recent progress provides considerable optimism. With electrical conductivities of doped polyacetylene comparable to that of copper—and still improving—this area continues to be exciting. Note that on a weight basis, doped polyacetylene has already been demonstrated to be better than copper. Moreover, as noted in Sec. II, the available data imply that the intrinsic conductivity of chain-oriented polyacetylene is still much greater than that achieved to date. Thus the achievement in conducting polymers of levels of conductivity not available from conventional metals appears to be a realistic possibility. Moreover, based on current understanding, there is no reason to expect that these remarkable transport properties will be limited to polyacetylene. With comparable materials quality and chain orientation, other conjugated conducting polymers should do just as well. Major materials problems remain to be solved, including the achievement of environmental stability, high degrees of chain alignment, higher molecular weight, better chain perfection, etc. Nevertheless, it appears that the intrinsic transport properties are sufficiently attractive that they represent a potentially important area of applications. Note that the combination of ultrahigh conductivities plus high anisotropy represents a combination that is not available with conventional metals.

A number of other areas of potential applications have developed, each directly traceable to specific aspects of the fundamental science. The novel electrochemistry of conducting polymers was discovered in an attempt to achieve high-precision reproducible control over the doping level. This resulted in the discovery that such polymers could reversibly store charge and energy and opened the possibility of high-energy-density, high-power-density polymer battery electrodes. The related electrochromic phenomena were discovered through spectroscopic studies carried out *in situ* during electrochemical doping; this technique was initially designed to detect the shift in oscillator strength from the interband transition into the midgap soliton transitions. The electrochemical properties of this class of polymers continue to be attractive. Polymer batteries are being developed in a number of countries throughout the world. The unique advantages of materials in which the chemical (and/or electrochemical) potential can be controlled continuously have only begun to be explored. The principal limitation is the maximum doping level, which in turn determines the maximum energy density. Some improvement in energy density can perhaps be expected from the use of self-doped polymers (i.e., systems where the counter ions are covalently attached via side chains to the backbone), since the use of such polymers may allow one to significantly reduce the amount of solvent in the cell. Other device concepts based on the novel electrochemistry include the possibility of efficient chemical sensors (three-terminal devices analogous to field-effect transistors but using electrochemical doping of the conducting polymer rather than depletion of the channel).

The large third-order nonlinear optical susceptibility $\chi^{(3)}$ was discovered in the context of the shifts in oscilla-

tor strength associated with photogeneration of nonlinear excitations (the Su-Schrieffer mechanism for photogeneration of solitons, polarons, and bipolarons). Whatever the mechanism, the large $\chi^{(3)}$, the ability to withstand relatively high peak pump powers without damage to the sample, and the subpicosecond response have all been demonstrated through detailed experimental studies. Most importantly, the magnitude of $\chi^{(3)}$ is large enough to generate considerable interest in these polymers as nonlinear optical materials.

Based on the novelty of this class of electronically active polymers, other areas of potential applications can be expected to develop, particularly as the materials become available in processed form with a high degree of anisotropy from chain alignment.

X. SUMMARY AND CONCLUSIONS

In judging the correctness of the soliton model of polyacetylene and its generalizations to related systems in which the ground-state degeneracy has been weakly lifted, one must not only evaluate how well the theory accounts for the experimental facts, but also to what extent the data uniquely identify the "soliton picture" as the correct point of view. These issues are discussed throughout this review in a segmented fashion. Here we assemble this information, and we attempt to assess the success of the soliton approach.

The first issue is fundamental: do solitons (or bond-alternation domain walls) really exist in $(CH)_x$, and are they stable over substantial periods of time?

The evidence for the existence of the neutral soliton (S^0) in *trans*-$(CH)_x$ is presented in Sec. V.A. In the undoped material, the presence of a small concentration ($\sim\frac{1}{3000}$) of spin-$\frac{1}{2}$ defects has been confirmed both by the observation of a Curie law in the static magnetic susceptibility, $\chi\sim 1/T$, and through spin resonance measurements. A number of studies were carried out to determine the charge of these defects. For instance, the observation that compensation of residual dopants (with an associated major decrease in conductivity) has no effect on the number of spins demonstrates that the spin and the charge are decoupled; the spin is associated with a neutral object. Another signature of electrical neutrality is the absence of the localized infrared-active vibrational (IRAV) modes in pristine samples. Since doping and photoexcitation experiments have demonstrated unambiguously that charges on the polymer chains always lead to infrared-active localized phonons at known characteristic frequencies, the absence of IRAV modes in pure samples indicates that the spin-$\frac{1}{2}$ defects are neutral. All available evidence supports the assignment of zero charge to these spin-$\frac{1}{2}$ objects. Clearly they are stable; they exist as stable defects in the ground state.

The evidence for the existence of charged solitons ($S^{\pm}$) is discussed in Sec. V.B. When *trans*-$(CH)_x$ is doped either *p*-type or *n*-type with associated dilute concentrations of appropriate counter ions, or when *trans*-$(CH)_x$ is optically pumped, charge is stored in a self-localized configuration. Three essential signatures of $S^{\pm}$ are observed.

(1) New infrared modes are seen in the frequency range predicted by the soliton model. The existence of these modes implies that there is structural relaxation around the injected charge; the large oscillator strength of these modes indicates a light dynamical mass.

(2) Associated with the charge, a single new electronic transition is observed with frequency of order half the energy gap.

(3) Electron-spin resonance and magnetic susceptibility experiments show that these objects carry no spin.

In cases where the ground-state degeneracy has been weakly lifted, the corresponding three signatures of *confined* soliton pairs (bipolarons) are observed either after doping or upon photoexcitation. The analogous infrared-active vibrational modes again imply structural relaxation around the injected charge, and the large oscillator strength of these modes again indicates a light dynamical mass. Magnetic measurements again demonstrate that the charged objects are spinless. The clear splitting of the "midgap" electronic transition into a pair, symmetric with respect to the gap center, is a signature of the confinement resulting from the nondegenerate ground state.

Taken together, the above evidence strongly supports the unique reversed spin-charge assignments of the soliton model. However, other pictures such as localized free radicals and localized charge defects might also be able to account for some of these results. Therefore one must probe the dynamics of these objects to determine whether they can move over substantial distances in space.

To define more precisely what we mean by dynamics, we note that an extended object such as a soliton (or a confined soliton pair) is expected to have a nontrivial internal structure as well as a center-of-mass coordinate. The internal structure of a soliton corresponds to an eigenstate with $E=0$, occupied by 0, 1, or 2 electrons. The model predicts that the size of this eigenstate is 2ξ. Thus the soliton's spin (occupancy 1) or charge (occupancy 0 or 2) is spread over a large number of lattice spacings, even if the center of mass is fixed. The soliton as a whole can undergo translation, unless it is trapped by some pinning center.

Both aspects of these dynamics have been unambiguously observed for the spin-$\frac{1}{2}$ object. As discussed in Sec. V.A, when the spin is fixed and immobile, as is the case in partially isomerized (nearly all-*cis*) polyacetylene, both the ESR linewidth (and line shape) and the ENDOR results indicate a spatial spread of the spin density over a distance consistent with $2\xi\sim 15$ lattice spacings, as predicted by the soliton model. After complete isomerization to the translationally invariant all-*trans* form, the ESR line is further narrowed and the ENDOR spectrum collapses into a single line indicative of rapid center-of-

mass motion over distances $L \gg 2\xi$. Thus both the internal quantum spatial delocalization (over $\sim 2\xi$) and the center-of-mass motion of the neutral object are observed.

The principal ways of creating the charged self-localized configurations are by doping or by photoexcitation. While the former method is simple and is capable of creating a high concentration of such objects, the charged counter ions provide pinning centers which may immobilize the charge carriers. It is not clear from the available data whether or not there is any experimentally accessible range of temperatures and dopant concentrations at which the dopant-induced charged solitons are significantly delocalized to contribute directly to the measured conductivity.

On the other hand, when the charged objects are created by photoexcitation, there are no such pinning centers and, except for interactions between the excitations, the objects are free to move until trapped by a structural defect or until recombination occurs. As discussed in Sec. V.B.3, following the onset of optical pumping, there is an abrupt increase in (photo)conductivity to remarkably high levels, while on the same time scale the signatures of charged solitons (e.g., the midgap absorption) are evident. Thus the photogenerated $S^{\pm}$ move with moderately high mobility over a distance of order 400 Å before trapping or recombination. Moreover, from the decay of the photoinduced dichroism, we know that some photogenerated species, presumably the charged soliton, diffuse over comparable distances.

The spatial extent of the charged soliton can be deduced indirectly from the giant oscillator strength associated with the midgap absorption in lightly doped polyacetylene; due to the width of the soliton, the transition dipole moment is enhanced by a factor proportional to ξ/a. From the intensity of this absorption and from the magnitude of the associated bleaching of the interband transition, the width of the self-localized charged object can be inferred to be $\xi \approx 7a$, in good agreement with the theory.

Another excitation predicted by the model is a polaron—an electron or a hole clothed by an accompanying lattice distortion (or, equivalently, a bound state of a neutral and a charged soliton). While injection of an even number of electrons is expected to produce the same number of solitons, an extra odd electron is predicted to produce a polaron as well. Although magnetic resonance experiments are consistent with one polaron per odd electron per chain, there is no strong evidence of polaron formation in $(CH)_x$. For polythiophene and related derivatives, where the ground-state degeneracy has been lifted, the results unambiguously indicate bipolaron formation in high-quality samples. Evidence has been presented for polaron formation in polypyrrole and in polyaniline.

An early concern with the soliton model was the suggestion that the time required to create a soliton pair following photoabsorption above the energy gap might be quite long (with so many internal degrees of freedom associated with all the CH units within 2ξ, it might take a very long time for the system to settle into the collective coordinate). It has been experimentally demonstrated through time-resolved photoinduced absorption that the creation time is on the scale of 10^{-13} s. Direct integration of the equations of motion show that this rapid evolution occurs since there is no barrier to the prompt decay of an electron-hole pair into a pair of charged solitons; thus the natural conversion time is the optical-phonon period.

An important test of the soliton model is the effective mass of the object. From the infrared oscillator strength associated with the translational mode of the charged species, the soliton mass is observed to be of the order of several electron masses, rather than on the scale of the CH mass. This is also true for the case of confined solitons in nondegenerate-ground-state materials. The rapid motion implied by the magnetic resonance results for *trans*-$(CH)_x$ also requires a comparably small mass. This result is an inherent property of the soliton approach.

Another issue is whether the neutral and charged objects are topological or nontopological in character. Only if the objects are topologically nontrivial will the electronic spectrum show a single state in the gap per object, rather than a pair of states on either side of the gap center, as would be the case for the topologically trivial polarons and bipolarons. The fact that only a single midgap peak has been observed associated with injected charges in lightly doped or photoexcited polyacetylene is strong evidence of the topological character of the charged soliton. Of course, it is possible that the single peak is actually two unresolved peaks (as would be the case for a weakly confined bipolaron), but there is no evidence of such structure. This is made even more convincing by the clear observation of a double-peaked structure in the gap when similar experiments are carried out on polythiophene (and all of its derivatives), in which the ground-state degeneracy is known to be weakly lifted.

The evidence for the topological nature of the neutral soliton is more subtle. In the absence of Coulomb interactions, the spin density is required by symmetry to vanish on odd-numbered sites. The inclusion of interactions between electrons of opposite spin leads to an exchange spin polarization of opposite sign, so that there is net spin $(\frac{1}{2}+\delta)$ on the even-numbered sites and $(-\delta)$ on the odd. This is a consequence of the single midgap state; for a polaron, the spin would be distributed equally on even- and odd-numbered sites. This even-odd asymmetry has been studied in ENDOR and triple magnetic resonance experiments in which a bimodal distribution of spin densities associated with each neutral, spin-$\frac{1}{2}$ object has been observed: those with spin density $+\alpha$ and those with spin density $-\beta$. One might be concerned that the oscillating spin distribution would be averaged out if the object translated over a distance $L \gg a$ during the resonance period (as is the case in the experimental studies). Again, the theory shows that for a soliton, the even-odd asymmetry persists even with rapid motion; the positive spin always sits on the even sites for a soliton and the odd

sites for an antisoliton, regardless of the location of the center of mass.

Taken together, the results summarized in the preceding paragraphs provide strong evidence for the validity of the soliton model and its specific predictions.

There are a number of areas that require further study.

(i) In the intermediate doping regime ($0.01 < y < 0.06$) *trans*-$(CH)_x$ is a good conductor, with a remarkably low spin density. It is possible that in this regime, motion of the charged solitons (which are certainly tightly bound to the counter ions at the lowest doping concentration) could contribute to the dc conductivity. This would imply either a movable soliton lattice or a more disordered mobile soliton liquid.

(ii) Despite a number of interesting suggestions, the origin of the metallic state in heavily doped *trans*-$(CH)_x$ is not understood. This is especially interesting in the context of the recent discovery of electrical conductivities for doped polyacetylene comparable to that of copper. Thus both the nature of the metallic state and the transport within that state are problems of fundamental importance.

(iii) Although experimental studies of the details of the recombination pathways subsequent to photoexcitation have begun, the theory of these processes remains to be fully developed.

(iv) Since the photoexcitation of nonlinear excitations leads to spectral shifts, these are inherently nonlinear optical processes. The photoinduced absorption studies have unambiguously demonstrated large resonant nonlinear optical coefficients ($\chi^{(3)}$). In addition, nonresonant pumping below the gap, even in regions well away from possible two- and three-photon resonances, leads to third-harmonic generation with $\chi^{(3)}$ values among the largest ever measured—4×10^{-10} esu in oriented samples for light polarized along the polymer chain direction (Sinclair, Moses, McBranch, *et al.*, 1988), with larger values deeper in the infrared (Kajzar *et al.*, 1987b). The origin of these nonresonant nonlinear optical properties and the possibility that they might arise from virtual creation of nonlinear excitations remain to be explored in detail.

The relation between solitons in quasi-one-dimensional materials and higher-dimensional systems exhibiting topological excitations is an interesting area. Fractionally charged excitations and fractional statistics have been discussed in quantum field theory and in the fractional quantum Hall effect and are intimately related to the reversed spin-charge relations seen in polyacetylene; these connections warrant further study. Excitations similar to those discussed in this review have been proposed in two-dimensional systems.

In conclusion, self-localized nonlinear excitations (solitons, polarons, and bipolarons) are fundamental and inherent features of quasi-one-dimensional conducting polymers. Their signatures are evident in many aspects of the physical (and chemical) properties of this growing class of materials. As a result, these polymers represent an opportunity for exploring the novel phenomena associated with topological solitons and their linear confinement, which results from weakly lifting the ground-state degeneracy.

ACKNOWLEDGMENTS

This review was supported in part by the Institute for Theoretical Physics (NSF Grant No. THY-82-7853 supplemented by NASA). W.P.S. was supported by the Texas Advanced Technology Research Program through the University of Houston and the Robert A. Welch Foundation. S.K. was supported by NSF Grant No. DMR-83-18051 and by an Alfred P. Sloan Foundation Fellowship. J.R.S. was supported by NSF Grant No. DMR-85-17276. A.J.H. was supported by the Office Naval Research and by NSF Grants Nos. DMR-85-21392 and DMR-86-15483.

REFERENCES

Akagi, K., S. Katayama, H. Shirakawa, K. Araya, A. Mutoh, and T. Norabara, 1987, Synth. Met. **17**, 241.

Akaishi, T., K. Miyasaka, K. Ishikawa, H. Shirakawa, and S. Ikeda, 1980, J. Polym. Sci. Polym. Phys. Ed. **18**, 745.

Arovas, D., J. R. Schrieffer, and F. Wilczek, 1984, Phys. Rev. Lett. **53**, 722.

Ashkanazi, J., E. Ehrenfreund, Z. Vardeny, and A. O. Brafman, 1985, Mol. Cryst. Liq. Cryst. **117**, 193.

Atiyah, M. F., V. K. Patodi, and I. M. Singer, 1975, Proc. Cambridge Philos. Soc. **77**, 43.

Auerbach, A., and S. Kivelson, 1986, Phys. Rev. B **33**, 8171.

Baeriswyl, D., and K. Maki, 1983, Phys. Rev. B **28**, 2068.

Baeriswyl, D., and K. Maki, 1985a, Phys. Rev. B **31**, 6633.

Baeriswyl, D., and K. Maki, 1985b, Mol. Cryst. Liq. Cryst. **118**, 1.

Ball, R., W.-P. Su, and J. R. Schrieffer, 1983, J. Phys. (Paris) **C3**, 429.

Bargon, J., S. Mohmand, and R. J. Waltman, 1983, IBM J. Res. Dev. **27**, 330.

Barisic, S., 1983, J. Phys. (Paris) **44**, 185.

Basescu, N., Z.-X. Liu, D. Moses, A. J. Heeger, H. Naarmann, and N. Theophilou, 1987, Nature (London) **327**, 403.

Basescu, N., Z.-X. Liu, D. Moses, H. Naarmann, and N. Theophilou, 1988, in *Electronic Properties of Conjugated Polymers,* edited by H. Kuzmany, M. Mehring, and S. Roth, Springer Series in Solid State Sciences, No. 76 (Springer, Berlin), p. 156.

Baughman, R. H., S. L. Hsu, L. R. Anderson, G. P. Pez, and A. J. Signorelli, 1979, in *Molecular Metals,* edited by W. Hatfield (Plenum, New York).

Baughman, R. H., L. W. Shacklette, N. S. Murthy, G. G. Miller, and R. B. Elsenbaumer, 1985, Mol. Cryst. Liq. Cryst. **118**, 253.

Benoit, C., O. Bernard, M. Palpacuer, M. Rolland, and M. J. M. Abadic, 1983, J. Phys. (Paris) **44**, 1307.

Bernier, P., 1986, in *Handbook of Conducting Polymers,* edited by T. A. Skotheim (Dekker, New York/Basel), Vol. 2, p. 1099.

Bernier, P., 1987, private communication.

Bishop, A. R., D. K. Campbell, P. S. Lomdahl, B. Horovitz,

and S. R. Phillpot, 1984a, Phys. Rev. Lett. **52**, 671.
Bishop, A. R., D. K. Campbell, P. S. Lomdahl, B. Horovitz, and S. R. Phillpot, 1984b, Synth. Met. **9**, 223.
Blanchet, G. B., C. R. Fincher, T.-C. Chung, and A. J. Heeger, 1983, Phys. Rev. Lett. **50**, 1938.
Blanchet, G. B., C. R. Fincher, and A. J. Heeger, 1983, Phys. Rev. Lett. **51**, 2132.
Bleier, H., S. Roth, and G. Leising, 1987, Synth. Met. **17**, 521.
Bott, D. C., C. S. Brown, C. K. Chaio, N. S. Walker, W. J. Feast, P. J. S. Foot, P. O. Calvert, N. C. Billingham, and R. A. Friend, 1986, Synth. Met. **14**, 245.
Bradley, D. D. C., R. H. Friend, T. Hartmann, E. A. Monseglia, M. M. Sckolowski, and P. D. Townsend, 1987, Synth. Met. **17**, 473.
Brazovskii, S. A., 1978, Pis'ma Zh. Eksp. Teor. Fiz. **28**, 656 [JETP Lett. **28**, 606 (1978)].
Brazovskii, S. A., 1980, Zh. Eksp. Teor. Fiz. **78**, 677 [Sov. Phys. JETP **51**, 342 (1980)].
Brazovskii, S. A., and N. Kirova, 1981, Pis'ma Zh. Eksp. Teor. Fiz. **33**, 6 [JETP Lett. **33**, 4 (1981)].
Brazovskii, S. A., and N. N. Kirova, 1984, Sov. Sci. Rev. A **5**, 99.
Brédas, J.-L., 1985, J. Chem. Phys. **82**, 3808.
Brédas, J.-L., 1987, Synth. Met. **17**, 123.
Brédas, J.-L., R. R. Chance, and R. Silbey, 1981a, Mol. Cryst. Liq. Cryst. **77**, 319.
Brédas, J.-L., R. R. Chance, and R. Silbey, 1981b, Phys. Rev. B **26**, 5843.
Brédas, J.-L., A. J. Heeger, and F. Wudl, 1986, J. Chem. Phys. **85**, 4673.
Brédas, J.-L., and G. B. Street, 1985, Accounts Chem. Res. **18**, 309.
Brédas, J.-L., B. Thémans, J. G. Fripiat, J. M. André, and R. R. Chance, 1984, Phys. Rev. B **29**, 6761.
Brédas, J.-L., F. Wudl, and A. J. Heeger, 1987, Solid State Commun. **63**, 577.
Brückner, S., W. Porzio, and F. Wudl, 1988, Makro. Molecular Chemie. (in press).
Campbell, D. K., and A. R. Bishop, 1981, Phys. Rev. B **24**, 4859.
Cambell, D. K., and A. R. Bishop, 1982, Nucl. Phys. B **200**, 297.
Campbell, D. K., A. R. Bishop, and M. J. Rice, 1986, in *Handbook of Conducting Polymers,* edited by T. A. Skotheim (Dekker, New York/Basel), Vol. 2, p. 937.
Campbell, D. K., T. A. DeGrand, and S. Mazumdar, 1984, Phys. Rev. Lett. **52**, 1717.
Campbell, D. K., J. Schonfeld, and C. A. Wingate, 1983, Physica D **9**, 1.
Chance, R. R., J.-L. Brédas, and R. Silbey, 1984, Phys. Rev. B **29**, 4491.
Chao, K. A., and Y. Wang, 1987, J. Phys. C. **18**, L1127.
Chen, J., T.-C. Chung, F. Moraes, and A. J. Heeger, 1985, Solid State Commun. **53**, 757.
Chen, J., and A. J. Heeger, 1986a, Phys. Rev. B **33**, 1990.
Chen, J., and A. J. Heeger, 1986b, Solid State Commun. **58**, 251.
Chen, J., and A. J. Heeger, 1988, Synth. Met. (in press).
Chiang, C. K., M. A. Druy, S. Gau, A. J. Heeger, H. Shirakawa, E. J. Louis, A. G. MacDiarmid, and Y. W. Park, 1978, J. Am. Chem. Soc. **100**, 1013.
Chiang, C. K., C. R. Fincher, Y. W. Park, A. J. Heeger, H. Shirakawa, E. J. Louis, S. Gau, and A. G. MacDiarmid, 1977, Phys. Rev. Lett. **39**, 1098.
Chiang, C. K., S. C. Gau, C. R. Fincher, Y. W. Park, A. G. MacDiarmid, and A. J. Heeger, 1978, Appl. Phys. Lett. **33**, 18.
Chiang, C. K., Y. W. Park, A. J. Heeger, H. Shirakawa, E. J. Louis, and A. G. MacDiarmid, 1978, J. Chem. Phys. **69**, 5098.
Chiang, J. C., P. Smith, A. J. Heeger, and F. Wudl, 1988, Polymer (in press).
Chroboczek, J. A., and S. Summerfield, 1983, J. Phys. (Paris) **44**, C3-517.
Chung, T.-C., A. Feldblum, A. J. Heeger, and A. G. MacDiarmid, 1981, J. Chem. Phys. **74**, 5504.
Chung, T.-C., J. H. Kaufman, A. J. Heeger, and F. Wudl, 1983, Phys. Rev. B **30**, 702.
Chung, T.-C., F. Moraes, J. D. Flood, and A. J. Heeger, 1984, Phys. Rev. B **29**, 2341.
Clark, W. G., K. Glover, G. Mozurkewich, S. Etemad, and M. Marfield, 1985, Mol. Cryst. Liq. Cryst. **117** (Part A), 447.
Clark, W. G., K. Glover, G. Mozurkewich, C. T. Murayama, J. Sanny, S. Etemad, and M. Maxfield, 1983, J. Phys. (Paris) Suppl. **44**, C3-239.
Clarke, T. C., and J. C. Scott, 1986, in *Handbook of Conducting Polymers,* edited by T. A. Skotheim (Dekker, New York/Basel), Vol. 2, p. 1127.
Clarke, T. C., and G. B. Street, 1980, Synth. Met. **1**, 119.
Colaneri, N., R. H. Friend, H. Schaffer, and A. J. Heeger, 1988, Phys. Rev. B (in press).
Colaneri, N., M. Nowak, D. Spiegel, S. Hotta, and A. J. Heeger, 1987, Phys. Rev. B **36**, 7964.
Coleman, S., and E. Weinberg, 1980, Phys. Rev. D **7**, 1888.
Conwell, E. M. 1985a, Synth. Met. **9**, 195.
Conwell, E. M., 1985b, Mol. Cryst. Liq. Cryst. **117**, 155.
Conwell, E. M., 1987, IEEE Trans. Electr. Insul. **EI-22**, 591.
Cross, M. C., and D. S. Fisher, 1979, Phys. Rev. B **19**, 402.
Danielson, P. L., and R. C. Ball, 1985, J. Phys. (Paris) **46**, 1611.
Devreux, F., F. Genoud, K. Holczer, M. Nechtschein, and J. P. Travers, 1981, Mol. Cryst. Liq. Cryst. **83** (Part A), 97.
Devreux, F., F. Genoud, M. Nechtschein, and B. Villeret, 1987, Synth. Met. **18**, 89.
Diaz, A., 1981, Chem. Scr. **17**, 145.
Dodd, R. K., J. C. Eilbeck, J. D. Gibbon, and H. C. Morris, 1982, *Solitons and Nonlinear Wave Equations* (Academic, London/New York).
Drechsler, S. L., and M. Bobeth, 1985, Phys. Status Solidi B **131**, 267.
Edwards, J. H., and W. J. Feast, 1980, Polymer **21**, 595.
Edwards, J. H., W. J. Feast, and D. C. Bott, 1984, Polymer **25**, 395.
Epstein, A. J., 1986, in *Handbook of Conducting Polymers,* edited by T. A. Skotheim (Dekker, New York/Basel), Vol. 2, p. 1041.
Epstein, A. J., R. W. Bigelow, A. Feldblum, H. W. Gibson, D. M. Hoffman, and D. B. Tanner, 1984, Synth. Met. **9**, 155.
Epstein, A. J., H. Rommelmen, R. Bigelow, H. W. Gibson, D. M. Hoffman, and D. B. Tanner, 1983, Phys. Rev. Lett. **50**, 1866.
Epstein, A. J., H. Rommelmann, M. A. Druy, A. J. Heeger, and A. G. MacDiarmid, 1981, Solid State Commun. **38**, 683.
Etemad, S., A. J. Heeger, and A. G. MacDiarmid, 1982, Annu. Rev. Phys. Chem. **33**, 443.
Etemad, S., M. Ozaki, T. Mitani, A. J. Heeger, and A. G. MacDiarmid, 1981, Solid State Commun. **40**, 75.
Etemad, S., A. Pron, A. J. Heeger, A. G. MacDiarmid, E. J. Mele, and M. J. Rice, 1981, Phys. Rev. B **23**, 5137.
Feast, W. J., 1986, in *Handbook of Conducting Polymers,* edited by T. Skotheim (Dekker, New York/Basel), Vol. 1, p. 1.
Feldblum, A., R. W. Bigelow, H. W. Gibson, A. J. Epstein, and

D. B. Tanner, 1984, Mol. Cryst. Liq. Cryst. **105**, 191.
Feldblum, A., J. H. Kaufman, S. Etemad, A. J. Heeger, T.-C. Chung, and A. G. MacDiarmid, 1982, Phys. Rev. B. **26**, 815.
Fesser, K., A. R. Bishop, and D. K. Campbell, 1983, Phys. Rev. B **27**, 4804.
Fincher, C. R., C. E. Chen, A. J. Heeger, A. G. MacDiarmid, and J. B. Hastings, 1982, Phys. Rev. Lett. **48**, 100.
Fincher, C. R., D. Moses, A. J. Heeger, and A. G. MacDiarmid, 1983, Synth. Met. **6**, 243.
Fincher, C. R., M. Ozaki, A. J. Heeger, and A. G. MacDiarmid, 1979, Phys. Rev. B **19**, 4140.
Fincher, C. R., M. Ozaki, M. Tanaka, D. L. Peebles, L. Lauchlan, A. J. Heeger, and A. G. MacDiarmid, 1979, Phys. Rev. B **20**, 1589.
Fincher, C. R., D. L. Peebles, A. J. Heeger, M. A. Druy, Y. Matsumura, A. G. MacDiarmid, H. Shirakawa, and S. Ikeda, 1978, Solid State Commun. **27**, 2849.
Fink, J., H. Fark, N. Nucker, B. Scheerer, G. Leising, and R. Weizenhofer, 1987, Synth. Met. **17**, 377.
Fink, J., and G. Leising, 1986, Phys. Rev. B **34**, 5320.
Fitchen, D. B., 1982, Mol. Cryst. Liq. Cryst. **83**, 1127.
Flood, J. D., E. Ehrenfreund, A. J. Heeger, and A. G. MacDiarmid, 1982, Solid State Commun. **44**, 1055.
Flood, J. D., and A. J. Heeger, 1983, Phys. Rev. B **28**, 2556.
François, B., M. Bernard, and J. J. André, 1981, J. Chem. Phys. **75**, 4142.
Frommer, J. E., and R. R. Chance, 1986, in *Encyclopedia of Polymer Science and Engineering* (Wiley, New York), Vol. 5, p. 462.
Fukutome, H., and M. Sasai, 1983, Prog. Theor. Phys. **69**, 1 (Part II); **69**, 373 (Part III).
Gammel, J. T., and J. A. Krumhansl, 1981, Phys. Rev. B **24**, 1035.
Garnier, F., G. Tourillon, Y. Barraud, and H. Dexpert, 1985, J. Mat. Sci. **20**, 2687.
Genoud, F., M. Guglielmi, M. Nechtschein, E. Genies, and M. Salmon, 1985, Phys. Rev. Lett. **55**, 118.
Gervais, J. L., and B. Sakita, 1975, Phys. Rev. D **11**, 2943.
Goldberg, I. B., H. R. Crowe, P. R. Newman, A. J. Heeger, and A. G. MacDiarmid, 1979, J. Chem. Phys. **70**, 1132.
Grant, P. M., and I. Batra, 1979, Solid State Commun. **29**, 225.
Grant, P. M., and I. Batra, 1983, J. Phys. (Paris) Colloq. **C-44**, 437.
Gross, D. J., and A. Neveu, 1974, Phys. Rev. D **10**, 3235.
Grupp, A., P. Hofer, H. Kass, M. Mehring, R. Weizenhofer, and G. Wegner, 1987, in *Electronic Properties of Conjugated Polymers,* edited by H. Kuzmany, M. Mehring, and S. Roth, Springer Series in Solid State Sciences No. 76 (Springer, Berlin), p. 156.
Guinea, F., 1984, Phys. Rev. B **30**, 1884.
Harada, I., Y. Furukawa, M. Tasumi, H. Shirakawa, and S. Ikeda, 1980, J. Chem. Phys. **73**, 4746.
Harbeke, G., 1986, Phys. Scr. **T13**, 302.
Harbeke, G., E. Meier, W. Kobel, M. Egli, H. Kiess, and E. Tassatti, 1985, Solid State Commun. **55**, 419.
Hattori, T., W. Hayes, K. Wong, K. Kaneto, and K. Yoshino, 1984, J. Phys. C **17**, L803.
Hayden, G. W., and E. J. Mele, 1985, Phys. Rev. B **32**, 6527.
Haden, G. W., and E. J. Mele, 1986, Phys. Rev. B **34**, 5484.
Hayes, W., F. L. Pratt, K. S. Wong, K. Kaneto, and K. Yoshino, 1985, J. Phys. C **18**, L555.
Heeger, A. J., 1981, Comments Solid State Phys. **10**, 53.
Heeger, A. J., 1985, Mol. Cryst. Liq. Cryst. **125**, 289.
Heeger, A. J., and A. G. MacDiarmid, 1981, Mol. Cryst. Liq. Cryst. **83** (Part A), 1.
Heeger, A. J., and J. R. Schrieffer, 1983, Solid State Commun. **48**, 207.
Hicks, J. C., and G. A. Blaisdell, 1985, Phys. Rev. B **31**, 919.
Hicks, J. C., J. Tinka Gammel, H.-Y. Choi, and E. J. Mele, 1987, Synth. Met. **17**, 57
Hirsch, J. E., 1983, Phys. Rev. Lett. **51**, 296.
Hirsch, J. E., and E. Fradkin, 1982, Phys. Rev. Lett. **49**, 402.
Hirsch, J. E., and E. Fradkin, 1983, Phys. Rev. B **27**, 1680 (Part I), 4302 (Part II).
Hirsch, J. E., and M. Grabowski, 1984, Phys. Rev. Lett. **52**, 1713.
Hirsch, J. E., R. L. Sugar, D. J. Scalapino, and R. Blankenbeckler, 1982 Phys. Rev. B **26**, 5033.
Hoffman, D., 1984, Ph.D. Thesis (Ohio State University).
Holczer, K., F. Devreux, M. Nechtschein, and J. P. Travers, 1981, Solid State Commun. **39**, 881.
Horovitz, B., 1982, Solid State Commun. **41**, 729.
Horovitz, B., and J. Solyom, 1985, Phys. Rev. B **32**, 2681.
Horovitz, B., Z. Vardeny, E. Ehrenfreund, and O. Brafman, 1984, Synth. Met. **9**, 215.
Horsch, P., 1981, Phys. Rev. B **24**, 7351.
Hotta, S., S. D. D. V. Rughooputh, A. J. Heeger, and F. Wudl, 1987, Macromolecules **20**, 212.
Hotta, S., W. Shimotsuma, and M. Taketani, 1984, Synth. Met. **10**, 85.
Hotta, S., W. Shimotsuma, M. Taketani, and S. Kohiki, 1985, Synth. Met. **11**, 139.
Ikehata, S., J. Kaufer, T. Woerner, A. Pron, M. A. Druy, A. Sivak, A. J. Heeger, and A. G. MacDiarmid, 1981, Phys. Rev. Lett. **45**, 1123.
Ito, H., and Y. Ono, 1985, J. Phys. Soc. Jpn. **54**, 1194.
Ito, H., A. Terai, Y. Ono, and Y. Wada, 1984, J. Phys. Soc. Jpn. **53**, 3519.
Jackiw, R., and C. Rebbi, 1976, Phys. Rev. D **13**, 3398.
Jackiw, R., and J. R. Schrieffer, 1981, Nucl. Phys. B **190**, 253.
Jeffries, C. D., 1963, *Dynamic Nuclear Polarization* (Interscience, New York).
Jen, K. Y., R. Oboodi, and R. L. Elsenbaumer, 1985, Polym. Mater. Sci. Eng. **53**, 79.
Jen, K. Y., R. Oboodi, and R. L. Elsenbaumer, 1986, Synth. Met. **15**, 169.
Jeyadev, S., and E. M. Conwell, 1987a, Phys. Rev. B **35**, 5917.
Jeyadev, S., and E. M. Conwell, 1987b, Phys. Rev. B **35**, 6253.
Kahlert, H., A. Leitner, and G. Leising, 1987, Synth. Met. **17**, 467.
Kajzar, F., S. Etemad, G. L. Baker, and J. Messier, 1987a, Synth. Met. **17**, 563.
Kajzar, F., S. Etemad, G. L. Baker, and J. Messier, 1987b, Solid State Commun. **63**, 1113.
Kaneto, K., Y. Kohno, K. Yoshio, and Y. Inuishi, 1983, J. Chem. Soc. Chem. Commun. 1983: 382.
Kaneto, K., and K. Yoshino, 1984, Solid State Commun. **51**, 267.
Kaneto, K., and K. Yoshino, 1987, Synth. Met. **18**, 133.
Kass, H., P. Hofer, A. Grupp, P. K. Kahol, R. Weizenhofer, G. Wegner, and M. Mehring, 1987, Europhys. Lett. **4**, 947.
Kaufman, J. H., T.-C. Chung, and A. J. Heeger, 1984, J. Electrochem. Soc. **131**, 2847.
Kaufman, J. H., N. Colaneri, J. C. Scott, and G. B. Street, 1984, Phys. Rev. Lett. **53**, 1005.
Kaufman, J. H., J. Kaufer, A. J. Heeger, R. Kaner, and A. G. MacDiarmid, 1983, Phys. Rev. B **26**, 4.
Kim, Y. H., S. Hotta, and A. J. Heeger, 1987, Phys. Rev. B **36**,

7486.
Kivelson, S., 1981, Phys. Rev. Lett. **46**, 1344.
Kivelson, S., 1982, Phys. Rev. B **25**, 3798.
Kivelson, S., 1983, Mol. Cryst. Liq. Cryst. **77**, 65.
Kivelson, S., 1986, in *Solitons,* edited by S. E. Trullinger, V. E. Zakharov, and V. L. Pokrovsky (Elsevier Science, Amsterdam), p. 30.
Kivelson, S., and A. J. Heeger, 1985, Phys. Rev. Lett. **55**, 308.
Kivelson, S., and A. J. Heeger, 1987, Synth. Met. **17**, 183.
Kivelson, S., and D. E. Heim, 1982, Phys. Rev. B **26**, 4278.
Kivelson, S., T. K. Lee, Y. R. Lin-Lliu, and Lu Yu, 1982, Phys. Rev. B **25**, 4173.
Kivelson, S., and J. R. Schrieffer, 1982, Phys. Rev. B **25**, 6447.
Kivelson, S., W.-P. Su, J. R. Schrieffer, and A. J. Heeger, 1987, Phys. Rev. Lett. **58**, 1899.
Kivelson, S., H. B. Thacker, and W.-K. Wu, 1985, Phys. Rev. B **31**, 3785.
Kivelson, S., and W.-K. Wu, 1986a, Mol. Cryst. Liq. Cryst. **118**, 9.
Kivelson, S., and W.-K. Wu, 1986b, Phys. Rev. B **34**, 5423.
Kobayashi, M., J. Chen, T.-C. Chung, F. Moraes, A. J. Heeger, and F. Wudl, 1984, Synth. Met. **9**, 77.
Kobayashi, M., N. Colaneri, M. Boysel, F. Wudl, and A. J. Heeger, 1985, J. Chem. Phys. **82**, 5717.
Kotani, A., 1977, J. Phys. Soc. Jpn. **42**, 408.
Krivnov, A., and A. Ovchinnikov, 1986, Zh. Eksp. Teor. Fiz. **90**, 709 [Sov. Phys. JETP **63**, 414 (1986)].
Krumhansl, J., and J. R. Schrieffer, 1975, Phys. Rev. B **11**, 3535.
Kuroda, S., H. Bando, and H. Shirakawa, 1984, Solid State Commun. **52**, 893.
Kuroda, S., H. Bando, and H. Shira Ka Wa, 1985, J. Phys. Soc. Jpn. **54**, 3956.
Kuroda, S., and H. Shirakawa, 1987, Synth. Met. **17**, 423.
Kuzmany, H., 1980, Phys. Status Solidi B **97**, 521.
Kuzmany, H., E. A. Imhoff, D. B. Fitchen, and A. Surhangi, 1982, Phys. Rev. B **26**, 7109.
Kwak, J. G., T. C. Clarke, R. L. Greene, and G. B. Street, 1979, Solid State Commun. **31**, 355.
Lauchlan, L., S. P. Chen, S. Etemad, M. Kletter, A. J. Heeger, and A. G. MacDiarmid, 1983, Phys. Rev. B **27**, 2301.
Lauchlan, L., S. Etemad, T.-C. Chung, A. J. Heeger, and A. G. MacDiarmid, 1981, Phys. Rev. B **24**, 3701.
Lee, T. K., and S. Kivelson, 1984, Phys. Rev. B **29**, 6687.
Lefrant, S., 1983, J. Phys. (Paris) **44**, C3-247.
Leising, G., 1987, talk given at Symposium on Conducting Polymers: Their Emergence and Future, American Chemical Society Meeting, Denver, CO (to be published).
Leising, G., R. Vitz, B. Angele, W. Ottinger, and F. Stelzer, 1985, Mol. Cryst. Liq. Cryst. **117** (Part A), 327.
Lichtmann, L. S., A. Sarhangi, and D. B. Fitchen, 1980, Solid State Commun. **36**, 869.
Longuet-Higgins, H. C., and L. Salem, 1959, Proc. R. Soc. London Ser. A **251**, 172.
MacDiarmid, A. G., and R. Kaner, 1986, in *Handbook of Conducting Polymers,* edited by T. A. Skotheim (Dekker, New York/Basel), Vol. 1, p. 689.
MacInnes, D., M. A. Druy, P. J. Nigrey, D. P. Nairns, A. G. MacDiarmid, and A. J. Heeger, 1981, J. Chem. Soc. Chem. Commun. 1981: 316.
Mazumdar, S., and S. M. Dixit, 1983, Phys. Rev. Lett. **51**, 292.
Mele, E. J., 1982, Phys. Rev. B **26**, 6901.
Mele, E. J., and J. C. Hicks, 1985, Phys. Rev. B **32**, 2703.
Mele, E. J., and J. C. Hicks, 1986, Synth. Met. **13**, 149.
Mele, E. J., and M. J. Rice, 1980a, Phys. Rev. Lett. **45**, 926.
Mele, E. J., and M. J. Rice, 1980b, Solid State Commun. **34**, 339.
Mele, E. J., and M. J. Rice, 1981, Phys. Rev. B **23** 5397.
Metropolis, V. A., Rosenbluth, M. Rosenbluth, A. Teller, and E. Teller, 1953, J. Chem. Phys. **21**, 1087.
Mizoguchi, K., K. Kume, and H. Shirakawa, 1984, Solid State Commun. **50**, 213.
Mo, Z., K.-B. Lee, Y. B. Moon, M. Kobayashi, A. J. Heeger, and F. Wudl, 1985, Macromolecules **18**, 1972.
Moon, Y.-B., M. Winokur, A. J. Heeger, J. Barker, and D. C. Bott, 1987, Macromolecules **20**, 2457.
Moraes, F., J. Chen. T.-C. Chung, and A. J. Heeger, 1985, Synth. Met. **11**, 271.
Moraes, F., Y. W. Park, and A. J. Heeger, 1986, Synth. Met. **13**, 113.
Moraes, F., H. Schaffer, M. Kobayashi, A. J. Heeger, and F. Wudl, 1984, Phys. Rev. B **30**, 2948.
Moses, D., J. Chen, A. Denenstein, A. J. Heeger, and A. G. MacDiarmid, 1981, Solid State Commun. **40**, 1007.
Moses, D., A. Denenstein, C. K. Chiang, A. J. Heeger, and A. G. MacDiarmid, 1980, Solid State Commun. **36**, 219.
Moses, D., A. Feldblum, A. Denenstein, E. Ehrenfreund, T.-C. Chung, A. J. Heeger, and A. G. MacDiarmid, 1982, Phys. Rev. B **26**, 2361.
Mulazzi, E., G. P. Brivio, E. Faulques, and S. Lefrant, 1983, Solid State Commun. **46**, 851.
Mulazzi, E., G. P. Brivio, E. Faulques, and S. Lefrant, 1985, Solid State Commun. **53**, 583.
Naarmann, H., 1987a, Synth. Met. **17**, 223.
Naarmann, H., 1987b, talk given at Symposium on Conducting Polymers: Their Emergence and Future, American Chemical Society Meeting, Denver, CO (to be published).
Naarmann, H., and N. Theophilou, 1987, Synth. Met. **22**, 1.
Nakahara, M., and K. Maki, 1982, Phys. Rev. B **25**, 7789.
Nakahara, M., and K. Maki, 1986, Synth. Met. **13**, 149.
Nechtschein, M., F. Devreux, F. Genoud, M. Guglielmi, and K. Holczer, 1983a, J. Phys. (Paris) Colloq. **44**, C3-209.
Nechtschein, M., F. Devreux, F. Genoud, M. Guglielmi, and K. Holczer, 1983b, Phys. Rev. B **27**, 61.
Nechtschein, M., F. Devreux, F. Genoud, E. Vieil, J. M. Pernant, and E. Genies, 1986, Synth. Met. **15**, 59.
Nechtschein, M., F. Devreux, R. L. Greene, T. C. Clark, and G. B. Street, 1980, Phys. Rev. Lett. **44**, 356.
Neuman, C.-S., and R. van Boltz, 1988, Phys. Rev. B (in press).
Nigrey, P. J., A. G. MacDiarmid, and A. J. Heeger, 1979, J. Chem. Soc. Chem. Commun. 1979: 594.
Nowak, M., S. D. D. V. Rughooputh, S. Hotta, and A. J. Heeger, 1987, Macromolecules **20**, 965.
Ogata, M., and Y. Wada, 1988, J. Phys. Soc. Jpn. (in press).
Onadera, Y., 1980, Phys. Rev. B **30**, 775.
Orenstein, J., and G. L. Baker, 1982, Phys. Rev. Lett. **49**, 1043.
Orenstein, J., Z. Vardeny, G. L. Baker, G. Eagle, and S. Etemad, 1984, Phys. Rev. B **30**, 786.
Park, Y. W., A. Denenstein, C. K. Chiang, A. J. Heeger, and A. G. MacDiarmid, 1979, Solid State Commun. **29**, 747.
Peierls, R. E., 1955, *Quantum Theory of Solids* (Clarendon, Oxford).
Piaggio, D., G. Dellepiane, L. Pisari, R. Tubino, and C. Taliana, 1984, Solid State Commun. **50**, 947.
Pines, D., 1961, Ed., *The Many Body Problem* (Benjamin, New York).
Pople, J. A., and S. H. Walmsley, 1962, Mol. Phys. **5**, 15.
Rabolt, J. F., T. C. Clarke, and G. B. Street, 1979, J. Chem.

Phys. **71**, 4614.
Rice, M. J., 1979, Phys. Lett. **71**, 152.
Robin, R., J. P. Pouget, R. Carres, H. W. Gibson, and A. J. Epstein, 1983a, Phys. Rev. B **27**, 3938.
Robin, R., J. P. Pouget, R. Carres, H. W. Gibson, and A. J. Epstein, 1983b, J. Phys. (Paris) **44**, C3-77.
Rothberg, L., T. M. Jedju, S. Etemad, and G. L. Baker, 1986, Phys. Rev. Lett. **57**, 3229.
Salem, L., 1966, *The Molecular Orbital Theory of Conjugated Systems* (Benjamin, New York).
Sato, M., S. Tanaka, and K. Kaseriyama, 1985, J. Chem. Soc., Chem. Commun. 1985: 713.
Sato, M., S. Tanaka, and K. Kaseriyama, 1986, Synth. Met. **14**, 289.
Schaffer, H., and A. J. Heeger, 1986, Solid State Commun. **59**, 415.
Schaffer, H., R. H. Friend, and A. J. Heeger, 1987, Phys. Rev. B **36**, 7537.
Schrieffer, J. R., 1964, *Theory of Superconductivity* (Benjamin, New York).
Schrieffer, J. R., 1985, in *Highlights of Condensed Matter Theory: Proceedings of the International School of Physics Enrico Fermi, Course LXXXIX. . .1983,* edited by F. Bassani (Elsevier, New York), Vol. 89, p. 300.
Scott, J. C., J. L. Bredas, K. Yakushi, P. Pfluger, and G. B. Street, 1984, Synth. Met. **9**, 165.
Scott, J. C., P. Pfluger, M. T. Krounbi, and G. B. Street, 1983, Phys. Rev. B **28**, 2140.
Seeger, K., W. D. Gill, T. C. Clarke, and G. B. Street, 1978, Solid State Commun. **28**, 873.
Sethna, J. P., and S. Kivelson, 1982, Phys. Rev. B **26**, 3613.
Shacklette, L. W., N. S. Murthy, and R. J. Baughman, 1985, Mol. Cryst. Liq. Cryst. **121**, 201.
Shacklette, L. W., and J. E. Toth, 1985, Phys. Rev. B **32**, 5892.
Schacklette, L. W., J. E. Toth, N. S. Murthy, and R. H. Baughman, 1985, J. Electrochem. Soc. **132**, 1529.
Shank, C. V., 1984, Science **219** (March), 1027.
Shank, C. V., R. Yen, R. L. Fork, J. Orenstein, and G. L. Baker, 1982, Phys. Rev. Lett. **49**, 1660.
Shank, C. V., R. Yen, J. Orenstein, and G. L. Baker, 1983, Phys. Rev. B **28**, 6095.
Shirakawa, H., and S. Ikeda, 1979/1980, Synth. Met. **1**, 175.
Shirakawa, H., E. J. Louis, A. G. MacDiarmid, C. K. Chiang, and A. J. Heeger, 1977, Chem. Commun. 1977: 578.
Sinclair, M., D. Moses, and A. J. Heeger, 1986, Solid State Commun. **57**, 343.
Sinclair, M., D. Moses, D. McBranch, A. J. Heeger, J. Yu, and W. P. Su, 1988, Phys. Scr. (in press).
Sinclair, M., D. Moses, A. J. Heeger, and K. Akagi, 1988, Phys. Rev. B (in press).
Skotheim, T. A., 1986, Ed., *Handbook of Conducting Polymers* (Dekker, New York/Basel).
Solyom, J., 1979, Adv. Phys. **28**, 201.
Su, W.-P., 1982, Solid State Commun. **42**, 497.
Su, W.-P., 1987, Phys. Rev. B **35**, 9245.
Su, W.-P., S. Kivelson, and J. R. Schrieffer, 1980, in *Physics in One Dimension,* edited by T. Bernasconi and T. Schneider (Springer, Berlin), p. 201.
Su, W.-P., and J. R. Schrieffer, 1980, Proc. Natl. Acad. Sci. U.S.A. **77**, 5626.
Su, W.-P., J. R. Schrieffer, and A. J. Heeger, 1979, Phys. Rev. Lett. **42**, 1698.
Su, W.-P., J. R. Schrieffer, and A. J. Heeger, 1980, Phys. Rev. B **22**, 2099.
Su, Z.-B., and L. Yu, 1983, Phys. Rev. B **27**, 5199.
Subbaswamy, K. R., and M. Grabowski, 1981, Phys. Rev. B **24**, 2168.
Sum, U., K. Fesser, and H. Buttner, 1987a, J. Phys. C **20**, L71.
Sum, U., K. Fesser, and H. Buttner, 1987b, Solid State Commun. **61**, 607.
Sun, X., C. Wu, and X. Shen, 1985, Solid State Commun. **56**, 1039.
Suzuki, H., M. Ozaki, S. Etemad, A. J. Heeger, and A. G. MacDiarmid, 1980, Phys. Rev. Lett. **45**, 1209.
Takayama, M., Y. R. Lin-Liu, and K. Maki, 1980, Phys. Rev. B **21**, 2388.
Tanner, D. B., G. Doll, K. Rao, M. H. Yang, P. C. Eckhurt, G. Arbuckle, and A. G. MacDiarmid, 1987, Bull. Am. Phys. Soc. **32**, 422.
Tanaka, M., A. Watanabe, and J. Tanaka, 1980, Bull. Chem. Soc. Jpn. **53**, 645, 3430.
Tavan, P., and K. Schulten, 1988, Phys. Rev. B **36**, 4337.
Terai, A., and Y. Ono, 1986, J. Phys. Soc. Jpn. **55**, 213.
Terai, A., Y. Ono, and Y. Wada, 1985, J. Phys. Soc. Jpn. **54**, 4468.
Terai, A., Y. Ono, and Y. Wada, 1986, J. Phys. Soc. Jpn. **55**, 2889.
Thomann, H., and G. L. Baker, 1987, J. Am. Chem. Soc. **109**, 1569.
Thomann, H., L. R. Dalton, M. Grabowski, Y. Tomkiewicz, N. S. Shiren, and T. C. Clarke, 1983, Phys. Rev. Lett. **50**, 533.
Thomann, H., H. Jin, and G. L. Baker, 1987, Phys. Rev. Lett. **59**, 509.
Tomboulis, T., 1975, Phys. Rev. D. **12**, 1678.
Tomkiewicz, Y., T. D. Schultz, H. B. Brom, A. R. Taranko, T. C. Clarke, and G. B. Street, 1981, Phys. Rev. B **24**, 4348.
Tomkiewicz, Y., N. S. Shiren, T. D. Schultz, H. Thomann, L. R. Dalton, A. Zettl, G. Gruner, and T. C. Clarke, 1981, Mol. Cryst. Liq. Cryst. **83** (Part D), 1049.
Tomkiewicz, Y., A. R. Taranko, and T. D. Schultz, 1979, Phys. Rev. Lett. **43**, 1532.
Tourillon, G., and F. Garnier, 1982, J. Electroanal. Chem. **135**, 173.
Townsend, P. D., D. D. C. Bradley, M. E. Horton, C. M. Pereira, R. H. Friend, N. C. Billingham, P. D. Calvert, P. J. S. Foot, D. C. Bott, C. K. Chai, N. S. Walker, and K. P. J. Williams, 1985, in *Proceedigns of the International Winter School on Electronic Properties of Polymers and Related Compounds, Kirchberg, Tyrol. . .,* Springer Series on Solid State Sciences No. 63, edited by H. Kuzmany, M. Mehring, and S. Roth (Springer, Berlin), p. 50.
Townsend, P. D., and R. H. Friend, 1987, in Proceedings ICSM 1986, Kyoto, Japan, Synth. Met. **17**, 361.
Vardeny, Z., 1984, Physica B **127**, 338.
Vardeny, Z., E. Ehrenfreund, O. Brafman, A. J. Heeger, and F. Wudl, 1987, Synth. Met. **18**, 183.
Vardeny, Z., E. Ehrenfreund, O. Brafman, and B. Horovitz, 1983, Phys. Rev. Lett. **51**, 2326.
Vardeny, Z., E. Ehrenfreund, O. Brafman, and B. Horovitz, 1985, Phys. Rev. Lett. **54**, 75.
Vardeny, Z., E. Ehrenfreund, O. Brafman, B. Horovitz, H. Fumimoto, J. Tanaka, and M. Tanaka, 1986, Phys. Rev. Lett. **57**, 2995.
Vardeny, Z., E. Ehrenfreund, O. Brafman, M. Nowak, H. Schaffer, A. J. Heeger, and F. Wudl, 1986, Phys. Rev. Lett. **56**, 671.
Vardeny, Z., J. Orenstein, and G. L. Baker, 1983a, Phys. Rev. Lett. **50**, 2032.

Vardeny, Z., J. Orenstein, and G. L. Baker, 1983b, J. Phys. (Paris) **44**, C3-325.
Vardeny, Z., J. Strait, D. Moses, T.-C. Chung, and A. J. Heeger, 1982, Phys. Rev. Lett. **49**, 1657.
Vardeny, Z., J. Tanaka, H. Fujimoto, and M. Tanaka, 1984, Solid State Commun. **50**, 937.
Wada, Y., and J. R. Schreiffer, 1978, Phys. Rev. B **18**, 3897.
Weinberger, B. R., E. Ehrenfreund, A. J. Heeger, and A. G. MacDiarmid, 1980, J. Chem. Phys. **72**, 4749.
Weinberger, B. R., C. B. Roxlo, S. Etemad, G. L. Baker, and J. Orenstein, 1984, Phys. Rev. Lett. **53**, 86.
Winokur, W., Y. B. Moon, A. J. Heeger, J. Barker, D. C. Bott, and H. Shirakawa, 1987, Phys. Rev. Lett. **58**, 2329.
Winokur, W., Y. B. Moon, A. J. Heeger, J. Barker, and D. C. Bott, 1988, unpublished.
Wu, C., X. Sun, and K. Nasu, 1987, Phys. Rev. Lett. **59**, 831.
Wu, W.-K., and S. Kivelson, 1986, Phys. Rev. B **33**, 8546.
Yang, X. Q., D. B. Tanner, M. J. Rice, H. W. Gibson, A. Feldblum, and A. J. Epstein, 1987, Solid State Commun. **61**, 335.
Yannoni, C. S., and T. C. Clarke, 1983, Phys. Rev. Lett. **51**, 1191.
Yoshino, K., S. Nakajima, M. Fujuii, and R. Sugimoto, 1987, Polymer Commun. **28**, 309.
Zabusky, N. J., and M. D. Kruskal, 1965, Phys. Rev. Lett. **15**, 240.
Zilcox, M., B. Francois, C. Mathis, B. Meurer, G. Weill, and K. Holczer, 1985, Mol. Cryst. Liq. Cryst. **117** (Part A), 483.
Ziman, J., 1980, *Electrons and Phonons: The Theory of Transport Phenomena in Solids* (Clarendon, Oxford).
Zoor, Z. G., and S. Ramasesha, 1983, Phys. Rev. Lett. **51**, 2374.

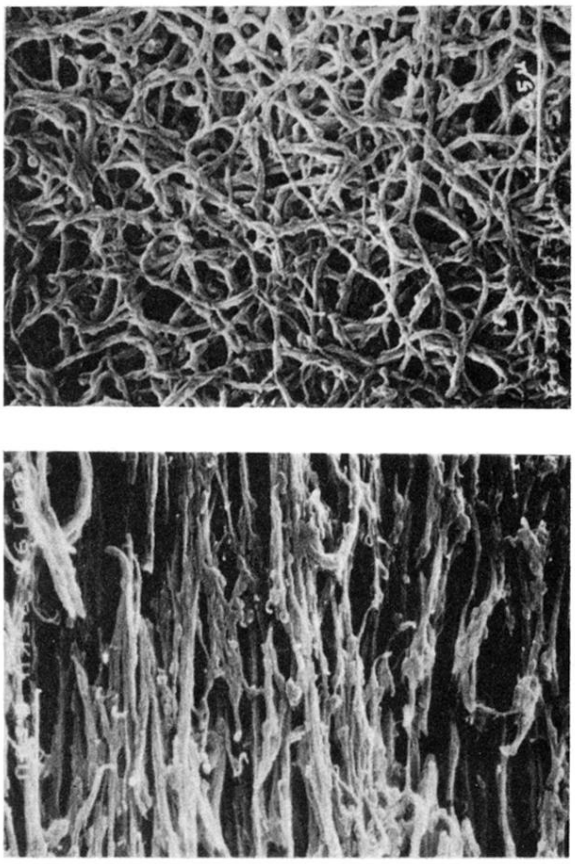

FIG. 3. Electron micrographs of polyacetylene; the upper panel shows the as-grown morphology, and the lower panel shows the effect of modest orientation by stretching. The typical fibril diameter is approximately 200 Å (from Shirakawa and Ikeda, 1979/1980).